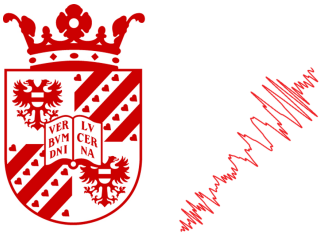

university of groningen

Effective Theory Approaches in Gravitational Wave Theory

About the use of effective theories, the effective field theory approach, and the effective one body approach in the development of gravitational wave theory describing binary inspiral systems

Submitted by
MYRTHE SCHEEPERS

Supervisor and first examiner
PROF. DR. DIEDERIK ROEST

Daily supervisor
DIJS DE NEELING, MSC

Second examiner
PROF. DR. ANUPAM MAZUMDAR

Van Swinderen Institute for Particle Physics and Gravity
Faculty of Science and Engineering

2020-2021

Abstract

Effective Theory Approaches in Gravitational Wave Theory

by MYRTHE SCHEEPERS

To study descriptions of gravitational waves originating from binary systems consisting of black holes and/or neutron stars, two different effective theory approaches are reviewed. The first, the effective field theory approach, integrates out the scales significantly smaller than the wavelength of gravitational waves and constructs an effective action that allows for a diagrammatic interpretation. The second, the effective one body approach, generalises the test particle limit and uses resummation methods to describe the gravitational waveform until the final stages of the merger, thus including the merger and ringdown. To understand these approaches better, they will be considered from the general notion of effective theories, and several cases of two-body systems will be discussed in other theories than the theory of General Relativity.

Acknowledgements

Throughout this research project, I received support and guidance from my supervisor, Prof. Dr. Diederik Roest. His enthusiasm and positive attitude have helped me to take up challenges and follow my interests within the project. I am thankful for everything that he has done to help me in both my academic and personal development during this research project.

In addition, I would like to thank Dijs de Neeling, who was my daily supervisor. From the start, he has been available to help me with the various challenges in this project, and I have enjoyed the diversity of topics that we have discussed. With the books added to my reading list, my recent fascination with football, and the other ideas and interests I have picked up from our conversations, I am looking forward to having some time off after finishing this project.

Finally, I am grateful for the meetings and seminars organised by the Kepler Journal Club, Gravity Journal Club, Basic Notions group, and the informal coffee meetings that I have appreciated very much. These have provided a sense of community and shared interests throughout the year.

Contents

Chapter 1

Introduction

The first direct detection of gravitational waves was performed on September 14th in 2015. The origin of these ripples in spacetime was the final moment of the merger of two black holes into one more massive spinning black hole. This detection was announced by the LIGO and Virgo collaborations on February 11th in 2016 (Abbott et al., 2016a) because it took a long time to verify the detection. Mainly due to the fact that the data acquired by the gravitational wave detectors is all but straightforward to interpret, as it requires a prediction of the shape of waveforms to be detected to filter out the noise. These waveforms are described by the theory of General Relativity, introduced by Albert Einstein in 1915 (Einstein, 1916).

The fact that gravitational waves, which were already predicted by Einstein's theory, have now been directly detected, is seen as an important verification of the theory of General Relativity. On top of that, the ability to detect gravitational waves is said to enable us to 'hear' phenomena, such as the mergers of heavy objects, like black holes or neutron stars, in the universe, instead of only being able to 'see' them by observing light- and other rays. It is as if we have acquired another sense to observe the universe. Since the first detection, the network of interferometers has been expanded and observational abilities have been improved to be able to perform more and better detections. By performing more of these gravitational wave observations, scientists would be able to study the fundamental nature of gravity, the structure of black holes and neutron stars, and the large-scale evolution of the universe.

However, analysis of gravitational waves requires an understanding the gravitational dynamics of the systems from which they are emitted, such as binary systems of black holes or neutron stars. This is not an easy job to do within the theory of General Relativity. In this theory, spacetime is described by the so-called Einstein field equations, which are non-linear. This makes them very hard to solve, and so far, only very few exact solutions have been found. Thus, to understand the data acquired from the interferometers, which are detecting the gravitational waves, we need a theory that approximates General Relativity but is easier to use for computations. Two important approaches which do this, the effective field theory approach and the effective one body approach, will be discussed in this project.

Effective field theories are very well known for their application in the Standard Model of particle physics. One of the most familiar examples of an effective field theory is the Fermi theory. In Fermi theory, four fermions interact with each other in one vertex and the coupling of that vertex is calculated. However, it later turned out that this is actually a low-energy effective description of the weak field interaction which occurs by the exchange of a virtual interaction boson and thereby splitting the one vertex in Fermi theory into two vertices.

The effective one body approach is a generalisation of the test particle limit and has been specifically developed for the description of gravitational binary systems. In this limit, there is one object, the 'test particle' with a significantly smaller mass or charge which therefore has a negligible effect on the other object with a larger mass or charge. The description of the system in the test particle limit can therefore be simplified by only considering the effects of the object with a larger mass or charge on the test particle. The generalisation of this limit extends the description to situations in which the masses or charges of the particles are more equal. The gravitational effective one body description was inspired by, although different from, an approach to electromagnetically interacting two body-systems. Its application in the current form to electrodynamically interacting two-body systems presents therefore an interesting case to study, because of the availability of exact solutions.

What stands out from the names of the two approaches, is that they are both classified as 'effective' approaches. The main implication of this characteristic is that they do not provide exact solutions or descriptions. An effective theory "systematizes what is irrelevant for the purposes at hand", it "enables a useful prediction with a finite number of input parameters" (Wells, 2012, p. 1). This can be useful in two types of cases: when you want to simplify a known complicated theory, and when you want to describe a system of which the theory is yet unknown. With the availability of the theory of General Relativity, it seems that we are looking at the first application of an effective theory for the description of coalescing binary systems.

In this thesis, we will start with an introduction to gravitational waves. We will cover some important moments in the theoretical development and the link between theory and experiment. After that, the chapters will be divided into three parts of the thesis: (I) effective theories, (II) effective field theory approach and (III) effective one body approach. The three approaches in the parts are not equal, since the first one will be studied as a foundation for the other two and reflect on the role of the broader class of effective theories in physics and theory development. The first part also includes a case study about a heuristic application of effective theories, which will at the same time provide a warm-up for the construction of an effective field theory. The second part then covers the main concepts and procedures of effective field theories for binary problems. Two cases will be studied, effective scalar field theory and effective electromagnetic field theory, before applying the approach to the gravitational dynamics of a binary system. The last part starts from the results from the second part and introduces an approach to extend these results to later stages of the merger of gravitational binaries. To study this approach, we

again analyse the case of electromagnetic interactions, before applying it to the gravitational situation. The concluding chapter of the thesis will then discuss the accumulated conclusions from the three parts.

The research question is: "How can we construct gravitational wave templates to detect gravitational waves originating from gravitational binary inspirals?" To answer this question, we will consider the role of effective theories in general, and the effective field theory formalism and the effective one body formalism in particular, in the development of our understanding of gravitational waves emitted by binary systems of compact objects.

1.1 Notation and conventions

There are several notations and conventions which are used consistently throughout this report, unless otherwise noted.

- Throughout the report we work with $\hbar = c = 1$ units, unless otherwise noted.
- We use a reduced Planck mass: $M_{Pl}^{-2} \equiv 32\pi G$, with G Newton's constant.
- We use Einstein's summation over repeated indices. Greek and Latin indices ranges are as usual, i.e. $\mu, \nu, \ldots = 0, 1, 2, 3$, and $i, j, \ldots = 1, 2, 3$. Sometimes we use the notation $x^0 = t$ where that is appropriate.
- We sometimes use the dot-notation for time derivatives, e.g. $\dot{\boldsymbol{x}} = \frac{d\boldsymbol{x}}{dt}$, and $\ddot{\boldsymbol{x}} = \frac{d^2\boldsymbol{x}}{dt^2}$.
- We denote 3-vectors in boldface, e.g. $\boldsymbol{x}, \boldsymbol{y}, \ldots$, and put hats on unit vectors, e.g. $\hat{\boldsymbol{x}}$. To avoid cluttering expressions, sometimes we omit the Greek indices when evaluating spacetime (scalar, vector, tensor) functions, e.g. $f^{\alpha\beta\cdots}(x, y, \cdots) \equiv f^{\alpha\beta\cdots}(x^\mu, y^\mu, \cdots)$.
- The Minkowski metric is given by $\eta_{\alpha\beta} \equiv \mathrm{diag}(+, -, -, -)$. The full metric tensor is denoted as usual, $g_{\mu\nu}(x)$, and often use the standard notation: $v^2 \equiv v^\mu v_\mu \equiv g_{\mu\nu} v^\mu v^\nu$.
- We use τ for the proper time: $d\tau^2 = g_{\alpha\beta} dx^\alpha dx^\beta$.
- We write spacetime velocities as $u^\mu(\sigma) \equiv \frac{dx^\mu}{d\sigma}$, with σ an affine parameter (sometimes the proper time), and $v^\mu(t) \equiv \frac{dx^\mu}{dt}$, when the choice $\sigma = t$ is made.
- The partial derivatives are denoted by $\partial_\mu \equiv \frac{\partial}{\partial x^\mu}$, and sometimes we simplify notation by repeating indices, e.g. $\partial_{ij} \equiv \partial_i \partial_j$.
- We use the shortened notation $\int_{\boldsymbol{p},\cdots,\boldsymbol{q}} \equiv \int \frac{d^3\boldsymbol{p}}{(2\pi)^3} \cdots \frac{d^3\boldsymbol{q}}{(2\pi)^3}$ and $\int_{p_0} \equiv \int \frac{dp_0}{2\pi}$.
- We denote the symmetric-trace-free electric- and magnetic-type multipole moments as I^L and J^L, respectively, using the compact notation $L \equiv (i_1 \ldots i_l)$. We also use the shortened notation $x^L \equiv x^{i_1} \cdots x^{i_l}$, $x^{ijL-2} \equiv x^i x^j x^{i_1} \cdots x^{i_{l-2}}$ etc., throughout.

- We denote the time average of a quantity as $\langle X(t) \rangle \equiv \frac{1}{T} \int_0^T dt X(t)$.
- We use $\langle T \cdots \rangle$ for the time-ordered product, which in our classical setting is short-hand for products of the Green's functions.
- The n-th order in the post-Newtonian expansion is denoted by $n\,\mathrm{PN} \equiv \mathcal{O}(v^{2n})$, this expansion is discussed in more detail in section 6.1.

Chapter 2

Gravitational Waves

As explained in the introduction, the theory of General Relativity predicted the existence of gravitational waves. However, the history of this prediction is less straightforward than often thought. We will therefore first briefly discuss part of the theoretical history of gravitational waves, and then discuss the current state of gravitational wave science including the detection of gravitational waves.

2.1 Theoretical history

The first known concept of gravitational waves was introduced by William Clifford in his published work in 1876 (Clifford, 1876). He did not use the term 'gravitational waves' but he described the following concept:

> I hold that (1) small portions of space *are* in fact of a nature analogous to little hills on a surface which is on average flat; namely that the ordinary laws of geometry are not valid for them. (2) That the property of being curved or distorted is continually being passed on from one portion of space to another after the manner of a wave (Chen, Nester, and Ni, 2017, pp. 4–5).

With this description, Clifford explained his concept of "curvature waves". The first known use of the term "gravitational waves" was then by Henri Poincaré in 1906 in relation to his speculation about relativistic gravity involving waves propagating at speed c originating from the acceleration of gravitational bodies (Poincaré, 1906, p. 174)(Chen, Nester, and Ni, 2017, p. 5).

The development of special relativity inspired some to think about a Lorentz covariant scalar theory. Nordström's suggestion in 1913 is one of the best-known (Nordström, 1913), it contained waves propagating at the speed of light and can be expressed in a generally covariant form, even though it does not predict the bending of light. This last characteristic was shown by Einstein and Fokker in 1914 for a theory with a generally covariant form (Einstein and Fokker, 1914), and one of the things it showed is that the Riemann curvature scalar is proportional to

the trace of the matter energy-momentum density:

$$R = 3\kappa T, \quad \kappa := \frac{8\pi G}{c^4} \tag{2.1}$$

where the factor κ depends on Newton's gravitational constant G and the speed of light c (Chen, Nester, and Ni, 2017, p. 5).

Einstein presented his generally covariant theory of gravitation for a dynamical spacetime metric, General Relativity, in 1915 (Einstein, 1916). The field equations,

$$R_{\mu\nu} - \frac{1}{2} g_{\mu\nu} R = \frac{8\pi G}{c^4} T_{\mu\nu}, \tag{2.2}$$

are found by taking the variation of the total gravitational action with respect to the spacetime metric tensor $g_{\mu\nu}$ (Maggiore, 2008, p. 4). More detail with regards to the gravitational action will be discussed in the field theory description. These field equations describe the relation between the density and flux of energy and momentum in spacetime, represented by the stress-energy-momentum tensor $T_{\mu\nu}$, and the curvature of spacetime, described by the spacetime metric $g_{\mu\nu}$, with spacetime interval $ds^2 = g_{\mu\nu} dx^\mu dx^\nu$. The Ricci curvature tensor, $R_{\mu\nu}$, is given by

$$R_{\mu\nu} = R^\alpha_{\mu\alpha\nu} = \partial_\mu \Gamma^\alpha_{\beta\nu} - \partial_\nu \Gamma^\alpha_{\beta\mu} + \Gamma^\alpha_{\gamma\mu} \Gamma^\gamma_{\beta\nu} - \Gamma^\alpha_{\gamma\nu} \Gamma^\gamma_{\beta\mu}, \tag{2.3}$$

in which the Christoffel symbols can be given in terms of the metric by

$$\Gamma^\alpha_{\beta\gamma} = \frac{1}{2} g^{\alpha\delta} (\partial_\beta g_{\delta\gamma} + \partial_\gamma g_{\delta\beta} - \partial_\delta g_{\beta\gamma}). \tag{2.4}$$

This allows us to define the Einstein tensor $G_{\mu\nu} = R_{\mu\nu} - \frac{1}{2} g_{\mu\nu} R$ (Chen, Nester, and Ni, 2017, p. 5).

Although now often seen as a logical consequence from the theory of General Relativity, at the time, Einstein was not convinced of the existence of gravitational waves. Three months after writing down these field equations, Einstein wrote to Schwarzschild:

> Since then [Nov 4], I have handled Newton's case differently according to the final theory. - Thus there are no gravitational waves analogous to light waves. This is probably also related to the one-sidedness of the sign of scalar T, incidentally. (Nonexistence of the "dipole".) (Einstein, 1998, p. 196)

Reconstructing what led Einstein to believe this, it is thought that he did not consider effects beyond dipole radiation. He might have understood that for purely attractive gravity, now considered a spin-two theory, there could be no dipole radiation. This explains why Einstein could have missed the damping due to radiation reactions from the emission of gravitational waves,

which we now know appear at order $\left(\frac{v}{c}\right)^5$, as he might have only found the first corrections of order $\left(\frac{v}{c}\right)^2$ and vanishing corrections at order $\left(\frac{v}{c}\right)^3$ (Chen, Nester, and Ni, 2017, p. 6).

A few months later, when Einstein developed the weak field linearized theory of General Relativity, which at the time still contained several mistakes, he changed his mind. He followed a suggestion from Willem de Sitter and used the coordinate condition $\sqrt{|g|} = 1$. This led to the prediction of the existence of gravitational waves that travel with a speed of c generated by the quadrupole moment of a time varying-source (Chen, Nester, and Ni, 2017, pp. 6–7).

In January 1918, Einstein published a new article in which he corrected many of the mistakes from his linearized gravity work since Nordström had pointed those out to him. This paper also provided the earlier missing arguments for the fact that two out of the three types of waves do not carry energy and depend on the choice of coordinates, these polarizations are therefore not physical, while only the transverse-transverse waves carry energy (Chen, Nester, and Ni, 2017, p. 7). In this paper, Einstein also introduced the "quadrupole formula" for the first time. This formula expresses the rate of emission of gravitational wave energy by a system of accelerating masses. Einstein showed that the power radiated in gravitational waves by a system of accelerating masses is proportional to the square of the third time derivative of the system's mass quadrupole moment, hence the name of the formula. The derivation of the quadrupole formula was the basis of the linearized approximation of General Relativity that we will discuss later in this chapter (Kennefick, 2017, p. 293). It would remain, however, for a long time an important question as to whether, and in which form, the quadrupole formula gives a reasonable approximation of the source strength of possible astrophysical sources of gravitational waves. We will see later in this chapter that the controversy of this question was eventually solved by the first indirect detections of gravitational waves.

Eddington examined the concept of 'waves of curvature' from Clifford in 1922 and concluded that the pure gauge degrees of freedom, which are the two types of waves depending on the choice of coordinates, can propagate at any speed. This verified Einstein's work from 1918 but also contained a small correction to the quadrupole amplitude (Chen, Nester, and Ni, 2017, pp. 7–8). However, the correct expression for the quadrupole radiation would not be finalised until many years later.

The arguments for and against the existence of gravitational waves kept on going back and forth between Einstein and others. Einstein submitted a paper together with Nathan Rosen in 1936 arguing against the existence of gravitational plane waves. However, the paper got rejected and Einstein decided to submit it elsewhere. A while later, one of Einstein's assistants became friends with the referee who was responsible for rejecting Einstein and Rosen's paper. This referee, H. P. Roberson, and Einstein worked on the theory of gravitational waves together and came back to the conclusion by arguing that cylindrical gravitational waves could exist.

Rosen was not involved in these revisions of the paper he and Einstein had published together, and he distanced himself from the new conclusions (Chen, Nester, and Ni, 2017, pp. 18–19).

These are only brief descriptions of the large amount of controversy surrounding the existence of gravitational waves and different restrictions on their characteristics. Since much of the further development of gravitational wave theory is strongly linked to the experimental ambitions and advances, we will mention some of the next highlights in the historical context in section 2.4 below. We will see how observations have been able to resolve some of the theoretical debates, or at least provide strong evidence for the existence of gravitational waves.

2.2 Linearized gravity

In linearized gravity the non-linear equations of motion from General Relativity are expanded to linear order in $h_{\mu\nu}$. This approach is applicable for weak gravitational fields, described by

$$g_{\mu\nu} = \eta_{\mu\nu} + h_{\mu\nu} \tag{2.5}$$

which can be treated as a classical field theory of the field $h_{\mu\nu}$ as a perturbation of the flat spacetime described by the Minkowsky metric $\eta_{\mu\nu}$, thus assuming that $|h_{\mu\nu}| \ll 1$ (Maggiore, 2008, p. 4).

2.2.1 Symmetries

The components of a tensor depend on the chosen reference frame, and hence we can always choose a reference frame for which equation 2.5 holds in a sufficiently large region of space. Fixing the reference frame has the consequence that the local invariance of General Relativity is broken under coordinate transformations, and pseudo-degrees of freedom are eliminated. A gauge symmetry remains, which can be associated with the coordinate transformation, or diffeomorphism,

$$x^\mu \to x'^\mu = x^\mu + \xi^\mu(x), \tag{2.6}$$

in which derivatives $|\partial_\mu \xi_\nu|$ are of the same order of smallness as $|h_{\mu\nu}|$. Under the transformation of the metric, given by

$$g_{\mu\nu}(x) \to g'_{\mu\nu}(x') = \frac{\partial x^\rho}{\partial x'^\mu} \frac{\partial x^\sigma}{\partial x'^\nu} g_{\rho\sigma}(x), \tag{2.7}$$

the transformation of $h_{\mu\nu}$, to lowest order, is

$$h_{\mu\nu}(x) \to h'_{\mu\nu}(x') = h_{\mu\nu}(x) - (\partial_\mu \xi_\nu + \partial_\nu \xi_\mu). \tag{2.8}$$

The condition $|h_{\mu\nu}| \ll 1$ is preserved when $|\partial_\mu \xi_\nu|$ are at most of the same order of smallness as $|h_{\mu\nu}|$, and if that is the case then the slowly varying diffeomorphisms described by equation 2.6 are a symmetry of linearized theory (Maggiore, 2008, pp. 4–5).

In addition to this local gauge symmetry, there is also a finite, global symmetry in linearized gravity. This symmetry is given by the Lorentz transformations

$$x^\mu \to \Lambda^\mu_\nu x^\nu. \tag{2.9}$$

In which the matrix Λ^μ_ν by definition has to satisfy

$$\Lambda^\rho_\mu \Lambda^\sigma_\nu \eta_{\rho\sigma} = \eta_{\mu\nu}. \tag{2.10}$$

For the transformation of the spacetime metric, this yields

$$\begin{aligned} g_{\mu\nu}(x) \to g'_{\mu\nu}(x') &= \Lambda^\rho_\mu \Lambda^\sigma_\nu g_{\rho\sigma}(x) && (2.11)\\ &= \Lambda^\rho_\mu \Lambda^\sigma_\nu [\eta_{\rho\sigma} + h_{\rho\sigma}(x)] && (2.12)\\ &= \eta_{\mu\nu} + \Lambda^\rho_\mu \Lambda^\sigma_\nu h_{\rho\sigma}(x). && (2.13) \end{aligned}$$

This shows that $h_{\mu\nu}$ transforms like a tensor under Lorentz transformations. We just have to make sure that the condition $|h_{\mu\nu}| \ll 1$ holds, which is always the case for rotations, and only poses a limitation for boosts (Maggiore, 2008, p. 5).

It is clear from equation 2.7 that constant translations leave $h_{\mu\nu}$ invariant. Constant translations are of the form $x^\mu \to x'^\mu = x^\mu + a^\mu$ in which a^μ has to be finite but not necessarily infinitesimal. We can summarise the symmetries of linearized gravity by saying that it is invariant under finite Poincaré transformations. This group of transformations includes the infinitesimal local transformations in equation 2.8, the Lorentz transformations in equation 2.9, and the finite translations (Maggiore, 2008, p. 5).

2.2.2 Wave equation

In linearized theory we use the flat metric $\eta_{\mu\nu} = \eta^{\mu\nu}$ to raise or lower indices. We define

$$h = \eta^{\mu\nu} h_{\mu\nu} \tag{2.14}$$

and

$$\bar{h}_{\mu\nu} = h_{\mu\nu} - \frac{1}{2}\eta_{\mu\nu} h. \tag{2.15}$$

Then by observing that

$$\bar{h} \equiv \eta^{\mu\nu} \bar{h}_{\mu\nu} = h - 2h = -h \tag{2.16}$$

thus

$$h_{\mu\nu} = \bar{h}_{\mu\nu} - \frac{1}{2}\eta_{\mu\nu}\bar{h}. \tag{2.17}$$

Combining this with the Riemann tensor to linear order in $h_{\mu\nu}$, given by

$$R_{\mu\nu\rho\sigma} = \frac{1}{2}(\partial_\nu\partial_\rho h_{\mu\sigma} + \partial_\mu\partial_\sigma h_{\nu\rho} - \partial_\mu\partial_\rho h_{\nu\sigma} - \partial_\nu\partial_\sigma h_{\mu\rho}), \tag{2.18}$$

we can compute the linearization of the Einstein tensor $G_{\mu\nu} = R_{\mu\nu} - \frac{1}{2}g_{\mu\nu}R$. And then the Einstein field equations become

$$\Box\bar{h}_{\mu\nu} + \eta_{\mu\nu}\partial^\rho\partial^\sigma\bar{h}_{\rho\sigma} - \partial^\rho\partial_\nu\bar{h}_{\mu\rho} - \partial^\rho\partial_\mu\bar{h}_{\nu\rho} = -\frac{16\pi G}{c^4}T_{\mu\nu}, \tag{2.19}$$

where $\Box = \eta_{\mu\nu}\partial^\mu\partial^\nu = \partial_\mu\partial^\mu$ is the flat space d'Alembertian. This can be simplified by using the gauge freedom from equation 2.8, and choose the harmonic gauge given by

$$\partial^\nu\bar{h}_{\mu\nu} = 0. \tag{2.20}$$

Which reduces equation 2.19 to

$$\Box\bar{h}_{\mu\nu} = -\frac{16\pi G}{c^4}T_{\mu\nu}, \tag{2.21}$$

which is a simple wave equation for the generation of a gravitational wave (Maggiore, 2008, pp. 6–7).

Observe that $h_{\mu\nu}$ has ten independent components because it is a symmetric 4×4 matrix. Equation 2.20 provides four conditions, thus reducing the number of independent parameters to six (Maggiore, 2008, p. 7). In the section about polarization, section 2.2.3 below, we will discuss the physical interpretation of the independent parameters.

We can also note that equations 2.20 and 2.21 together imply that

$$\partial^\nu T_{\mu\nu} = 0, \tag{2.22}$$

equivalent to the conservation of energy-momentum in this linearized theory. This is in contrast with the full conservation given by $D^\nu T_{\mu\nu} = 0$, where D^ν is the covariant derivative, in the full, non-linear theory of General Relativity (Maggiore, 2008, p. 7). For many situations, only retaining the terms up to order $\mathcal{O}(h)$ suffices and higher-order terms can be dropped.

The physical interpretation of approximations in linearized gravity for a self-gravitating binary system is that the bodies are moving in a flat space-time, $\eta_{\mu\nu}$, along trajectories determined by their mutual influence. This means that the system, up to certain order, is described by the dynamics of Newtonian gravity, rather than that of full General Relativity. The response of the objects to the presence of gravitational waves in the system is computed using $g_{\mu\nu} = \eta_{\mu\nu} + h_{\mu\nu}$,

where terms $\mathcal{O}(h^2)$ are neglected in the Christoffel symbols and Riemann tensor (Maggiore, 2008, p. 7).

2.2.3 Polarization

The wave equation in equation 2.21 describes the generation of gravitational waves. To study the propagation of gravitational waves, we are interested in the equations outside the source, when $T_{\mu\nu} = 0$. The wave equation then reduces to

$$\Box \bar{h}_{\mu\nu} = 0, \tag{2.23}$$

where

$$\Box = -\frac{1}{c^2}\partial_0^2 + \nabla^2. \tag{2.24}$$

Outside the source, the metric can also be simplified, because the harmonic gauge in equation 2.20 does not fix the gauge completely. This can be seen in the transformation of $\bar{h}_{\mu\nu}$:

$$\bar{h}_{\mu\nu} \to \bar{h}'_{\mu\nu} = \bar{h}_{\mu\nu} - (\partial_\mu \xi_\nu + \partial_\nu \xi_\mu - \eta_{\mu\nu}\partial_\rho \xi^\rho), \tag{2.25}$$

which implies

$$\partial^\nu \bar{h}_{\mu\nu} \to (\partial^\nu \bar{h}_{\mu\nu})' = \partial^\nu \bar{h}_{\mu\nu} - \Box \xi_\mu. \tag{2.26}$$

From which we can see that a coordinate transformation $x^\mu \to x^\mu + \xi^\mu$ with the condition $\Box \xi_\mu = 0$ does not violate the condition that $\partial^\mu \bar{h}_{\mu\nu} = 0$. This allows us to define

$$\xi_{\mu\nu} \equiv \partial_\mu \xi_\nu + \partial_\nu \xi_\mu - \eta_{\mu\nu}\partial_\rho \xi^\rho, \tag{2.27}$$

which must satisfy $\Box \xi_{\mu\nu} = 0$, given that the d'Alembertian $\Box$ commutes with ∂_μ. Looking back at equation 2.25, it now shows how from the six independent components of $\bar{h}_{\mu\nu}$, satisfying $\Box \bar{h}_{\mu\nu} = 0$, we can subtract the functions $\xi_{\mu\nu}$. The functions $\xi_{\mu\nu}$ depend on four arbitrary functions ξ_μ, and satisfy $\Box \xi_{\mu\nu} = 0$. This means that four extra conditions can be imposed on $h_{\mu\nu}$. In particular, ξ^0 can be chosen such that the trace $\bar{h} = 0$, which has as a consequence that $\bar{h}_{\mu\nu} = h_{\mu\nu}$. And the three functions $\xi^i(x)$ are chosen such that $h^{0i}(x) = 0$ (Maggiore, 2008, pp. 7–8).

The condition from equation 2.20, taking $\mu = 0$, reads

$$\partial^0 h_{00} + \partial^i h_{0i} = 0, \tag{2.28}$$

and since we have also fixed $h_{0i} = 0$, this simplifies to

$$\partial^0 h_{00} = 0. \tag{2.29}$$

As a consequence, h_{00} is a constant in time, corresponding to the Newtonian potential of the source that generated the gravitational wave. Since the gravitational wave itself is time-dependent, only the spatial components h_{ij} are non-zero after removing all redundant degrees of freedom. This is all summarised in the transverse-traceless (TT) gauge, in which the metric is denoted by h_{ij}^{TT}, which has to satisfy:

$$h^{0\mu} = 0, \quad h_i^i = 0, \quad \partial^j h_{ij} = 0. \tag{2.30}$$

The six degrees of freedom of $h_{\mu\nu}$ that remained after imposing the harmonic gauge, have now been reduced to two degrees of freedom by fixing the residual gauge freedom, with the four constraints of the functions ξ^μ (Maggiore, 2008, p. 8).

The two remaining degrees of freedom correspond to the two physical polarizations of gravitational waves. They are given in the plane wave solutions to equation 2.23, given by

$$h_{ij}^{TT}(x) = e_{ij}(\boldsymbol{k}) e^{ikx}, \tag{2.31}$$

in which $k^\mu = (\omega/c, \boldsymbol{k})$, $\omega/c = |\boldsymbol{k}|$, and $e_{ij}(\boldsymbol{k})$ is called the polarization tensor. For a single plane wave with wave-vector $\boldsymbol{k}$, the non-zero components of h_{ij}^{TT} are in the plane transverse to $\hat{\boldsymbol{n}} = \boldsymbol{k}/|\boldsymbol{k}|$ because the condition $\partial^j h_{ij} = 0$ becomes $n^i h^{ij} = 0$. Choosing $\hat{\boldsymbol{n}}$ along the z-axis, and imposing that h_{ij} is symmetric and traceless, we find

$$h_{ij}^{TT}(t,z) = \begin{pmatrix} h_+ & h_\times & 0 \\ h_\times & -h_+ & 0 \\ 0 & 0 & 0 \end{pmatrix}_{ij} \cos[\omega(t - z/c)], \tag{2.32}$$

in which h_+ and $h_\times$ are the amplitudes of the "plus" and "cross" polarizations of the wave (Maggiore, 2008, p. 9).

2.2.4 Field theory description

So far, we have described General Relativity in its geometric formalism. Complementary to this, there is also the field-theoretic tradition. The field theory language is most familiar in the context of classical and quantum field theory. Both formalisms describe General Relativity at different levels. The macroscopic level is most clear in the geometric tradition, in which the metric describes the collective excitations of the gravitational field. The fundamental level is best described by the field theory tradition, in which linearized gravity is the field theory of a massless particle called the graviton. Both descriptions have their advantages, and they both provide a better understanding of different conceptual challenges (Maggiore, 2008, p. xiv).

The basis of the field-theoretic description is the action, in the case of General Relativity the action is given by $S = S_{EH} + S_M$, consisting of the Einstein-Hilbert action, and the matter

action respectively. The first is given by

$$S_{EH} = \frac{c^3}{16\pi G} \int d^4x \sqrt{-g} R \tag{2.33}$$

in which c is the speed of light, G is Newton's gravitational constant, g is the determinant of the spacetime metric $g_{\mu\nu}$, and R is the Ricci scalar (Maggiore, 2008, pp. 4, 59).

For the matter action, we often look at its variation because that enables us to define the energy-momentum tensor $T_{\mu\nu}$. The variation of the matter action under the change of the metric $g_{\mu\nu} \to g_{\mu\nu} + \delta g_{\mu\nu}$ is given by

$$\delta S_M = \frac{1}{2c} \int d^4x \sqrt{-g} T^{\mu\nu} \delta g_{\mu\nu}, \tag{2.34}$$

in which c is the speed of light, g is the determinant of the spacetime metric $g_{\mu\nu}$, and $T^{\mu\nu}$ is the stress-energy tensor (Maggiore, 2008, pp. xvii, 4).

Because we are looking at linearized theory here, we expand $g_{\mu\nu} = \eta_{\mu\nu} + h_{\mu\nu}$. This is the same expansion as used in the geometric approach, however, now $h_{\mu\nu}$ is treated like any other field, and not specifically interpreted as a space-time metric as in the geometric tradition (Maggiore, 2008, p. 52). The loss of the metric aspect of the theory is related to the fact that in the Newtonian approximation of General Relativity, the leading-order term comes from just one component of the Einstein equations. This poses a problem for the description of gravitational waves because they travel far from the sources that generate them and the Newtonian approximation weakens according to the inverse-square of the radial distance from the source (Kennefick, 2017, p. 48). However, as we will see, the field theoretical description, without the metric interpretation of the spacetime perturbation, has found a way to describe gravitational waves.

The linearized gravity theory yields for the Ricci scalar

$$R = g^{\mu\nu} R_{\mu\nu} = (\eta^{\mu\nu} - h^{\mu\nu} + \mathcal{O}(h^2)) \left(R^{(1)}_{\mu\nu} + R^{(2)}_{\mu\nu} + \mathcal{O}(h^3) \right), \tag{2.35}$$

where $R^{(1)}_{\mu\nu}$ is linear in h and $R^{(2)}_{\mu\nu}$ is quadratic in h, and they are given by (Maggiore, 2008, pp. 30, 59):

$$R^{(1)}_{\mu\nu} = \frac{1}{2}(\bar{D}^\alpha \bar{D}_\mu h_{\nu\alpha} + \bar{D}^\alpha \bar{D}_\nu h_{\mu\alpha} - \bar{D}^\alpha \bar{D}_\alpha h_{\mu\nu} - \bar{D}_\nu \bar{D}_\mu h), \tag{2.36}$$

$$\begin{aligned} R^{(2)}_{\mu\nu} = \frac{1}{2}\bar{g}^{\rho\sigma}\bar{g}^{\alpha\beta} \Bigg[& \frac{1}{2}\bar{D}_\mu h_{\rho\alpha} \bar{D}_\nu h_{\sigma\beta} + (\bar{D}_\rho h_{\nu\alpha})(\bar{D}_\sigma h_{\mu\beta} - \bar{D}_\beta h_{\mu\sigma}) \\ & + h_{\rho\alpha}(\bar{D}_\nu \bar{D}_\mu h_{\sigma\beta} + \bar{D}_\beta \bar{D}_\sigma h_{\mu\nu} - \bar{D}_\beta \bar{D}_\nu h_{\mu\sigma} - \bar{D}_\beta \bar{D}_\mu h_{\nu\sigma}) \\ & + \left(\frac{1}{2}\bar{D}_\alpha h_{\rho\sigma} - \bar{D}_\rho h_{\alpha\sigma} \right) (\bar{D}_\nu h_{\mu\beta} + \bar{D}_\mu h_{\nu\beta} - \bar{D}_\beta h_{\mu\nu}) \Bigg]. \end{aligned} \tag{2.37}$$

In these expressions, $\bar{D}_\mu$ is the covariant derivative with respect to the flat background metric (Maggiore, 2008, p. 30).

With the expansion given by

$$\sqrt{-g} = \sqrt{\det(\delta^\mu_\nu + h^\mu_\nu)} = \sqrt{1 + \eta^{\mu\nu}h_{\mu\nu} + \mathcal{O}(h^2_{\mu\nu})}, \tag{2.38}$$

and some algebra and integration by parts, we arrive at the linearized Einstein action, up to and including orders of h^2, given by

$$S_E = -\frac{c^3}{64\pi G}\int d^4x[\partial_\mu h_{\alpha\beta}\partial^\mu h^{\alpha\beta} - \partial_\mu h\partial^\mu h + 2\partial_\mu h^{\mu\nu}\partial_\nu h - 2\partial_\mu h^{\mu\nu}\partial_\rho h^\rho_\nu]. \tag{2.39}$$

From which we can identify

$$\mathcal{L} = -\frac{c^3}{64\pi G}[\partial_\mu h_{\alpha\beta}\partial^\mu h^{\alpha\beta} - \partial_\mu h\partial^\mu h + 2\partial_\mu h^{\mu\nu}\partial_\nu h - 2\partial_\mu h^{\mu\nu}\partial_\rho h^\rho_\nu] \tag{2.40}$$

as the corresponding Lagrangian density (Maggiore, 2008, p. 59).

2.3 Sources

In general, every acceleration that is not spherically or cylindrically symmetric will produce gravitational waves. This brings us to four main types of gravitational waves caused by sources with different kinds of motion and changing distributions of mass (*Sources of Gravitational Waves*):

- **Continuous** gravitational waves are caused by systems with a relatively constant and well-defined frequency. For example, binary systems of stars or black holes orbiting each other before the inspiralling and merger stage, or a star with a large irregularity fastly orbiting around its axis. These sources of gravitational waves are expected to be relatively weak compared to the other types of sources (*Continuous Gravitational Waves*).
- **Inspiral** gravitational waves are caused by the later stage of binary systems that merge into one object. These systems often consist of two neutron stars, two black holes, or a neutron star and a black hole. Their orbits have degraded from the continuous stage because the orbital distances decrease and the speeds increase. This causes the frequency of the gravitational waves to increase until the merger, and hence the source is not continuous anymore (*Inspiral Gravitational Waves*).
- **Burst** gravitational waves are short-duration signals from mostly unknown or unanticipated sources. The hypotheses are that systems such as supernovae or gamma-ray bursts can produce these types of gravitational waves, but too little is yet known to make predictions and anticipate the sources of these gravitational waves (*Burst Gravitational Waves*).

- **Stochastic** gravitational waves have their origin in the early evolution of the universe. They are expected to arise from a large number of random, independent events combining to a cosmic gravitational wave background, similar to the Cosmic microwave background for electromagnetic radiation (*Stochastic Gravitational Waves*).

For this project, we focus on the inspiral gravitational waves caused by binary systems of neutron stars and black holes. Although there are systems emitting continuous gravitational waves for which the discussion in this project is relevant, not all continuous signals will fit within this theory. One of the assumptions or starting points for the approaches that will be discussed is that the orbits are quasi-circular, which is always the case for the inspiral stage of a merger due to circularization but is not always applicable to the binary sources of continuous gravitational waves.

Figure 2.1 shows an example of a gravitational wave originating from a binary coalescence, namely the first directly detected gravitational wave, GW150914. Characteristic of these signals is that they cover a large range of scales, both in terms of separation distance, and in terms of relative velocity. The accompanying increase in the frequency of the gravitational wave is often referred to as the "chirp" of the signal because it becomes higher and higher pitched (Blanchet, 2016, p. 11).

2.4 Detection

It was most importantly the experimental evidence that led to the consensus about the existence of gravitational waves. Initially with the indirect detections in a binary pulsar, and later with the direct detection by laser interferometers. We will briefly discuss both below, in which we will pay special attention to the requirements for filtering out the signal from the detector output of laser interferometer detectors.

2.4.1 Indirect: binary pulsar

In 1974, the binary pulsar PSR B1913+16 was discovered (Chen, Nester, and Ni, 2017, p. 27). A pulsar is a fast rotating neutron star that emits radio signals in the shape of two cones. Due to the rotation of the source, the radio signals are received in pulses, like the light from a lighthouse, rather than a continuous signal (Falcke, 2020, p. 91). The frequency of these pulses provides a lot of information about the evolution of the dynamics of such a system involving one or multiple pulsars.

Taylor first announced in 1978 that the orbital parameters of the binary pulsar were decaying according to the quadrupole formula, analogous to the dipole formula in electromagnetism (Taylor, Fowler, and McCulloch, 1979). For a gravitational system, the quadrupole formula gives the first approximation of the radiation emitted by a weakly relativistic system (Schutz,

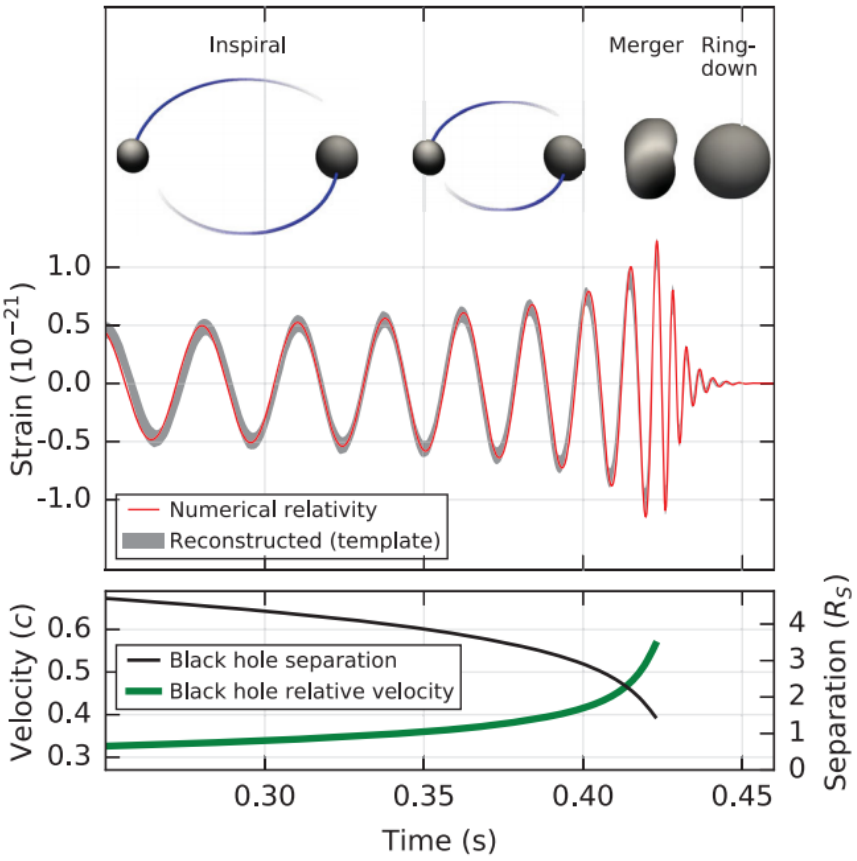

FIGURE 2.1: *Top:* The estimated gravitational-wave amplitude from GW150914. *Bottom:* The Keplerian effective black hole separation in units of Schwarzschild radii ($R_S = 2GM/c^2$) and the effective relative velocity given by the parameter $v/c = (GM\pi f/c^3)^{1/3}$, where f is the gravitational-wave frequency calculated with numerical relativity and M is the total mass of the objects in the system (Abbott et al., 2016a, p. 3).

2000, p. 6). This was strong indirect evidence for the existence of gravitational waves (Chen, Nester, and Ni, 2017, p. 27).

Thibault Damour was able to solve the quadrupole formula controversy, mentioned in sections 2.1, in 1983. He provided quantitative results that both agreed with the observational data from the binary pulsar, and with theoretical results at that time (Damour, 1983). After a few more years, around 1985, the consensus had spread and the controversy about the existence of gravitational waves was over (Chen, Nester, and Ni, 2017, pp. 26–27).

After the original results of the binary pulsar, scientists continued to monitor the relativistic binary pulsar PSR B1913+16 and collected over three decades of data. During this extensive period, the measured orbital decay of the binary system is still in agreement with the value predicted by the theory of General Relativity, as can be seen in figure 2.2 (Weisberg, Nice, and Taylor, 2010).

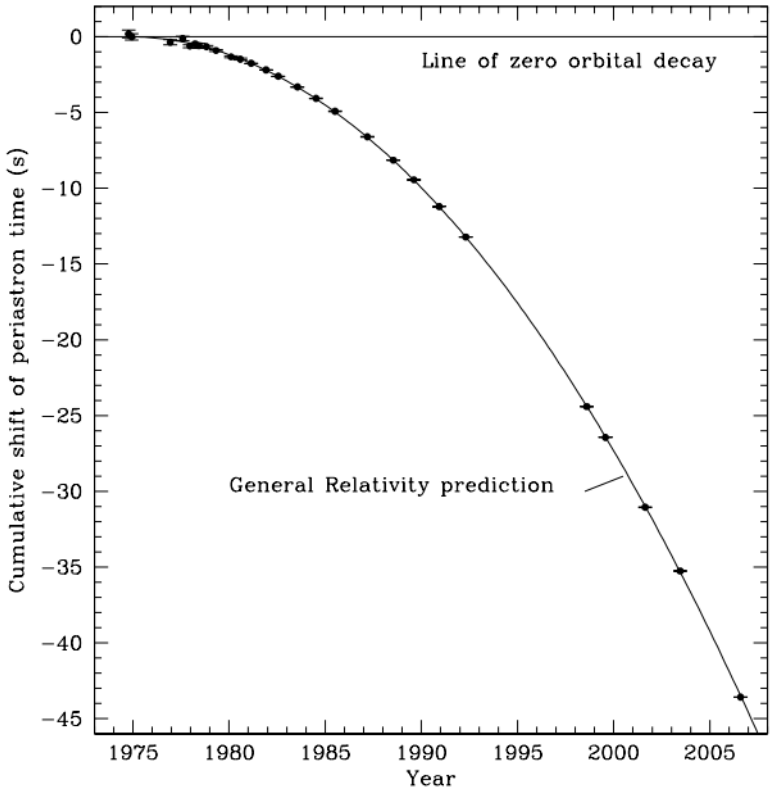

FIGURE 2.2: "Orbital decay caused by the loss of energy by gravitational radiation. The parabola depicts the expected shift of periastron time relative to an unchanging orbit, according to General Relativity. Data points represent our measurements, with error bars mostly too small to see." (Weisberg, Nice, and Taylor, 2010, p. 14)

2.4.2 Direct: laser interferometry

The efforts to develop methods for direct detection of gravitational waves started with Joseph Weber in 1958. At the time, the gap between predicted gravitational wave strength and detection capabilities was still approximately 15-16 orders of magnitude (Chen, Nester, and Ni, 2017, p. 28). With a lot of hard work and different detector designs based on the compression of a large cylinder, Weber reported having detected gravitational waves in both 1969 and 1970. Even though no attempts to verify his results were successful, this did lead to an increase in interest in gravitational wave detection (Chen, Nester, and Ni, 2017, pp. 29–32).

The first people thought to have come up with the idea to use interferometers for gravitational wave detection were M. Gerstenshtein and V. I. Pustovoit who published about this in 1962. Independently, Weber and his students also considered this idea in 1964. It eventually was Robert Forward who was the first one to build an interferometer to detect gravitational waves. However, this first device was too small to actually perform any detections (Chen, Nester, and Ni, 2017, p. 32).

In 1966, a group of scientists, among who also Forward, started building the first laser interferometer at the Hughes Research Laboratories. In that same year, Weber published an article describing how to improve detectors' sensitivity which would reduce the gap to the expected gravitational wave signals to 6 orders of magnitude (Chen, Nester, and Ni, 2017, p. 29). The first laser interferometer was later finished in 1972 but did not generate any conclusive results (Chen, Nester, and Ni, 2017, pp. 32–33). However, laser interferometer detectors did become the new standard for detection efforts by 1980, and in 1981 the first public proposal for a space-bound interferometer was presented by Faller and Bender (Chen, Nester, and Ni, 2017, p. 35).

All these attempts paved the road for the 'second generation detectors', such as advanced LIGO, advanced Virgo, and KAGRA, to eventually become the first generation of detectors to successfully perform direct detections of gravitational waves (Chen, Nester, and Ni, 2017, p. 36). One of the biggest challenges for these detectors to succeed was to overcome amounts of noise in which the actual gravitational wave signals are hidden.

The four main sources of noise for a laser interferometer to detect gravitational waves are:

- **Shot noise** due to the quantized nature of light. The photodetectors measure the power of a laser signal as the number of incoming photons, which for a large number of N photons behaves according to a Gaussian distribution with a standard deviation of $\sqrt{N}$. This type of noise cannot be eliminated but it can be quantified (Dimastrogiovanni, 2021, pp. 8–10).
- **Radiation pressure** is the pressure extorted by photons upon hitting the detector or mirror. This source of noise is not trivial to balance out since it depends on the intensity of the light and is related to the shot noise (Dimastrogiovanni, 2021, pp. 8–10).
- **Thermic noise** is caused by vibrations in the detector system due to temperature fluctuations, it can be minimised by keeping the temperature as stable as possible (Dimastrogiovanni, 2021, pp. 8–10).
- **Seismic and Newtonian noise** is caused by micro-seismic background, seismic activity, and human activity (Dimastrogiovanni, 2021, pp. 8–10).

These types of noise show that it is not possible to eliminate or quantify all of the noise. The last type of noise is expected to be fully eliminated in the Laser Interferometer Space Antenna (LISA) which is planned to launch before 2035. This detector consisting of three spacecrafts will follow the earth in its orbit around the sun and have arm lengths given by the distance between the spacecrafts of 2.5 million kilometres (Barausse et al., 2020). But even such an advancement in gravitational wave detection will still have to make use of data analysis tools to identify the signal in the detector output which mainly consists of noise.

The detector output is called the "strain" and will have the general form of $s(t) = h(t) + n(t)$ in which $s(t)$ is the strain at moment t in time, and $h(t)$ and $n(t)$ are the gravitational wave signal and noise respectively at that same moment. Intuitively it makes sense to think that the signal

can only be detected when $|h(t)| > |n(t)|$, but that would make detections on Earth, where generally the situation resembles $|h(t)| \ll |n(t)|$, impossible. The method called "matched filtering" offers a solution since that enables us to filter out noise even when it is much stronger than the signal (Maggiore, 2008, p. 343).

A requirement for this technique is to know, at least to some level of accuracy, the form of the signal $h(t)$. Additionally, we must have an idea of the scales of variation of the noise $n(t)$, to be able to exploit the difference in the behaviour of the two. To illustrate the procedure, you can think of matched filtering as in the following example. Suppose that both $s(t)$ and the form of $h(t)$ are known. Multiply these two with each other, integrate over an observation time T, and divide by T. This looks as follows (Maggiore, 2008, p. 343):

$$\frac{1}{T}\int_0^T dt s(t)h(t) = \frac{1}{T}\int_0^T dt h^2(t) + \frac{1}{T}\int_0^T dt n(t)h(t). \tag{2.41}$$

The essential characteristic of $h(t)$ and $n(t)$ is that both are oscillating functions. This makes the first integral on the right hand side definite positive, for instance the integral of $\cos^2 \omega t$ times an amplitude, which is a slowly varying function of time. For large T, the integral will then grow as T, and due to the average over the time, this gives:

$$\frac{1}{T}\int_0^T dt h^2(t) \sim h_0^2, \tag{2.42}$$

where h_0 represents the amplitude of the signal template $h(t)$. Considering that $n(t)$ and $h(t)$ are uncorrelated, their product will oscillate. For large T, the integral of $n(t)h(t)$ will, therefore, grow as $T^{1/2}$, as shown in

$$\frac{1}{T}\int_0^T dt n(t)h(t) \sim \left(\frac{\tau_0}{T}\right)^{1/2} n_0 h_0, \tag{2.43}$$

in which τ_0 is the period of the signal waveform $h(t)$, and n_0 is the amplitude of the noise function $n(t)$ (Maggiore, 2008, p. 343).

For the limit $T \to \infty$, this means that the term with the noise function averages to zero, and the contribution from the noise is "filtered out" of the strain. In practice, the observation time T is limited, and the signal itself has a finite temporal duration. However, this method is successful in reducing the requirement of $h_0 > n_0$ to $h_0 > (\tau_0/T)^{1/2} n_0$ (Maggiore, 2008, p. 344).

This description stresses the importance of constructing possible waveforms for the signals we would like to extract from the detector outputs. The matched filtering procedure can be further improved by, for example, adding a "filter function", comparing signals from different detectors, and applying statistical methods, but the dependency on the template $h(t)$ remains (Maggiore, 2008, pp. 344, 356, 400).

The template waveform is even more complex because it does not just depend on a temporal variable t. Instead, it also depends on a collection of other parameters, just like the actual signal depends on parameters describing the characteristics of the source of the gravitational waves. This collection of parameters, such as the object's masses, the time of coalescence, the luminosity distance, etc., is often denoted by $\theta = \theta_1, ..., \theta_N$ in the "template" waveform $h(t; \theta)$ (Maggiore, 2008, p. 351).

2.5 Analogy with electromagnetic waves

The analogy between gravitational and electromagnetic waves has been very important. Especially before the physical proof of the existence of gravitational waves had been found, this analogy offered a way to describe the gravitational field. The analogy has two purposes: a heuristic one, and to represent a real underlying structural connection. In his book *Traveling at the speed of thought*, Daniel Kennefick associates the two purposes with the 'sceptics' and 'nonsceptics' among the theorists. The sceptics regarded the analogy of gravity with electromagnetism as inappropriate or misleading. They either doubted the existence of gravitational waves altogether or, more commonly, thought that gravitational waves would not be emitted by freely falling gravitational systems, such as binary stars. Even though the sceptics did use the analogy, they were not necessarily committed to making every point of the analogy correspond, thus only using it with a heuristic purpose. The nonsceptics, on the other hand, considered the analogy as a first step towards unifying the two areas of physics. Therefore, they emphasised the points of similarity between the two theories, which enabled them to adopt insights, intuition, and calculation tools from the better understood electromagnetic theory of radiation. Despite this distinction between sceptics and nonsceptics, it is important to emphasise that both used the analogy as a guide. The difference was that the sceptics were looking for a point of breakdown of the analogy, while the nonsceptics were searching for a unified theory in which both gravity and electromagnetism would be brought together (Kennefick, 2017, pp. 7–17).

The similarity between gravity and electromagnetism lies in the description by the Einstein field equations and the Maxwell equations respectively, which can both be used to describe waves. The differences between the theories are that there exist no negative masses, unlike the existence of both positive and negative charges in nature, and that there is no electromagnetic analogue for the conservation of momentum in gravity.

This description of the analogy between gravitational and electromagnetic waves completes this chapter that has introduced some concepts of gravitational waves. The analogy will be used in chapters 8 and 12, where we will study binary systems in electromagnetism.

Part I

Effective Theories

Chapter 3

Effective Theory Basics

There is a risk of presenting effective theories as a new concept or method. However, effective theories have in principle existed for as long as theories have existed. The relatively new part is that we have started to use them more actively. There has been a change of mindset in the understanding and the use of effective theories in a more explicit way.

In this chapter, we will discuss different aspects of the approach, or notion, that we mean when we talk about "effective theories". Starting with a brief overview of the history of the approach. Then continuing with a definition and description of different types of how effective theory approaches are used. When these general defining aspects have been made clear, we look a bit more closely to why and when it is beneficial to use the effective theory approach. There are both advantages and disadvantages to using effective theories, which will both be discussed. That will make clear which situations are most suitable for applying this approach and how they strongly relate to the types of effective theories. The chapter will be concluded with a brief discussion of some more philosophical reflections on the impact of effective theories on scientific progress and reduction.

3.1 History

Effective theories have existed for as long as science has, however, we have only started to give them a name relatively recently. This change arrived around the same time as the understanding that finitely written theories are in principle never complete, and with the development of renormalisation techniques, in the 1970s (Hartmann, 2001, pp. 2–3). James Wells describes, in the preface of his book *Effective Theories in Physics*, the existence of two different, opposing camps. On one side, the physicists who started working on effective theories who were "celebrating their ignorance", and on the other side, the physicists who shared their belief in being close to the 'Theory of Everything' (Wells, 2012, p. v).

The history of a specific kind of effective theories, the effective field theories, started with the reconceptualisation of renormalisation. Stephan Hartmann describes that while many effective

field theories were previously were seen as problematic due to the divergences at higher orders in perturbation expansions, which blocked the road to obtaining finite results from those theories. In the 1970s, however, the cut-off parameter in quantum field theories started to be interpreted in a realistic way, opposed to its previous formalistic way. Together with the insights of renormalisation group theory, this shift in interpretation relaxed the condition of renormalisation for theories and thus paved the way for acceptance of effective field theories (Hartmann, 2001, pp. 2–3).

The start of the introduction of effective theories in gravitational dynamics can be traced back to the middle of the last century, when the Einstein field equations of General Relativity were derived from the assumption of massless spin-2 particles in a flat background (Rothstein, 2014, pp. 1–2). Pioneers in the development of these ideas were (Gupta, 1954), (Kraichnan, 1955), and (Feynman, 1996). The non-geometric, quantum-based approach to General Relativity added the benefit that the machinery developed for quantum field theory could be applied to gravity. Together with the reconceptualisations and change in mindset in quantum field theory research, this led to the first effective theory descriptions of systems governed by gravity, such as the Schwarzschild solution generated by coupling the graviton to a point particle classical source (Duff, 1973). The work of Goldberger and Rothstein in (Goldberger and Rothstein, 2006a) and (Goldberger and Rothstein, 2006b) is often considered to be the first application of the effective field theory approach to the gravitational binary inspiral problem (Porto, 2016, p. 3).

Now, after getting more used to the concept of effective theory, the culture and language of the approach have infiltrated all of physics (Wells, 2012, p. v). As we will see in the definition, types, and motivation of effective theories, there is no way of doing physics, and science in general, without effective theories. This also sheds more light on the comment about how effective theories are not a new concept, it is just the evolution from a passive into an active use of the approach that has changed and helped us further develop theories and methods in physics.

3.2 Definition

The definition of an 'effective theory' is essentially just the combination of the definitions of 'effective' and 'theory'. Wells sums it up as follows:

> "Effective Theories" are theories because they can organise phenomena under an efficient set of principles, and they are effective because it is not impossibly complex to compute outcomes. The only way a theory can be effective is if it is manifestly incomplete. "Everything affects anything" is generally correct, but it saps confidence in our ability to predict outcomes. Effective Theories modify this depressing maxim

> by pointing out that "most things are irrelevant for practical purposes. (Wells, 2012, p. 1)

This description suggests that all theories that are not infinite are effective, and you can wonder what the added value of the term 'effective theory' thus is. There are two important reasons for the explicit emphasis that comes with the use of the term. The first concerns the historical awareness, it is an important reminder that we have not always been convinced of the fact that most theories are incomplete. It provides a good nuance for the belief that theories are either correct or useless because it adds the option that theories are "correct enough for our purposes in [a given] domain". And the second reason for the use of the term 'effective theory' has a more heuristic purpose, to refer to the new approach to theory development. This approach acknowledges the theory's incompleteness and domain of applicability. When the domain of applicability is well known, the uncertainties of the theory can be parametrically assessed (Wells, 2012, p. 1).

3.3 Types

Since the definition of effective theories is still broad and includes all finite theories, it is no surprise that there are different types of effective theories to be distinguished. A specific type that is often used is the group of 'effective field theories' which are effective theories used in field theories. However, as we will later find by an example of an effective theory in part III of this project, there are other effective approaches that are hard to classify. Therefore we will consider a distinction between types of effective theories based on the relation between the effective theory with another theory or other theories. This classification results in the notions of 'top-down' and 'bottom-up' types of effective theories. In the top-down approach, the higher-energy theory is understood, but for practical purposes, it is useful to have a simpler theory for the lower energies. The bottom-up approach is used when the underlying more fundamental theory is unknown, or when matching the theories turns out to be too difficult to carry out (Stewart, 2013).

Roberto Emparan makes the same distinction but phrases it differently. According to him, effective theories can be used either as "a scheme to systematically parametrize our ignorance about short-distance dynamics", or as "an approach to simplify the long-distance physics of a known complex theory" (Emparan, 2020). These uses correspond to the bottom-up and top-down approaches respectively.

3.4 Motivation

The motivation for using effective theories can already be recognised in the different ways in which effective theories are used. However, in this section, we will state more explicitly what

the disadvantages and advantages of the effective theory approach are. Doing so will also provide a better understanding of the situations in which effective theories can be helpful.

The most important disadvantage to using an effective theory is that it does not provide the underlying fundamental principles which govern the system. Therefore, before the effective theory approach was accepted as a valuable tool in physics, theories that would have fit into the effective theory mindset were dismissed based on their lack of logic and reasoning. We will see an example of the dismissal of such a theory in the next chapter (Wells, 2011).

Another related disadvantage is that we might prefer a theoretical description that applies to the largest range of scales (Porto, 2016, p. 1). The basis of this preference is that we believe that all phenomena should be possible to be reduced to a set of universal laws, and having different theories for different scales does not fit this belief. A compromise on this point is to have different theories which can be shown to reduce to the same principles in their appropriate limits, such as how the classical limit of quantum mechanics relates to the theory of classical mechanics.

In return for giving up the more fundamental explanation and applicability to all scales in effective theories, we get some nice things back. The most important one is that effective theories simplify the computations compared to most more fundamental theories (Porto, 2016, p. 2). This advantage is directly related to the type of use of effective theories that simplifies a known more fundamental theory.

The other important advantage of effective theories is related to the other type of their use, the parametrization of our ignorance, which is the case where we do not know what the more fundamental theory is. By using an effective theory, we can improve our understanding of the limits of the known theory and quantitatively predict for which parameters and scales we expect to require a new description of phenomena. This advantage will also be further elaborated on in the case discussed in the next chapter (Wells, 2011).

3.5 Impact on theory development

The relatively new mindset of effective theories and its effect on how we see and do physics ought to also affect the theory of science that describes theory development in physics. Although this is a bit of a different project on its own, it is interesting to discuss some of these considerations very briefly. Starting with two views on scientific progress described by Kuhn and Feyerabend, which have one aspect in common: 'incommensurability'. It is followed by a discussion of the concept of 'reduction'. As we will see, there are some trends in these two stories that could be related to effective theories.

3.5.1 Scientific progress

There is a very well-known theory of science described by Thomas Kuhn. He puts a lot of emphasis on the revolutionary character of science. The revolutions as described by Kuhn are characterised by replacing one theoretical structure with another theoretical structure, where both structures are 'incommensurable' with each other (Chalmers, 1999, pp. 132, 142). 'Incommensurability' typically means "to have no common measure" and is used by Kuhn "to characterize the holistic nature of the changes that take place in a scientific revolution" (Oberheim and Hoyningen-Huene, 2018).

In 1962, Kuhn published his book *The structure of scientific revolutions* (Kuhn, 1962) introducing his theory about scientific progress in which sociological characteristics play an important role (Chalmers, 1999, p. 133). In that same year, Paul Feyerabend first used the term 'incommensurable' in his article 'Explanation, Reduction, and Empiricism' (Feyerabend, 1962) by which he meant that two incommensurable fundamental theories were conceptually incompatible (Oberheim and Hoyningen-Huene, 2018). "The main concepts of one could neither be defined based on the primitive descriptive terms of the other nor related to them via a correct empirical statement" (Feyerabend, 1962, p. 74). As an example, Feyerabend claims that the concepts of mass, length and time have a different meaning in Newtonian mechanics compared to those same concepts in relativistic mechanics (Oberheim and Hoyningen-Huene, 2018).

Both authors include a certain discontinuous aspect of scientific progress, in which theories are in some way incompatible. However, based on the development of physics of the past decades, we might consider changing this view. Even though concepts are in some cases still different in their meaning depending on the theory in which they occur, as the examples for Newtonian and relativistic mechanics, more attention started to be paid to describing these differences. The more detailed description of the relation between theories, indicated by a more precise requirement of being able to reduce one theory to another, does not remove the conceptual incompatibilities but does introduce a common measure to describe the theories. This can be seen as related to the mindset that is also behind the use of effective theories as we will discuss below.

3.5.2 Reduction

A term often used in describing the relationship between different (part of) theories is 'reduction'. Despite its prevalent uses, it lacks a clear definition and is not used consistently. This is already unmistakable from the between the philosophers' convention and the physicists' convention of defining reduction. Typically when philosophers say that theory A can be reduced to theory B, physicists will state exactly the opposite, thus that theory B can be reduced to theory A (Crowther, 2018, p. 1441). Despite these ambiguities in the definition of the 'direction' of

reduction, there are also other ways in which it is hard to use the word 'reduction' without the possibility of going into a discussion of what is precisely meant by the term.

Different types of reduction are defined to distinguish between different uses of the notion. To give some examples, we first discuss the distinction described by William Wimsatt (Wimsatt, 1976) between 'explanatory' reduction and 'successive' reduction. The first is an inter-level relation representing the relation between different levels of explanation rather than different theories. An example of this type of reduction is the explanation of the behaviour of a gas in terms of a could of colliding molecules. This is different from 'successive' reduction, which is an intra-level relation common in mathematically expressed theories that are either on the same level of composition or not level-specific. The reduction relation localises similarities and differences between theories through mathematical transformations. This form of reduction includes the example of special relativity reducing to classical mechanics in taking the limit $\frac{v}{c} \to 0$ (Wimsatt, 2006, pp. 450–451).

Another definition of types of reduction is described by Karen Crowther (Crowther, 2018) and distinguishes 'weak' and 'strong' reduction. Weak reduction holds in the cases where the successful results from one theory can be obtained, within an acceptable degree of error, in the other theory. The strong conception of reduction requires that the successful parts of one theory can be derived or deduced in principle from the other theory (Crowther, 2018, p. 1443).

In general, successive reduction and strong reduction are the stricter types of reduction and are also the types of reduction that are often desired in contemporary physics. This fits the view that "everything depends on everything else" that is also on the fundamental basis of effective theories because the success of theories is often determined based on their 'fit' to other successful theories. For example, candidates for a theory of quantum gravity have to satisfy certain conditions in their relation to General Relativity and quantum field theory. Whether these relations are relations of reduction, and what type of reduction is desired depends on the research programme.

Chapter 4

Case: Mercury's Perihelion Precession

In one of the chapters of his book, *Effective Theories in Physics*, James Wells describes an alternative history to the discovery of the perihelion precession of Mercury (Wells, 2012, Chapter 3). This is a simple example of how a bottom-up approach of an effective theory could be used to make new predictions. The author argues that the effective theory mindset could have predicted the perihelion precession, which is shown in figure 4.1, before it was discovered by LeVerrier in 1845.

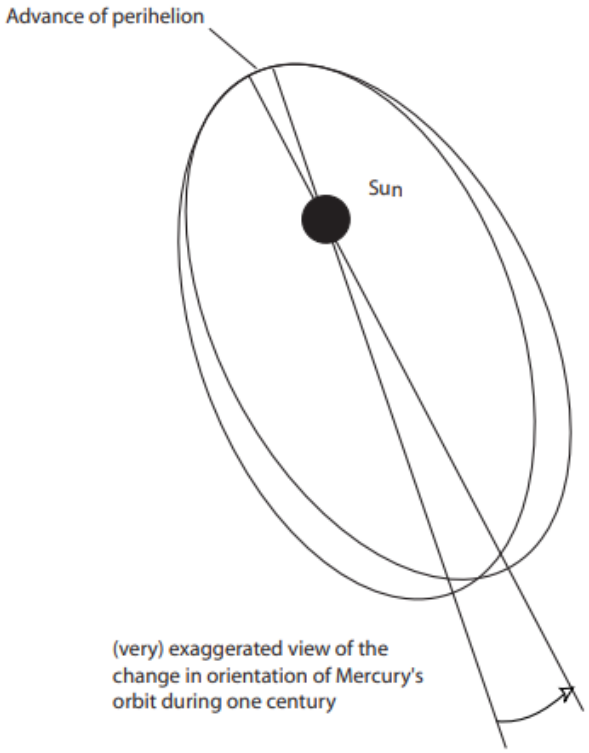

FIGURE 4.1: Every revolution the perihelion of Mercury's orbit advances a little bit. This effect, which is called the 'precession of the perihelion' is explained by the theory of General Relativity (Magnan, 2007, p. 11).

The theory under consideration is Newton's law of gravity for a system of a test particle moving in the gravitational field of another object with a much larger mass. We can assume that the relative velocity between the two bodies is small relative to the speed of light, and therefore neglect special relativistic effects. This system describes the orbit of Mercury around the Sun and is described by the Lagrangian

$$L = \frac{1}{2}m\boldsymbol{v}_r^2 + \frac{\alpha}{r} \tag{4.1}$$

in which m is the mass of a test particle orbiting a particle of mass $M \gg m$, and $\alpha = GMm$ with G being Newton's constant (Wells, 2012, p. 17).

Due to the rotational invariance of the system, we can express the equations of motion in polar coordinates.

$$m(\ddot{r} - rv_\phi) = -\frac{\alpha}{r^2} \qquad \text{(radial equation)} \tag{4.2}$$

$$m(2v_r v_\phi + r\ddot{\phi}) = \frac{d}{dt}(mr^2 v_\phi) = 0 \qquad \text{(angular equation)} \tag{4.3}$$

The solution to the radial equation is given by a harmonic oscillator equation ($r \equiv \frac{1}{u}$):

$$u(\phi) = u_0 \cos\phi + \frac{\alpha m}{l^2} \tag{4.4}$$

$$r(\phi) = \frac{\rho}{1 + e\cos\phi} \tag{4.5}$$

in which u_0 is a constant determined by the initial conditions, $\rho = \frac{l^2}{\alpha m}$, and $e = u_0\rho$ is the eccentricity. For our case we focus on $0 \leq e < 1$ corresponding to circular and elliptical orbits (Wells, 2012, pp. 17–18).

This shows that Newton's theory of gravity does not allow any advancement of the perihelion. The minimum where $\frac{du}{d\phi} = 0$ occurs for $\sin\phi = 0$ and therefore the successive perihelions start at $\phi = 0, 2\pi, 4\pi, ...$ (Wells, 2012, p. 20). Therefore the situation shown in figure 4.1 does not apply to the situation described by Newtonian gravity.

4.1 Symmetries

The symmetries of this system can be seen from considering some characteristics on the closest and furthest points of the orbits, called the perigee and apogee respectively. At those points the radius vector $\hat{\boldsymbol{r}}$, angular vector $\hat{\phi}$, and angular momentum vector $\boldsymbol{L} = \boldsymbol{r} \times \boldsymbol{p} = mr^2\boldsymbol{v}_\phi$ are perpendicular to each other. Since we also know that angular momentum and $mr^2 v_\phi$ are conserved, we can conclude that $l = mr^2 v_\phi$ on all points of the orbit. This proves, among other things, that the motion is in a plane (Wells, 2012, p. 17).

The existence of an additional conserved vector can be derived by first taking the cross product of $\frac{d\boldsymbol{p}}{dt}$ with $\boldsymbol{L}$:

$$\frac{d\boldsymbol{p}}{dt} \times \boldsymbol{L} = \frac{mk}{r^3}[\boldsymbol{r} \times (\boldsymbol{r} \times \boldsymbol{v}_r)] = \frac{mk}{r^3}[\boldsymbol{r}(\boldsymbol{r} \cdot \boldsymbol{v}_r - r^2\boldsymbol{v}_r]. \tag{4.6}$$

Where $\frac{d\boldsymbol{p}}{dt} = \frac{\boldsymbol{r}}{r^3}$ has been given by Newton's second law, and Laplace's identity was used. Noting that

$$\boldsymbol{r} \cdot \boldsymbol{v}_r = \frac{1}{2}\frac{d}{dt}(\boldsymbol{r} \cdot \boldsymbol{r}) = rv_r \tag{4.7}$$

and using that $\boldsymbol{L}$ is constant, you can rewrite this into

$$\frac{d}{dt}(\boldsymbol{p} \times \boldsymbol{L}) = \frac{d}{dt}\left(\frac{mk\boldsymbol{r}}{r}\right). \tag{4.8}$$

This implies that there is a constant vector

$$\boldsymbol{A} = \boldsymbol{p} \times \boldsymbol{L} - mk\frac{\boldsymbol{r}}{r} \tag{4.9}$$

which is called the Laplace-Runge-Lenz vector and its conservation implies the hidden symmetry in closed Kepler-orbits (Goldstein, Poole, and Safko, 2002, p. 103).

4.2 Effective potential

We can rewrite the description of this system into a one-dimensional Hamiltonian description in which the orbit is considered from the perspective of the radial effective potential.

First expand $\boldsymbol{v}_r$ into radial and angular coordinates, where you can take $\sin\theta = 1$ for the fixed orbital plane. This gives

$$\boldsymbol{v}_r^2 = v_r^2 + r^2\sin^2\theta v_\phi^2 + r^2 v_\theta^2 = v_r^2 + r^2 v_\phi^2 \tag{4.10}$$

The Hamiltonan is then constructed from

$$H = \sum_i v_i p_i - L \tag{4.11}$$

in which the factors p_i are given by

$$p_r = \frac{\partial L}{\partial v_r} = mv_r, \text{ and } p_\phi = \frac{\partial L}{\partial v_\phi} = mr^2 v_\phi \tag{4.12}$$

for the radial and angular momentum respectively (Wells, 2012, p. 19).

This implies

$$H = \frac{1}{2}mv_r^2 + \frac{1}{2}mr^2v_\phi^2 - \frac{\alpha}{r} \tag{4.13}$$

where we can see that it is independent of the angle ϕ. Using one of Hamilton's equations, we thus can deduce that p_ϕ is a conserved quantity

$$\frac{dp_\phi}{dt} = \frac{\partial H}{\partial \phi} = 0 \tag{4.14}$$

This is another way to see that the angular momentum of the system is conserved because

$$l = p_\phi = mr^2 v_\phi \tag{4.15}$$

Substituting this back into the Hamiltonian yields

$$H = \frac{p_r^2}{2m} + V_{eff}(r), \tag{4.16}$$

where

$$V_{eff}(r) = \frac{l^2}{2mr^2} - \frac{\alpha}{r} \tag{4.17}$$

in which the first term of the effective (radial) potential pushes the particle away, and the second term attracts the particle to the origin (Wells, 2012, pp. 19–20).

4.3 Effective theory corrections

The symmetries in Newton's theory of gravitation tell us that the effective theory must be invariant with respect to any transformation of rotation, spatial translation, and time translation, together referred to as Galilean invariance. For Newton's theory, introducing all terms consistent with these symmetries gives

$$V_{ET}(r) = \frac{GMm}{r}\left[1 + \sum_{n=1}^{\infty} \lambda_n \left(\frac{r_0}{r}\right)^n\right] + ... \tag{4.18}$$

where r_0 is some dimensionful effective theory length scale and λ_n are dimensionless coefficients, which together with r_0 can be found by performing precise experiments. There are an infinite variety of other terms that could be added, including r^j and v_r^k interactions, but we streamline the argument by looking only at one class of corrections that decouple as $r \to \infty$ (Wells, 2012, p. 29).

From this, we can deduce that any deviation from the pure inverse square law will lead to a perihelion precession of planets. We also know that Newton's law is approximately correct and thus we should add terms that decouple as $r \gg r_0$. Our expectation, based on the small precession of Mercury, is that r_0 should be much less than the orbital radius of Mercury around the sun (Wells, 2012, p. 29).

Following Wells, we will discuss the two first terms, with $n = 1$ and $n = 2$. First by considering the new dynamics of the system, then by calculating the specific length scale of the term, and then by showing how the term can be derived from General Relativity.

4.3.1 First correction, $n = 1$

The first correction term adds a $\frac{1}{r^2}$-correction to the potential, this changes the Lagrangian into

$$L_1 = \frac{1}{2}m\boldsymbol{v}_r^2 + \frac{\alpha}{r}\left(1 + \frac{R_1}{r}\right) \tag{4.19}$$

where R_1 will be fixed later, it represents the new fundamental length scale, corresponding to the cut-off scale of the effective theory. The solution to the radial equation of motion of this theory is given by

$$u(\phi) = \left(\frac{1}{\rho - 2R_1}\right)\left[e\cos\left(\phi\sqrt{1 - \frac{2R_1}{\rho}}\right) + 1\right] \tag{4.20}$$

where $e = u_0(\rho - 2R_1)$. This time, calculating the minimum from $\frac{du}{d\phi} = 0$, we find that the successive perihelion shifts start at $\phi\sqrt{1 - \frac{2R_1}{\rho}} = 0, 2\pi, 4\pi, ...$ Assuming that $\frac{2R_1}{\rho}$ is small we can thus derive that the ellipse now has a small perihelion advance given by (Wells, 2012, pp. 20–21):

$$\delta = 2\pi\frac{R_1}{\rho}. \tag{4.21}$$

When the perihelion advance is measured, you can use it to calculate the value for the length scale R_1. Or, when you have a theory for what the length scale is, you can make a prediction for the perihelion advance in units of arc seconds per century. The relation between the length scale and the perihelion advance is expressed by the relation (Wells, 2012, p. 22):

$$\frac{\delta}{T_{orbit}} = \frac{2\pi R_1}{\rho T_{orbit}} = (0.866 \text{ arcsec} \cdot \text{century}^{-1})\left(\frac{1 \text{ au}}{\rho}\right)\left(\frac{\text{years}}{T_{orbit}}\right)\left(\frac{R}{1 \text{ km}}\right)\text{''}. \tag{4.22}$$

The length scale R_1 can be expressed as a multiple value of some invariants of the system: $R_1 = \lambda_1 R$, where $R \equiv \frac{GM}{c^2}$. Fitting the data clarifies that $\lambda_1 = 3$, yielding a new theory of gravity

$$L_1 = \frac{1}{2}m\boldsymbol{v}_r^2 + \frac{GMm}{r}\left(1 + 3\frac{GM/c^2}{r}\right) \tag{4.23}$$

This lagrangian looks "natural" given that there are no really big or really small numbers. Furthermore, it provides the information that the "natural" next known threshold of speed is the speed of light (Wells, 2012, p. 32).

A problem in this theory is that if $\rho < 2R_1 = \frac{6GM}{c^2}$, the orbits do not make sense anymore, as the equations formally say $r < 0$ which is nonsensical. Since for the situation of orbits around

the Sun this radius is only 9 km, which is below the radius of the Sun (7×10^5 km), there is no danger that some small object rotating around the sun would have no chance to be described by this theory. Nevertheless, it is a bit uncomfortable because it means that you can imagine a configuration in which this theory cannot provide a description (Wells, 2012, p. 33). The limitation in the range of validity of the description is a fundamental characteristic of effective theories, we will see and discuss this also in later chapters.

The effective theory including the first correction term has been discussed as a bottom-up type of effective theory, without referring to a more fundamental theory. Even though the effective theory is valid without relating it to the higher energy theory, we will now briefly discuss how the same effective theory can be constructed in a top-down way, deriving it from the theory of General Relativity. We start by looking at the Schwarzschild metric given by

$$ds^2 = \left(1 - \frac{r_g}{r}\right) c^2 dt^2 - \frac{dr^2}{\left(1 - \frac{r_g}{r}\right)} - r^2 \left(\sin^2\theta d\phi^2 + d\theta^2\right) \tag{4.24}$$

in which $r_g = \frac{2GM}{c^2}$ is the gravitational radius of the Sun with G Newton's constant and M the mass of the Sun, and r, θ, and ϕ are spherical coordinates in their normal use (Landau et al., 1971, p. 284).

We can plug this metric into the Hamilton-Jacobi equation,

$$g^{\mu\nu} \frac{\partial S}{\partial x^\mu} \frac{\partial S}{\partial x^\nu} - m^2 c^2 = 0, \tag{4.25}$$

which gives

$$\left(1 - \frac{r_g}{r}\right)^{-1} \left(\frac{\partial S}{c \partial t}\right)^2 - \left(1 - \frac{r_g}{r}\right) \left(\frac{\partial S}{\partial r}\right)^2 - \frac{1}{r^2} \left(\frac{\partial S}{\partial \phi}\right)^2 - m^2 c^c = 0 \tag{4.26}$$

applying the approximations $r(r - r_g) = r'^2$ and $r - \frac{r_g}{2} \approx r'$, and expanding some terms in powers of $\frac{r_g}{r'}$, we can solve for S_r which yields

$$S_{r'} = \int \left[\left(2E'm + \frac{E'^2}{c^2}\right) + \frac{1}{r'}(2m^2 MG + 4E'mr_g) - \frac{1}{r'^2}\left(l^2 - \frac{3m^2 c^2 r_g^2}{2}\right)\right]^{\frac{1}{2}} dr' \tag{4.27}$$

in which E' is the non-relativistic energy without the rest energy, M the mass of the Sun, m the mass of Mercury, and l angular momentum (Landau et al., 1971, pp. 287–288).

The last term is proportional to $\frac{G^2 M^2/c^2}{r^2}$ and thus is the first correction term that we found in our effective theory.

4.3.2 Second correction, $n = 2$

We can do the same for the second correction term, which adds a $\frac{1}{r^3}$-correction to the potential

$$L_2 = \frac{1}{2}m\boldsymbol{v}_r^2 + \frac{\alpha}{r}\left(1 + \frac{R_2^2}{r^2}\right) \tag{4.28}$$

in which R_2 is a new fundamental length scale. Because this theory is different from the one with the first correction, we also have a different cut-off scale, meaning that R_1 from the previous section is not equal to R_2 and we need to determine the value of the new fundamental length scale for this effective theory separately. The changed radial equation of motion can be solved using perturbation theory. Treat the last term in the following equation as a small perturbation, then the solution to the unperturbed equation will be the standard Newtonian orbit solution

$$\frac{d^2u}{d\phi^2} + u = \frac{\alpha m}{l^2}\left(1 + 3R_2^2u^2\right) \tag{4.29}$$

$$u_N(\phi) = \frac{1}{\rho}(1 + e\cos\phi) \tag{4.30}$$

where $e = u_0\rho$. Substitute $u \to u_N(\phi) + \delta u$ into the differential equation and keep one order in perturbation theory. Then solve for δu to obtain the complete solution

$$\delta u = \frac{3}{\rho^3}R_2^2\left(1 + e\phi\sin\phi + \frac{e^2}{3}\cos 2\phi + e^2\sin^2\phi\right) \tag{4.31}$$

Solving for δ in the perturbation expansion results in a perihelion advance of

$$\delta = 6\pi\frac{R_2^2}{\rho^2} \tag{4.32}$$

Yielding a value for the new length scale and a prediction for the perihelion advance:

$$\frac{\delta}{T_{orbit}} = \frac{6\pi R_2^2}{\rho^2 T_{orbit}} = (1.74\ \text{arcsec}\cdot\text{century}^{-1})\left(\frac{R}{10^7\ \text{meters}}\right)^2\left(\frac{1\ \text{au}}{\rho}\right)^2\left(\frac{\text{years}}{T_{orbit}}\right) \tag{4.33}$$

(Wells, 2012, pp. 22–24).

This time, the value for R_2 depends the planet for which you are considering the theory, it is proportional to the angular momentum divided by the mass of the planet, $R_2^i \propto \frac{l_i}{m_i}$. Where the proportionality constant given by the inverse of the speed of light (Wells, 2012, p. 34).

This theory thus has the same fundamental speed threshold as the previous one, and the theory is now given by

$$L_2 = \frac{1}{2}m\boldsymbol{v}_r^2 + \frac{GMm}{r}\left(1 + \frac{1}{c^2}\frac{l^2/m^2}{r^2}\right) \tag{4.34}$$

Reflecting on this theory and noting that angular momentum is $l \sim mrv$, where v is the velocity of the planet orbiting the sun, the second term inside the parenthesis can be thought of as an m-independent $\frac{v^2}{c^2}$ correction to the Newtonian gravitational potential. As the speed of the planet gets closer to the speed of light, Newton's theory begins to crack. So far the basic assumptions of spacetime, symmetries are not breaking down, just the simple form of Newton's theory of gravity (Wells, 2012, p. 34).

We can also derive this theory from the theory of General Relativity. Starting from the trajectory of a particle subject to a central, radially symmetric gravitating source in General Relativity, we use the Schwarzschild metric. The Schwarzschild metric is unperturbed by making shifts in the time direction and by making shifts in the angular direction ϕ. These define Killing vectors $\xi^\lambda_{time} = (1, 0, 0, 0)$ and $\xi^\lambda_{rot} = (0, 0, 0, 1)$, which, when dotted into the four-velocity vector $\frac{dx^\alpha}{d\tau}$, the result must be constant along the geodesic motion:

$$\xi^\lambda \frac{dx_\lambda}{d\tau} = g_{\alpha\beta}\xi^\alpha \frac{dx^\beta}{d\tau} = \text{constant} \tag{4.35}$$

Applied to the Schwarzschild metric, this gives:

$$g_{\alpha\beta}\xi^\alpha_{time}\frac{dx^\beta}{d\tau} = \eta(r)\frac{dt}{d\tau} = c_1 \tag{4.36}$$

$$g_{\alpha\beta}\xi^\alpha_{rot}\frac{dx^\beta}{d\tau} = r^2 \sin^2\theta \frac{d\phi}{d\tau} = c_2, \tag{4.37}$$

in which $\eta(r) \equiv 1 - \frac{r_g}{r}$ is the Schwarzschild factor. We know that the independence of time implies conservation of energy, and the independence of rotation implies conservation of angular momentum. Thus, c_1 is some function of energy, and c_2 is some function of angular momentum (Wells, 2012, pp. 37–38).

Solve for $\frac{dt}{d\tau} = \frac{c_1}{\eta(r)}$ and $\frac{d\phi}{d\tau} = \frac{c_2}{r^2 \sin^2\theta}$. Simplify by taking the orbit in the $\theta = \frac{\pi}{2}$ plane. Note that conservation laws have given us this, and this is where deep physics lies. Expand out the defining equation for the four-velocity, substitute values for the Killing equations, and doing some algebra and rewriting with some substitutions, we find:

$$E = \frac{1}{2}m\left(\frac{dr}{dt}\right)^2 + \frac{l^2}{2mr^2} - \frac{GMm}{r}\left(1 + \frac{l^2/m^2c^2}{r^2}\right) \tag{4.38}$$

This is the energy equation for a particle in Newtonian gravity except for the small shift in the effective potential

$$\Delta V_{eff}(r) = -\frac{GMm}{r}\left(\frac{l^2/m^2c^2}{r^2}\right) \tag{4.39}$$

which is the same correction to Newton's theory as we derived for the second correction term of the effective theory (Wells, 2012, pp. 38–39).

Chapter 5

Discussion of Part I

In this part, we have seen how 'effective theories' are really about a certain mindset. It is a broad category of theories but what they all have in common is that they provide a comprehensive manner to organise phenomena under an efficient set of principles. The difference with non-effective theories is that effective theories do not aim to generate descriptions that include all details and interactions, instead, they focus on the practical purposes of the theory. These practical purposes should then be restricted to a certain domain or region on which the effective theory is defined.

The concept of effective theories is not new in itself, but the awareness and mindful application of them is. Therefore, the use of the term 'effective theory' serves as a reminder of the shift in mindset that occurred around the 1970s which made the use of effective theories more acceptable, and it serves as a new heuristic approach to exploring new phenomena and testing theories on a specified domain.

The two main types in which effective theories are used are referred to as 'top-down' and 'bottom-up', corresponding to simplifying a known theory for use on the long-range and parametrizing the ignorance of short-range dynamics respectively. Therefore, the use and type of an effective theory are significantly determined by its relation to other known theories.

In an effective theory, one has to compromise on the fundamental descriptions and the range of applicability. But simplified computations and describing systems for which the fundamental descriptions are not available are two important qualities that compensate for those disadvantages.

Even though the discussion about the relationship between effective theories and the development of physics that was provided here is nowhere near complete, some trends are can be identified and reflected upon in the development in physics of the past decades. Depending on your exact definitions of concepts involved, the relatively recent revolutions in physics are less characterised by the incommensurability of different theories compared to scientific revolutions from centuries ago on which many theories of science are based. Nowadays, physicists

are interested in quantifying the differences between theories by writing them in terms of effective theories, thus overcoming, or at least describing the incompatibilities between theories. Furthermore, there is a shift towards requiring more strict types of reduction between theories, fuelled by an understanding of how theories in different ranges of validity can be connected. More often than in the past, instead of rejecting a theory in favour of a more successful theory, physicists aim to describe the domain on which the theory can make accurate predictions.

The case that was studied in this part, about the perihelion precession of Mercury, showed that there are multiple ways to derive the effective theory predicting the phenomenon. The difference between the different effective theories is due to different corrections to Newton's gravity law. We have seen that both the first and second correction terms can reproduce the correct predictions and they can both be derived from the theory of General Relativity. The two theories based on the different correction terms are not equivalent though. They yield equivalent results for this problem as all approximations and computations of the coupling terms have been carried out with the sole purpose of finding perihelion precession. In the end, the precession rate angle per orbit period from either correction is the same:

$$\delta = \frac{6\pi GM/c^2}{a(1-e^2)} \tag{5.1}$$

Algebraically, the orbital identity $l^2 = GMm^2a(1-e^2)$ is what guarantees that the two solutions predict the same anomalous perihelion precession rate (Wells, 2012, p. 39).

An important point that Wells puts forward, is that the understanding of the concept of effective theories could have lead to an earlier discovery of the anomalous perihelion precession of Mercury. And even after the measured advancement of the perihelion, a lot of theories were dismissed because they did not provide a fundamental explanation but only gave a description of the phenomena. These theories were rejected at the time, while they were accurate effective theories (Wells, 2012, p. 35). This case, therefore, supports the argument made in the effective theory chapter that an understanding of effective theories can lead to new predictions and possibly the discovery of new physics.

Part II

Effective Field Theory Approach

Chapter 6

Effective Field Theory Basics

In section 2.4.2, we saw that in order to detect a gravitational wave, given the noise that the detectors deal with, a suitable template for the signal is required. The sensitivity of current and planned gravitational wave detectors is highest for inspiralling compact binaries containing neutron stars and/or black holes. A useful characteristic of such systems is that the orbit of the objects can be considered to be circular after the gradual inspiral because the gravitational radiation reaction forces are responsible for a rapid decrease towards zero of the eccentricity (Peters and Mathews, 1963). Therefore, only non-isolated systems will have a non-negligible eccentricity (Blanchet, 2016, p. 12).

Furthermore, in the first approximation, the objects in the system can be considered to be structureless. This means that, for example, their magnetic properties and internal structure can be neglected, and only their masses and spins need to be taken into account (Blanchet, 2016, pp. 12–13).

One of the requirements for using an effective field theory (EFT) is that there is a separation of scales. The dynamics of the binary problem can be separated into the following zones (Porto, 2016, p. 25), which are also depicted in figure 6.1:

- **Internal zone:** the scale of finite-size effects. For compact neutron stars or black holes we have $R_s \simeq 2G_N m$;
- **Near (or potential) zone:** the intermediate region, or orbit scale, given by the typical separation between the objects of the binary, r;
- **Far (or radiation) zone:** the scale of (gravitational) waves emitted with a typical wavelength $\lambda_{rad} \sim r/v$.

The hierarchy among these scales can be justified by looking at the virial theorem given by

$$v^2 \simeq \frac{GM}{r}, \tag{6.1}$$

which is equivalent on circular orbits to Kepler's law

$$\omega^2 \simeq \frac{GM}{r^3}. \tag{6.2}$$

These expressions are exact at the Newtonian level, but not in General Relativity. For the hierarchy of scales this results in $R_s < r \sim \frac{R_s}{v^2} < \lambda \sim \frac{r}{v}$, where for the gravitational wave-length the relation $v = \omega r$ was used (Sturani, 2014, pp. 8–9).

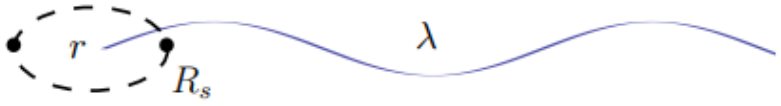

FIGURE 6.1: Schematic description of an inspiralling compact binary where the relevant length scales are shown (Cannella, 2011, p. 48).

After discussing more the different types of approximations, which are together collected under the term 'post-Newtonian' approximations, we will continue by setting up an introduction to the systematic effective field theory approach. The first situation in which we will do this is an effective scalar field theory. Then we apply the same approach to a vector-theory, Maxwell's electromagnetism, to then get to the gravitational situation with all of its extra challenges and complications.

6.1 Post-Newtonian approach

To define and keep track of the order of approximations, we talk about the "post-Newtonian" (PN) orders of approximation. This is an expansion in $1/c^2$ which means that 0PN order corresponds to $\mathcal{O}(\left(\frac{1}{c^2}\right)^0)$, 1PN order corresponds to $\mathcal{O}(\left(\frac{1}{c^2}\right)^1)$, and so forth. The expansion does not have to be explicitly around a parameter containing $1/c^2$, because expansions in other parameters can also result in post-Newtonian terms.

There are several different approximations connected to corresponding expansion parameters that can be used to determine the terms in the post-Newtonian expansion of General Relativity. The most used ones are the following (Blanchet, 2016, p. 5):

- **Post-Newtonian** method is a non-linear expansion in $1/c$, with c the speed of light. The post-Newtonian expansion is therefore both the encompassing scheme in which expansions in different parameters are ordered, as well as an expansion in a parameter, $1/c$, itself.
- **Post-Minkowskian** method is a non-linear expansion in the Newtonian constant, G.
- **Multipole decomposition** is an expansion in the source radius.

- **Far-zone expansion** is an expansion in $1/R$, with R the radial separation between the objects.
- **Perturbation in the small mass limit** is an expansion in the mass ratio, ν, of a binary system.

Since the orbital and wave frequencies of the gravitational binary system vary quicker towards the later stages of the merger, the assumption of slow variation is violated. To handle the time-varying frequency, the $\cos(2\omega(t)t)$ factor in the interferometer signal $h(t)$ can be replaced with $\cos(2\Phi(t))$, where

$$\Phi(t) = 2\int_{t_i}^{t} \omega(t')dt' \tag{6.3}$$

is the integrated phase of the orbital motion, in which ω is the orbital angular velocity of the individual binary component, and t_i indicates the time at which the signal enters the detector's band-with (Hilborn, 2018, p. 36)(Sturani, 2014, pp. 7–8). The laser interferometer detectors discussed in section 2.4.2 are particularly sensitive to this factor in the gravitational wave signal.

To calculate this phase, we can consider two quantities: the energy E, and the radiated flux $\mathcal{F}$. They are related by the equation

$$\frac{dE}{dt} = -\mathcal{F}, \tag{6.4}$$

and can both be expressed in terms of a single parameter, which is the relative velocity of the binary system, v. The energy of a circular orbit can be expressed as

$$E(v) = -\frac{1}{2}\frac{Gm_1m_2}{r}(1 + c_{1PN}(\nu)v^2 + c_{2PN}(\nu)v^4 + \cdots), \tag{6.5}$$

in which $\nu \equiv m_1m_2/M^2$ is the symmetric mass ratio, with $M \equiv m_1 + m_2$ the total mass, and $c_{nPN}(\nu)$ the coefficients that stand for the corrections to the Newtonian case. Note that only the even powers in v are involved in the conservative energy. The leading term of the radiated flux $\mathcal{F}(v)$ is the Einstein quadrupole formula, and for circular orbits it is given by the following expansion:

$$\mathcal{F}(v) = \frac{32\nu^2}{5G}v^{10}(1 + d_{1PN}(\nu)v^2 + d_{1.5PN}(\nu)v^3 + \cdots). \tag{6.6}$$

Using the relation $v = \omega r$ together with the virial theorem $v^2 \simeq \frac{GM}{r}$, we can use

$$\omega \simeq \frac{1}{GM}v^3 \tag{6.7}$$

to rewrite the gravitational phase:

$$\Phi(v) \simeq \frac{2}{GM}\int_{v_i}^{v} v^3\frac{dE/dv}{-\mathcal{F}}dt = \frac{5}{16\nu}\int_{v_i}^{v}\frac{1}{v^6}(1 + f_{1PN}v^2 + f_{1.5PN}v^3 + \cdots)dv. \tag{6.8}$$

The precision of the detection of the phase is of order $\mathcal{O}(1)$, thus we need to consider the energy and radiation flux at least to $\mathcal{O}(v^6)$, which corresponds to the third post-Newtonian order (Sturani, 2014, p. 8) (Blanchet, 2016, p. 13).

Chapter 7

Case: Effective Scalar Field Theory

Building on the field theory formalism introduced in section 2.2.4, we can describe one of the methods to expand the theory of General Relativity. The analysis will be restricted to scalar fields in $d = 4$ spacetime dimensions. Initially, studying a linear static case, and later incorporating time-dependence and non-linearities. The methods have their origin in quantum field theory, however, for the General Relativity context we do not need to take quantum effects into account and therefore we will consider the classical limit of the quantum field theory methods (Porto, 2016, p. 6).

Quantum field theory, in its path-integral representation, takes the action as the main actor of the functional integral

$$Z[J] \equiv \int D\phi e^{iS[\phi,J]}. \tag{7.1}$$

The action is represented by $S[\phi, J]$ and describes a set of fields, $\phi(x)$, coupled to external sources, $J(x)$. Classical objects with an action $S[\phi, J] \gg 1$ are subject to rapid oscillatory behaviour, in which case the path-integral is dominated by the saddle-point

$$Z[J] \simeq e^{iS[\phi=\phi_J,J]}. \tag{7.2}$$

Here, $\phi_J(x)$ is defined by

$$\left.\frac{\delta S[\phi, J]}{\delta\phi(x)}\right|_{\phi\to\phi_J} = 0, \tag{7.3}$$

which minimizes the action (Porto, 2016, p. 6).

For simplicity, we define

$$W[J] \equiv -i \log Z[J], \tag{7.4}$$

for which we can take $W[J] \to S[\phi_J, J]$ in the classical limit. And we concentrate on a single massless scalar field, with the action given by

$$S[\phi, J] = \int d^4x \left(-\frac{1}{2}\phi(x)\partial^2\phi(x) - V(\phi) + J(x)\phi(x)\right). \tag{7.5}$$

For now, we can also remove self-interactions, by setting $V(\phi) = 0$ (Porto, 2016, pp. 6–7).

With these choices in place, we can find a solution to the field equations 7.3:

$$\phi_J(x) = \phi_{J=0}(x) + i \int d^4y \Delta_F(x-y) J(y). \tag{7.6}$$

In this expression, $\phi_{J=0}(x)$ is a solution to the Klein-Gordon equation with $J(x) = 0$, and the propagator, or Green's function, $\Delta_F(x-y)$ is given by

$$\Delta_F(x-y) \equiv \int_{\boldsymbol{p}} \int_{p_0} \frac{i}{p_0^2 - \boldsymbol{p}^2 + i\epsilon} e^{-ip_0(x_0-y_0)} e^{i\boldsymbol{p}\cdot(\boldsymbol{x}-\boldsymbol{y})}. \tag{7.7}$$

The inclusion of $i\epsilon$ is known as Feynman's prescription and is a choice of boundary condition. This only matters when the momenta go 'on-shell' when $p_0^2 = \boldsymbol{p}^2$ (Porto, 2016, p. 7).

With equation 7.6 as an expression for $\phi_J(x)$, we can rewrite the action and find an expression for the functional $W[J]$:

$$S[\phi = \phi_J, J] \to \frac{i}{2} \int d^4x d^4y J(x) \Delta_F(x-y) J(y) = W[J]. \tag{7.8}$$

This expression has an important role in the development of our classical effective field theory approach. However, it is only exact for scalar fields coupled to external sources and does not include self-interactions (Porto, 2016, p. 7).

From the functional derivative, we can read off the propagator,

$$\Delta_F(x-y) = -i \frac{\delta^2 W[J]}{\delta J(x) \delta J(y)}\bigg|_{J=0} = (-i)^2 \frac{\delta^2 Z[J]}{\delta J(x) \delta J(y)}\bigg|_{J=0}, \tag{7.9}$$

with normalization $Z[0] = 1$. This expression will be useful to set up the perturbative approach and include non-linearities later (Porto, 2016, p. 7).

7.1 Binding potential

7.1.1 Static sources

We introduce a mass scale M_ϕ related to the strength of the coupling of ϕ and consider static point-like sources described by

$$J(\boldsymbol{x}) = J_1(\boldsymbol{x}) + J_2(\boldsymbol{x}) \equiv \frac{1}{M_\phi} \left[m_1 \delta^3(\boldsymbol{x} - \boldsymbol{x}_1) + m_2 \delta^3(\boldsymbol{x} - \boldsymbol{x}_2) \right]. \tag{7.10}$$

We can ignore the $i\epsilon$ in the propagator for off-shell configurations, and write the expression from equation 7.8 as

$$W[J] = \left(\int dt\right) \frac{1}{2} \int d^3\boldsymbol{x} d^3\boldsymbol{x'} J(\boldsymbol{x}) J(\boldsymbol{x'}) \int_{\boldsymbol{p},p_0} \frac{-1}{p_0^2 - \boldsymbol{p}^2} \delta(p_0) e^{i\boldsymbol{p}\cdot(\boldsymbol{x}-\boldsymbol{x'})}. \tag{7.11}$$

The factor $\delta(p_0)$ comes from performing the integral $\int dt' e^{-ip_0(t-t')} = 2\pi\delta(p_0)$ for static sources (Zee, 2010, pp. 27–28). Rewrite $r \equiv \boldsymbol{x}_1 - \boldsymbol{x}_2$ and use that

$$\int_{\boldsymbol{p}} \frac{1}{\boldsymbol{p}^2} e^{-i\boldsymbol{p}\cdot\boldsymbol{r}} = \frac{1}{4\pi r}, \tag{7.12}$$

such that via

$$W[J] \to -\int_{t_{in}}^{t_{out}} dt V[J], \tag{7.13}$$

it is possible to identify the binding potential $V[J]$ when taking $t_{in} \to -\infty$ and $t_{out} \to +\infty$. This yields

$$W[J] = \left(\int dt\right) \frac{m_1 m_2}{4\pi M_\phi^2} \frac{1}{r} \to V[J] = -\frac{m_1 m_2}{4\pi M_\phi^2} \frac{1}{r}, \tag{7.14}$$

where the Coulomb-like potential can be recognised. From products of the sources at the same point, you can also find self-energy contributions given by

$$\int d^3\boldsymbol{x} d^3\boldsymbol{y} \delta^3(\boldsymbol{x} - \boldsymbol{x}_1(t)) \Delta_F(\boldsymbol{x} - \boldsymbol{y}, t) \delta^3(\boldsymbol{y} - \boldsymbol{x}_1(t)) = \Delta_F(0,t) \propto \int_{\boldsymbol{p}} \frac{1}{\boldsymbol{p}^2}. \tag{7.15}$$

This integral is divergent and therefore it is necessary to introduce a UV cutoff. It can be shown that the cutoff's contribution can be absorbed into the mass coupling(s) of the sources. This process is referred to as adding a 'counter-term'. Instead, you can use dimensional regularization, which sets the scale-less integrals to zero, and allows you to ignore these terms (Porto, 2016, p. 8).

7.1.2 Time-dependent sources

The static situation can be generalised to the case of time-dependent sources by taking for the sources the expression

$$J(t,\boldsymbol{x}) = J_1(t,\boldsymbol{x}) + J_2(t,\boldsymbol{x}) \equiv \frac{1}{M_\phi} \left[m_1 \delta^3(\boldsymbol{x} - \boldsymbol{x_1}) + m_2 \delta^3(\boldsymbol{x} - \boldsymbol{x_2})\right]. \tag{7.16}$$

For this situation the time integrals no longer lead to $\delta(p_0)$, as they did in equation 7.11. And hence we need to assume that the sources move slowly, which means that $|\boldsymbol{v}_a| \equiv |\dot{\boldsymbol{x}}_a| \ll 1$ for both sources $a = 1, 2$. The off-shell Green's function can be expanded in powers of $\frac{p_0}{|\boldsymbol{p}|}$, which

due to the scaling $(p_0, \boldsymbol{p}) \sim (\frac{v}{r}, \frac{1}{r})$ corresponds to an expansion in v:

$$\frac{1}{p_0^2 - \boldsymbol{p}^2} \simeq -\frac{1}{\boldsymbol{p}^2}\left(1 + \frac{p_0^2}{\boldsymbol{p}^2} + \cdots\right). \tag{7.17}$$

The static propagator and its expansion are shown in figure 7.1. The leading term in this expansion yields

$$W_{(0)}[J] = \frac{m_1 m_2}{4\pi M_\phi^2}\int \frac{dt}{|\boldsymbol{r}(t)|}, \tag{7.18}$$

as we have also found in equation 7.14 (Porto, 2016, pp. 8–9).

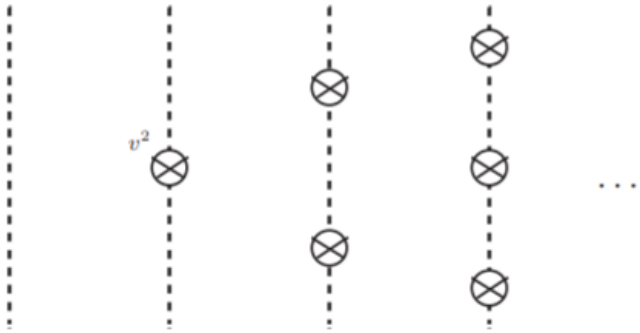

FIGURE 7.1: Diagrammatic representation of the static propagator as a dashed line, with $p_0 = 0$, and correction factors of $p_0^2/\boldsymbol{p}^2$ in subsequent diagrams, corresponding to the expansion in equation 7.17 (Porto, 2016, p. 9).

Using the integral

$$\int_{\boldsymbol{p}} \frac{\boldsymbol{p}^i \boldsymbol{p}^j}{\boldsymbol{p}^4} e^{i\boldsymbol{p}\cdot\boldsymbol{r}(t)} = \frac{1}{8\pi r^3}(r^2\delta_{ij} - \boldsymbol{r}^i\boldsymbol{r}^j), \tag{7.19}$$

the first correction can be written in the form

$$W_{(v^2)}[J] = \frac{m_1 m_2}{M_\phi^2}\int dt dt' \int_{\boldsymbol{p},p_0} \frac{p_0^2}{\boldsymbol{p}^4} e^{-ip_0(t-t')} e^{i\boldsymbol{p}\cdot(\boldsymbol{x}_1(t) - \boldsymbol{x}_2(t))} \tag{7.20}$$

$$= \frac{m_1 m_2}{M_\phi^2}\int dt \boldsymbol{v}_1^i(t)\boldsymbol{v}_2^j(t)\int_{\boldsymbol{p}} \frac{\boldsymbol{p}^i\boldsymbol{p}^j}{\boldsymbol{p}^4} e^{i\boldsymbol{p}\cdot\boldsymbol{r}(t)} \tag{7.21}$$

$$= \frac{m_1 m_2}{M_\phi^2}\int dt \boldsymbol{v}_1^i(t)\boldsymbol{v}_2^j(t)\frac{1}{8\pi r^3}(r^2\delta_{ij} - \boldsymbol{r}^i\boldsymbol{r}^j). \tag{7.22}$$

Then the following first-order potential can be identified (Porto, 2016, p. 9):

$$V_{(v^2)}[J] = \frac{m_1 m_2}{8\pi M_\phi^2}\frac{1}{|\boldsymbol{r}(t)|^3}\left[|\boldsymbol{r}(t)|^2(\boldsymbol{v}_1(t)\cdot\boldsymbol{v}_2(t)) - (\boldsymbol{v}_1(t)\cdot\boldsymbol{r}(t))(\boldsymbol{v}_2(t)\cdot\boldsymbol{r}(t))\right]. \tag{7.23}$$

Higher-order corrections can be computed using the same approach. The validity of performing the Taylor series from equation 7.17 inside the integral depends on the method of regions[,

which is explained in section ...] (Porto, 2016, p. 9).

7.1.3 Non-linearities

Adding self-interactions makes the field equations more difficult to solve in closed analytic form, and this requires numerical methods or perturbative techniques. For this discussion, we consider perturbative techniques applied to an example of a cubic potential, $V(\phi) = \lambda\phi^3$, which leads to IR divergences for a massless field. The singular integrals can later be tamed by introducing regulators, thus we can proceed by assuming that λ is small and writing the field equations in the form

$$\partial^2\phi(x) = J(x) - 3\lambda\phi^2(x). \tag{7.24}$$

With the ansatz

$$\phi_J(x) = \phi_J^{\lambda=0}(x) + \phi_J^{\lambda}(x) + \cdots + \phi_J^{\lambda^n}(x) + \cdots, \tag{7.25}$$

inserted into equation 7.24, we can solve for ϕ_J in powers of λ. When assuming static sources, at first order in λ this gives

$$\partial^2\phi_J^{\lambda}(\boldsymbol{x}) = J_\lambda(\boldsymbol{x}), \text{ with } J_\lambda(\boldsymbol{x}) \equiv -3\lambda(\phi_J^{\lambda=0})^2(\boldsymbol{x}). \tag{7.26}$$

Solving for ϕ_J^{λ} by using the Green's function as follows:

$$\phi_J^{\phi}(\boldsymbol{x}) = 3i\lambda \int d^3\boldsymbol{y}d^3\boldsymbol{z}d^3\boldsymbol{w}\Delta_F(\boldsymbol{x}-\boldsymbol{y})\Delta_F(\boldsymbol{y}-\boldsymbol{z})\Delta_F(\boldsymbol{y}-\boldsymbol{w})J(\boldsymbol{z})J(\boldsymbol{w}). \tag{7.27}$$

Then you can use

$$\int_{\boldsymbol{q}} \frac{1}{\boldsymbol{q}^2(\boldsymbol{k}+\boldsymbol{q})^2} = \frac{1}{8|\boldsymbol{k}|}, \tag{7.28}$$

to write down the contributions from particle 1 in Fourier space (Porto, 2016, p. 10):

$$\phi_J^{\lambda}(\boldsymbol{k}) = -3\lambda\frac{m_1^2}{M_\phi^2}\frac{e^{i\boldsymbol{k}\cdot\boldsymbol{x}_1}}{\boldsymbol{k}^2}\int_{\boldsymbol{q}}\int_{\boldsymbol{q}}\frac{1}{\boldsymbol{q}^2(\boldsymbol{k}+\boldsymbol{q})^2} + \cdots = -3\lambda\frac{m_1^2}{8M_\phi^2}\frac{e^{i\boldsymbol{k}\cdot\boldsymbol{x}_1}}{|\boldsymbol{k}|^3} + \cdots. \tag{7.29}$$

To compute $W_{(\lambda)}[J]$ we use the expression from equation 7.8. Then, we plug the above expression for ϕ_J^{λ} into the action from equation 7.5. We can see that the first term becomes

$$-\frac{1}{2}\phi_J^{\lambda}\partial^2\phi_J^{\lambda=0} \to -\frac{1}{2}J\phi_J^{\lambda}, \tag{7.30}$$

based on the field equations in equation 7.24. Combined with the source term in equation 7.5, $J\phi_J^\lambda$, and equation 7.13, we can compute the binding potential from $W_{(\lambda)}[J]$.

$$W\left[J, V[J]=0\right] \to \left(\int dt\right) S[\phi_J(\boldsymbol{x}), J(\boldsymbol{x}), V[J]=0] = \frac{1}{2}J(\boldsymbol{x})\phi_J^\lambda(\boldsymbol{x}) \tag{7.31}$$

$$V_{(\lambda)}[J] = -\frac{1}{2}\int d^3\boldsymbol{x} J(\boldsymbol{x})\phi_J^\lambda(\boldsymbol{x}) + \cdots = 3\lambda\frac{m_1^2 m_2}{64\pi^2 M_\phi^3}\log(\mu r) + 1 \leftrightarrow 2 \cdots . \tag{7.32}$$

Where $1 \leftrightarrow 2$ accounts for the contributions from particle 2, and μ is introduced as an IR regulator and could be, for example, a scalar mass. The introduction of the regulator is desired to be able to tame singular integrals. The logarithm in the potential is responsible for a long-range force scaling as $1/r$ (Porto, 2016, p. 10).

The procedure can be continued to all orders in λ, and it can be extended to the case of non-static sources like we have done in section 7.1.2. This will introduce some divergences. We will discuss an example of such a divergence: the contribution given by the cubic potential in the evaluation of the unperturbed solution, $\lambda(\phi_J^{\lambda=0})^3$. The divergent integral produced by this contribution represents the self-energy in the scalar field produced by a point-like object,

$$\lambda\frac{m^3}{M_\phi^3}\int d^3\boldsymbol{x}\frac{1}{|\boldsymbol{x}_1 - \boldsymbol{x}|^3} \propto \int \frac{dr}{r} = \log(\Lambda/\mu). \tag{7.33}$$

Where Λ^{-1} is introduced as a short-distance cutoff. The dependence on this UV cutoff can be absorbed into the couplings of the theory, while the IR singularities cancel out after long-distance effects are properly incorporated (Porto, 2016, pp. 10–11).

7.1.4 Diagrammatic approach

A diagrammatic approach would help to simplify the collection of all possible contributions to $W[J]$, and for this, we can use Wick's theorem. This theorem helps to sum the different contributions from combinations of field variables at different spacetime points. We will discuss how this works based on a simple one-dimensional model described by

$$Z[J,\lambda] = \int dx e^{-\frac{a}{2}x^2 - \lambda x^3 + Jx}. \tag{7.34}$$

The propagator for this case follows from expanding $Z[J, \lambda = 0]$ to second order in J, and evaluating at $J = 0$:

$$\langle x^2\rangle = \frac{1}{Z_0}\frac{\delta^2 Z[J,\lambda=0]}{\delta J^2}\bigg|_{J=0} = \frac{\int dx x^2 e^{-\frac{a}{2}x^2}}{\int dx e^{-\frac{a}{2}x^2}} = a^{-1}, \tag{7.35}$$

where $Z_0 \equiv Z[J=0, \lambda=0]$. Higher moments can then be obtained by further differentiating with respect to J,

$$\langle x^{2n} \rangle = \frac{\int dx x^{2n} e^{-\frac{a}{2}x^2}}{\int dx e^{-\frac{a}{2}x^2}} = a^{-n}(2n-1)!!, \tag{7.36}$$

where each factor of $\frac{1}{a}$ is replaced by a propagator. These propagators are defined by the 'time-ordering' of the different Wick contractions of the field variables evaluated at different spacetime points. This looks as follows for the two-point function, connecting two distinct points:

$$\langle T\{\phi(x_1)\phi(x_2)\}\rangle_{\lambda=0} \equiv \int D\phi\phi(x_1)\phi(x_2)e^{iS[\phi,\lambda=0]} = (-i)^2 \frac{\delta^2 Z[J,\lambda=0]}{\delta J(x_1)\delta J(x_2)}\bigg|_{J=0} = \Delta_F(x_1-x_2). \tag{7.37}$$

When the cubic interaction is turned on, that is for $\lambda \neq 0$, $Z[J,\lambda]$, as given in equation 7.34, needs to be expanded around the linear theory:

$$Z[J,\lambda] = \sum_n \frac{1}{n!}\frac{\partial^n Z[J,\lambda]}{\partial \lambda^n}\bigg|_{\lambda=0} \lambda^n = \sum_n \frac{1}{n!}\lambda^n \langle (-x)^{3n}\rangle_{(J,\lambda=0)}, \tag{7.38}$$

in which $Z[J,\lambda]$ was redefined as $Z[J,\lambda]/Z_0$. The next step is expanding this expression in powers of the source J, this yields

$$Z[J,\lambda] = \sum_{n,l} \frac{1}{n!}\frac{1}{l!}\frac{\partial^n \partial^l Z[J,\lambda]}{\partial\lambda^n \partial J^l}\bigg|_{\lambda=0,J=0} J^l\lambda^n = \sum_{n,l}(-1)^n J^l \lambda^n \langle x^{3n+l}\rangle_{(J=0,\lambda=0)}. \tag{7.39}$$

Restoring the is for Minkowski space, we have

$$Z[J,\lambda] = \sum_{n,l}\frac{(-1\lambda)^n}{n!}\frac{i^l}{l!}\int d^4x_1 \cdots d_l^4 J(x_1)\cdots J(x_l)\times \left\langle T\left\{\phi(x_1)\cdots\phi(x_l)\left(\int d^4y_1\phi^3(y_1)\cdots\int d^4y_n\phi^3(y_n)\right)\right\}\right\rangle_{(J=0,\lambda=0)}. \tag{7.40}$$

Where Wick's theorem can be applied to every one of these moments of a Gaussian integral (Porto, 2016, pp. 11–13).

We can now construct the diagrammatic approach. This consists of the following Feynman rules, also represented in figure 7.2 (Porto, 2016, p. 13):

- **Propagator:** Include a factor of $\frac{-i}{\boldsymbol{p}^2}\delta(t_1-t_2)$ for each dashed line connecting two points in the diagram.
- **Non-instantaneity:** Replace the factor of $\delta(t_1-t_2)$ by $\frac{d^2}{dt_1 dt_2}\delta(t_1-t_2)$ for one of the (two) propagator(s) connected by a cross.

- **Point-like sources:** Include a factor of $i\sum_{a=1,2}\frac{m_a}{M_\phi}\int dt e^{i\boldsymbol{p}\cdot\boldsymbol{x}_a(t)}$, or $i\sum_{a=1,2}\frac{m_a}{M_\phi}\int dt\delta(\boldsymbol{x}-\boldsymbol{x}_a(t))$ in coordinate space, for each propagator ending in a source.
- **Vertex:** Include a factor of $-i\lambda\int d\tilde{t}\delta^3\left(\sum_{i=1}^{i=3}\boldsymbol{p}_k\right)$ for each ϕ^3-vertex. This guarantees conservation of momenta, with $\boldsymbol{p}_i$ incoming.

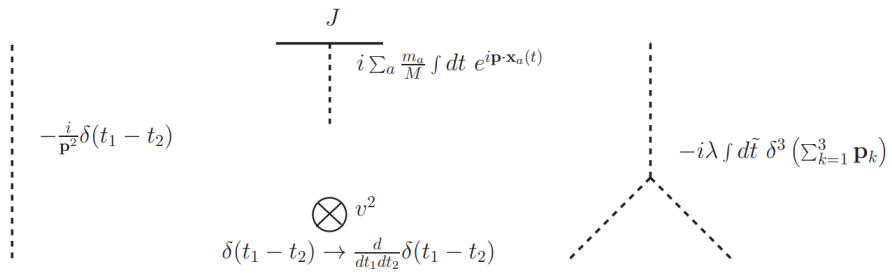

FIGURE 7.2: These are the Feynman rules for the diagrammatic approach to General Relativity. The solid line represents a point-like external source which does not propagate. The dashed lines represent the static propagators (Porto, 2016, p. 13).

We start by constructing the diagrams for the linear theory for static sources, as was described in section 7.1.1. We know the exact result of this theory, which was given in equation 7.11 and can be written using propagators in the following form

$$W[J]=-i\log Z[J]=\left(\int dt\right)\frac{1}{2}\int d^3\boldsymbol{x}d^3\boldsymbol{x'}J(\boldsymbol{x})(i\Delta_F(\boldsymbol{x}-\boldsymbol{x'}))J(\boldsymbol{x'}). \tag{7.41}$$

The contributing diagrams for $W[J]$ are therefore only one-scalar diagrams, these are the tree-level connected diagrams. From this result for $W[J]$, it is straightforward to see that the contributing diagrams for $Z[J]$ are found by exponentiation of the result for $W[J]$. The diagrams contributing to $Z[J]$ are shown in figure 7.3 (Porto, 2016, p. 14).

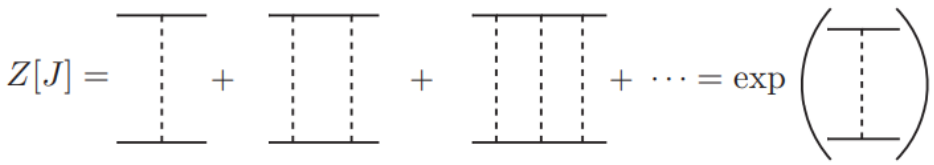

FIGURE 7.3: (Porto, 2016, p. 14)

Diagrams with self-interactions only occur after adding the non-linear terms to the theory. Diagrams with loops do not occur since they are responsible for quantum effects, and we are considering a classical field theory. The exclusion of self-interactions and loops makes sense for the linear theory because only one-scalar exchanges contribute to $Z[J]$ when $\lambda=0$.

We can further consider the relation between $Z[J]$ and $W[J]$ by considering that

$$Z[J] = \sum_{n}^{\infty} \frac{\left(\frac{i}{\hbar} W[J]\right)^n}{n!}, \tag{7.42}$$

which is the series expansion of the exponential. In the classical limit, we can see from equation 7.2 and Stirling's approximation, $e^N \simeq \frac{N^{N+1/2}}{N!}$ for $N \gg 1$, that $Z[J]$ involves a large number of terms, because

$$n \simeq N \equiv S[\phi_J]/\hbar \gg 1. \tag{7.43}$$

The series of N one-scalar exchanges can be interpreted as building blocks for the classical field $\phi_J(t, \boldsymbol{x})$. The typical momentum exchanged by each of these contributions is of order $|\boldsymbol{q}| \sim \frac{\hbar}{r}$ due to the quantum nature of the off-shell exchange particles. While the total momentum transferred due to the force induced by the binding potential is given by

$$\Delta \boldsymbol{p} \simeq N \frac{\hbar}{r} \simeq mv. \tag{7.44}$$

Considering the fraction of linear momentum exchanged and the total momentum due to the binding potential,

$$\frac{|\boldsymbol{q}|}{|\Delta \boldsymbol{p}|} \sim \frac{\hbar}{L} \ll 1, \tag{7.45}$$

in which $L = mvr$ is the angular momentum. We can see that this yields

$$S[\phi_J] \simeq \int \Delta \boldsymbol{p} d\boldsymbol{x} \simeq L \gg \hbar, \tag{7.46}$$

which support an analogy with heavy particle effective field theories. Based on this analogy you can argue that for the effective theory of gravity we can treat macroscopical objects as non-propagating sources (Porto, 2016, pp. 14–15) (Goldberger and Rothstein, 2006a, p. 3).

7.2 Radiated power loss

In the discussion of the equations of motion and binding potential in the previous section, the choice of boundary conditions is innocuous because it involves quasi-instantaneous modes, where $p_0 \ll |\boldsymbol{p}|$ applies. But when the theory allows the objects to move, they will accelerate due to the binding forces and hence emit radiation. To derive the power of the scalar field that is radiated, we can introduce retarded boundary conditions, in contrast to the Feynman propagator used in the previous part. The $i\epsilon$-prescription is re-introduced here, because the scalar field can only be emitted on-shell for $p_0^2 = \boldsymbol{p}^2$ (Porto, 2016, p. 16).

7.2.1 Retarded boundary conditions

The standard approach to compute the total radiated power of a system is by introducing the retarded propagator given by

$$\Delta_{ret}(x-y) = \int_{\boldsymbol{p}}\int_{p_0} \frac{i}{(p_0+i\epsilon)^2-\boldsymbol{p}^2} e^{-ip_0(x_0-y_0)} e^{i\boldsymbol{p}\cdot(\boldsymbol{x}-\boldsymbol{y})} \tag{7.47}$$

in momentum space. This propagator has, unlike the Feynman propagator, only poles in the lower-half complex plane, thus enforcing the causal condition that is required. We can also define the retarded propagator in coordinate space, then it is given by

$$i\Delta_{ret}(x-y) = \frac{1}{2\pi}\theta(x^0-y^0)\delta((x-y)^\mu(x-y)_\mu). \tag{7.48}$$

The retarded propagator can be inserted into equation 7.6, which gives the solution to the field equations that minimises the action. It becomes

$$\phi_J^{ret}(x) = \sum_{a=1,2}\frac{m_a}{4\pi M_\phi}\int_{-\infty}^{x^0} dt \frac{1}{|\boldsymbol{x}-\boldsymbol{x}_a(t)|}\delta(x^0-t-|\boldsymbol{x}-\boldsymbol{x}_a(t)|) \tag{7.49}$$

$$= \sum_{a=1,2}\frac{m_a}{4\pi M_\phi}\left[\frac{1}{|\boldsymbol{x}-\boldsymbol{x}_a(t)|-\boldsymbol{v}_a(t)\cdot(\boldsymbol{x}-\boldsymbol{x}_a(t))}\right]_{ret}, \tag{7.50}$$

in which the conditions for the last expression are given by replacing $t = x^0 - \boldsymbol{R}(t)$, where $\boldsymbol{R}(t) \equiv \boldsymbol{x} - \boldsymbol{x}_a(t)$ (Porto, 2016, pp. 16–17).

The derivatives of this expression are given by

$$\partial_i\phi_J^{ret}(x) = \sum_{a=1,2}\frac{m_a}{4\pi M_\phi}\left[\frac{\hat{\boldsymbol{R}}-\boldsymbol{v}_a}{\boldsymbol{R}^2(1-\boldsymbol{v}_a\cdot\hat{\boldsymbol{R}})^2} + \frac{\hat{\boldsymbol{R}}}{(1-\boldsymbol{v}_a\cdot\hat{\boldsymbol{R}})}\left(\frac{\dot{\boldsymbol{v}}_a\cdot\boldsymbol{R}-\boldsymbol{v}_a\cdot\hat{\boldsymbol{R}}+\boldsymbol{v}_a^2}{\boldsymbol{R}^2(1-\boldsymbol{v}_a\cdot\hat{\boldsymbol{R}})^2}\right)\right]_{ret} \tag{7.51}$$

$$\partial_0\phi_J^{ret}(x) = \sum_{a=1,2}\frac{m_a}{4\pi M_\phi}\left[\frac{\dot{\boldsymbol{v}}_a\cdot\boldsymbol{R}-\boldsymbol{v}_a\cdot\hat{\boldsymbol{R}}+\boldsymbol{v}_a^2}{\boldsymbol{R}^2(1-\boldsymbol{v}_a\cdot\hat{\boldsymbol{R}})^2}\right]_{ret}, \tag{7.52}$$

which can be used together with Noether's theorem to compute the momentum density, $\boldsymbol{P}_i(x) = \partial_i\phi(x)\partial_0\phi(x)$. We will expand in small velocities, thus assuming $|\boldsymbol{v}| \ll 1$, at leading order this yields

$$\hat{\boldsymbol{R}}_i\cdot\partial_i\phi_J^{ret} = \partial_0\phi_J^{ret} = \sum_{a=1,2}\frac{m_a}{4\pi M_\phi}\left[\frac{\dot{\boldsymbol{v}}_a\cdot\boldsymbol{R}}{\boldsymbol{R}^2}\right]_{ret}. \tag{7.53}$$

Giving a total radiated power loss at leading order given by (Porto, 2016, p. 17):

$$\frac{dP_{LO}}{d\Omega} = \frac{1}{16\pi^2 M_\phi^2} \sum_{a\neq b} m_a m_b \left(\dot{\boldsymbol{v}}_a \cdot \hat{\boldsymbol{R}}\right)\left(\dot{\boldsymbol{v}}_b \cdot \hat{\boldsymbol{R}}\right), \tag{7.54}$$

$$P_{LO} = \frac{1}{12\pi M_\phi^2}\left\langle \left(\sum_{a=1,2} m_a \dot{\boldsymbol{v}}_a\right)\cdot\left(\sum_{b=1,2} m_b \ddot{\boldsymbol{x}}_b\right)\right\rangle = \frac{(m_1+m_2)^2}{12\pi M_\phi^2}\langle \boldsymbol{a}_{cm}^2\rangle. \tag{7.55}$$

Using the retarded boundary conditions is one way to compute the total radiated power loss. However, another procedure that allows us to compute the radiated power uses the optical theorem. In the next section, we will discuss this second procedure, as it will also be relevant for the next two chapters.

7.2.2 Optical theorem

Before discussing the optical theorem, we have a brief look at the Feynman propagator in coordinate space, given by

$$i\Delta_F(x-y) = -i\frac{1}{(2\pi)^2}\frac{1}{(x-y)^\mu (x-y)_\mu + i\epsilon}. \tag{7.56}$$

Using that

$$\mathrm{Im}\left\{\frac{1}{x+i\epsilon}\right\} = -\pi\delta(x), \tag{7.57}$$

we can write the real part of the Feynman propagator as

$$\mathrm{Re}\, i\Delta_F(x-y) = \frac{1}{4\pi}\delta((x-y)^\mu (x-y)_\mu). \tag{7.58}$$

This is a procedure to include the retarded boundary conditions such that the propagators satisfy the causal conditions. In fact, with this procedure we have included (half of) both retarded and advanced contributions (Porto, 2016, p. 17).

We can split the effective action in terms of the real and imaginary parts,

$$Z[J] = e^{iW[J]} \to e^{i\int_{t_{in}}^{t_{out}} dt\, \mathrm{Re}\, E[J]} \times e^{-\int_{t_{in}}^{t_{out}} dt\, \mathrm{Im}\, E[J]}, \tag{7.59}$$

where we take t_{in} and t_{out} to be (infinitely) long times. Note that $\mathrm{Re}\, E[J]$ accounts for the binding energy as studied in the previous section. For the imaginary part we can consider

$$\frac{1}{T}\,\mathrm{Im}\, W[J] = \langle \mathrm{Im}\, E[J]\rangle \to \frac{1}{2}\int \frac{d^2\Gamma}{dE d\Omega} dE d\Omega, \tag{7.60}$$

where $T = t_{out} - t_{in} \to \infty$, and $d\Gamma$ the differential rate of radiation. Multiplying this by the energy of the emitted (massless) scalars, and integrating over energy and solid angle, we find

$$P \equiv \int dP = \int E d\Gamma = \int E \frac{d^2\Gamma}{d\Omega dE} dE d\Omega. \tag{7.61}$$

The scalar field has to be taken on-shell here, and hence the $i\epsilon$-prescription is crucial (Porto, 2016, pp. 17–18).

The intuitive interpretation of the optical theorem is that the in-out boundary conditions represent a system that first emits radiation, and later absorbs that radiation again. The optical theorem can be intuitively thought of as computing (twice) the imaginary part, which can be represented as sending the radiation backwards in time. Figure 7.4 is a diagrammatic representation of this procedure (Porto, 2016, p. 19).

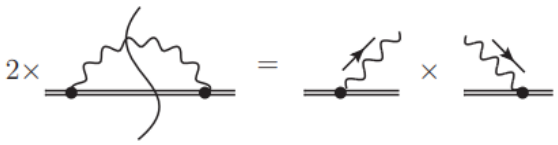

FIGURE 7.4: The optical theorem in an intuitive, diagrammatic representation. The double lines are non-propagating constituents of the source which are separated by a distance much shorter than the scale of radiation.

We can introduce a mixed Fourier space representation, with a source given by

$$J(t, \boldsymbol{p}) \equiv \int d^3\boldsymbol{x} J(t, \boldsymbol{x}) e^{-i\boldsymbol{p}\cdot\boldsymbol{x}} = \frac{1}{M_\phi} \sum_a m_a e^{-i\boldsymbol{p}\cdot\boldsymbol{x}_a(t)}. \tag{7.62}$$

This expression can be used to consider the imaginary part of $W[J]$, defined in equation 7.8, by also using equation 7.57:

$$\begin{aligned} \operatorname{Im} W[J] &= \frac{1}{2} \int dt dt' \int_{p_0, \boldsymbol{p}} \frac{1}{2|\boldsymbol{p}|} (\delta(p_0 - |\boldsymbol{p}|) + \delta(p_0 + |\boldsymbol{p}|)) e^{-ip_0(t-t')} J(t, \boldsymbol{p}) J(t', -\boldsymbol{p}) && (7.63) \\ &= \int dt dt' \int_{\boldsymbol{p}} \frac{1}{2|\boldsymbol{p}|} e^{-i|\boldsymbol{p}|(t-t')}. && (7.64) \end{aligned}$$

Together with equation 7.60, this yields for the total radiated power that

$$\frac{d^2P}{d|\boldsymbol{p}|d\Omega} = \frac{1}{T} \frac{|\boldsymbol{p}|^2}{16\pi^3 M_\phi^2} \left| \sum_{a=1,2} \int dt_a m_a e^{i|\boldsymbol{p}|t_a} e^{-i\boldsymbol{p}\cdot\boldsymbol{x}_a(t_a)} \right|^2. \tag{7.65}$$

This can be expanded in powers of $\boldsymbol{p}\cdot\boldsymbol{x}_a \sim v$:

$$P = \frac{1}{T}\int_{\boldsymbol{p}} \frac{1}{2M_\phi^2}\left|\sum_{a=1,2}\int dt_a m_a e^{i|\boldsymbol{p}|t_a}\left(1+\boldsymbol{p}\cdot\boldsymbol{x}_a(t_a)+\frac{1}{2}(\boldsymbol{p}\cdot\boldsymbol{x}_a(t_a))^2+\cdots\right)\right|^2 = P_{(0)}+P_{(1)}+\cdots . \tag{7.66}$$

The first term, $P_{(0)}$, vanishes, and for the next term we find (Porto, 2016, pp. 18–19):

$$P_{(1)} = \frac{1}{T}\int_{\boldsymbol{p}} \frac{1}{2M_\phi^2}\sum_{a\neq b}\int dt_a dt_b m_a m_b e^{i|\boldsymbol{p}|(t_a-t_b)}\boldsymbol{p}^i\boldsymbol{p}^j\boldsymbol{x}_b^i(t_b)\boldsymbol{x}_a^j(t_a) \tag{7.67}$$

$$= \frac{1}{T}\int_{\boldsymbol{p}} \frac{1}{2M_\phi^2}\boldsymbol{p}^i\boldsymbol{p}^j\left(\sum_{b=1,2} m_b\tilde{\boldsymbol{x}}_b^i(|\boldsymbol{p}|)\right)\left(\sum_{a=1,2} m_a\tilde{\boldsymbol{x}}_a^j(-|\boldsymbol{p}|)\right) \tag{7.68}$$

$$= \frac{1}{12\pi M_\phi^2}\frac{1}{T}\int_0^\infty \frac{d|\boldsymbol{p}|}{\pi}|\boldsymbol{p}|^4\left(\sum_{b=1,2} m_b\tilde{\boldsymbol{x}}_b^i(|\boldsymbol{p}|)\right)\left(\sum_{a=1,2} m_a\tilde{\boldsymbol{x}}_a^j(-|\boldsymbol{p}|)\right) \tag{7.69}$$

$$= \frac{1}{12\pi M_\phi^2}\left\langle\left(\sum_{b=1,2} m_b\ddot{\boldsymbol{x}}_b(t)\right)\cdot\left(\sum_{a=1,2} m_a\ddot{\boldsymbol{x}}_a(t)\right)\right\rangle . \tag{7.70}$$

The expressions in equations 7.63 and 7.65 have the form of the square of an on-shell amplitude (Porto, 2016, p. 19):

$$i\mathcal{A}(p_0=|\boldsymbol{p}|,\boldsymbol{p}) = i\sum_{a=1,2}\frac{m_a}{M_\phi}\int dt_a e^{i|\boldsymbol{p}|t_a\cdot\boldsymbol{x}_a(t_a)}, \tag{7.71}$$

$$P = \frac{1}{T}\int_{\boldsymbol{p}}\frac{1}{2|\boldsymbol{p}|}|\boldsymbol{p}||\mathcal{A}|^2. \tag{7.72}$$

7.2.3 Multipole expansion

The discussion in the previous subsection, without self-interactions, was able to provide an exact result in equation 7.65. However, after adding the self-interactions of gravity, an analytic result is no longer possible, and therefore we introduce a perturbative approach to the radiation problem. This approach is based on the multipole expansion, similar to the one in electromagnetism in which a combined system can be approximated by a single localized source with a series of time-dependent multipole moments. The assumption for this approach is that the typical wavelength of the radiation is much larger than the typical change of positions and velocities in the system, thus $\lambda_{rad} \sim r/v \gg r$. For such a system, we have an effective action given by

$$S_{eff}^{rad} = \frac{1}{M_\phi}\int dt\left(J_{(0)}(t)\phi(t,\boldsymbol{x}_{cm})+J_{(1)}^i(t)\partial_i\phi(t,\boldsymbol{x}_{cm})+\frac{1}{2}J_{(2)}^{ij}(t)\partial_i\partial_j\phi(t,\boldsymbol{x}_{cm})+\cdots\right), \tag{7.73}$$

where $\boldsymbol{x}_{cm}$ is the centre-of-mass of the bound state. The time-dependent couplings, $J_{(n)}^{i_1,\cdots,i_n}$, can be computed by using a matching procedure. Starting with inserting the multipole expansion,

$$\phi(t,\boldsymbol{x}) = \phi(t,\boldsymbol{x}_{cm}) + (\boldsymbol{x}-\boldsymbol{x}_{cm})^i\partial_i\phi(t,\boldsymbol{x}_{cm}) + \frac{1}{2}(\boldsymbol{x}-\boldsymbol{x}_{cm})^i(\boldsymbol{x}-\boldsymbol{x}_{cm})^j\partial_i\partial_j\phi(t,\boldsymbol{x}_{cm}) + \cdots, \quad (7.74)$$

into the $J\phi$-interaction from the original action, as given in equation 7.5. For simplicity, we can take $\boldsymbol{x}_{cm} = 0$, and then we can write

$$\int dt d^3\boldsymbol{x} J(t,\boldsymbol{x})\phi(t,\boldsymbol{x}) \to \int dt \left\{ \left(\int d^3\boldsymbol{x} J(t,\boldsymbol{x}) \right) \phi(t,0) + \left(\int d^3\boldsymbol{x} J(t,\boldsymbol{x})\boldsymbol{x}^i \right) \partial_i\phi(t,0) \right\} + \cdots. \quad (7.75)$$

The following multipole moments term can be read of:

$$J_{(n)}^{i_1,\cdots,i_n}(t) = M_\phi \int d^3\boldsymbol{x} J(t,\boldsymbol{x})\boldsymbol{x}^{i_1}\cdots\boldsymbol{x}^{i_n}. \quad (7.76)$$

And in mixed Fourier space:

$$J(t,\boldsymbol{k}) = \int d^3\boldsymbol{x} e^{-i\boldsymbol{k}\cdot\boldsymbol{x}} J(t,\boldsymbol{x}) = \sum_n \frac{(-i)^n}{n!} \left(\int d^3\boldsymbol{x} J(t,\boldsymbol{x})\boldsymbol{x}_i\cdots\boldsymbol{x}_{i_n} \right) \boldsymbol{k}^i\cdots\boldsymbol{k}^{i_n}, \quad (7.77)$$

where the coefficients in the expansion correspond to the $J_{(n)}^{i_1,\cdots,i_n}(t)$-factors in equation 7.76. For example, the first two terms are:

$$J_{(0)} = m_1 + m_2, \quad (7.78)$$

$$J_{(1)} = m_1\boldsymbol{x}_1 + m_2\boldsymbol{x}_2. \quad (7.79)$$

The total radiated power loss can be computed in a similar way as in equation 7.71. For example, the dipole term contributes as

$$i\mathcal{A}_{(1)}(p) = i\frac{1}{M_\phi}\boldsymbol{p}\cdot\boldsymbol{J}_{(1)}(t), \quad (7.80)$$

which gives the same power as was already calculated in equation 7.54 (Porto, 2016, p. 20):

$$P_{(1)} = \frac{1}{T}\frac{1}{M_\phi^2}\left\langle \int_{\boldsymbol{p}} \boldsymbol{p}^i\boldsymbol{p}^j\boldsymbol{J}_{(1)}^i(t)\boldsymbol{J}_{(1)}^j \right\rangle = \frac{1}{12\pi M_\phi^2}\left\langle \ddot{\boldsymbol{J}}_{(1)}\cdot\ddot{\boldsymbol{J}}_{(1)} \right\rangle \quad (7.81)$$

$$= \frac{1}{12\pi M_\phi^2}\left\langle \left(\sum_{b=1,2} m_b\ddot{\boldsymbol{x}}_b(t) \right)\cdot\left(\sum_{a=1,2} m_a\ddot{\boldsymbol{x}}_a(t) \right) \right\rangle = \frac{(m_1+m_2)^2}{12\pi M_\phi^2}\langle \boldsymbol{a}_{cm}^2 \rangle. \quad (7.82)$$

This procedure can be continued to all orders, for which it is useful to decompose the multipoles into irreducible symmetric-trace-free (STF) parts. More details about this procedure are

given in (Porto, 2016, p. 21). With the expression

$$\mathcal{J}^L(t) = \sum_k \frac{(2l+1)!!}{(2l+2k+1)!!(2k)!!} \int d^3\boldsymbol{x} \partial_0^{2k} J(t,\boldsymbol{x}) |\boldsymbol{x}|^{2k} \boldsymbol{x}^L_{STF}, \tag{7.83}$$

in which $L = (i_1 \cdots i_l)$ and $l = 0, 1, 2, \ldots$ corresponds to the order of the multipole expansion, the flux to all orders can be computed:

$$i\mathcal{A}_{(l)}(p) = i\frac{1}{M_\phi}\frac{(-1)^l}{l!}\mathcal{J}^L p^L, \tag{7.84}$$

$$P = \frac{1}{4\pi M_\phi^2} \sum_l \frac{1}{l!(2l+1)!!} \left\langle \left(\frac{d^{l+1}\mathcal{J}^L(t)}{dt^{l+1}} \right)^2 \right\rangle. \tag{7.85}$$

7.3 Method of regions

In the introduction of this chapter, the separation of scales for the binary problem in General Relativity was discussed. Here we will briefly look at how this separation of scales is implemented for the effective scalar theory we have just developed.

The conservative dynamics, described in terms of the binding potential above, can be seen as independent from the radiation field when there are no non-linear contributions. The 'method of regions' describes how these two aspects relate to each other. For the situation described above, the scalar field can be decomposed into separate regions based on their length scale. For slowly moving objects, $v \ll c$, the wavelength of the radiation is much longer than the separation of the objects, $\lambda_{rad} \sim r/v \gg r$. That means that we can create two non-overlapping regions: one corresponding to the field mode representing the dynamics of potential forces, and the other region corresponding to the field mode representing the radiation effects. The scalar field can then be written as

$$\phi(t,\boldsymbol{x}) = \underbrace{\Phi(t,\boldsymbol{x})}_{\text{potential}} + \underbrace{\bar{\phi}(t,\boldsymbol{x})}_{\text{radiation}}. \tag{7.86}$$

The scaling of the terms is as follows:

$$\partial_0 \Phi(t,\boldsymbol{x}) \sim \frac{v}{c}\Phi(t,\boldsymbol{x}), \tag{7.87}$$

$$\partial_i \Phi(t,\boldsymbol{x}) \sim \frac{1}{r}\Phi(t,\boldsymbol{x}), \tag{7.88}$$

$$\partial_\mu \bar{\phi}(t,\boldsymbol{x}) \sim \frac{v}{c}\bar{\phi}(t,\boldsymbol{x}). \tag{7.89}$$

For a static source J there are only potential modes without a temporal component, thus described by $|\boldsymbol{p}| \sim 1/r$. The dynamics of slowly moving sources is described by a deviation

parameterized in powers of $p_0 \sim v/r \ll c/r$. As asymptotic states in the EFT, on-shell radiation modes appear, with a typical momentum of order $(p_0, \boldsymbol{p}) \sim (v/r, v/r)$. In this region the potential modes must be solved for, or in the language of particle physics: these modes need to be 'integrated out' (Porto, 2016, pp. 21–22).

For the linear theory, this procedure is still relatively straightforward since the two regions decouple and the binding energy and emitted power can be computed separately. However, when non-linearities are added to the theory, the two regions get mixed, and terms like $\Phi^2\bar{\phi}$ and $\bar{\phi}^2\Phi$ might occur. This is what is called the 'coupling' of the potential modes and the radiation modes (Porto, 2016, p. 22).

Chapter 8

Case: Effective Classical Electrodynamics

After introducing the effective field theory approach in the previous chapter in a scalar theory, we will now apply the approach to a system governed by Maxwell's laws. The electromagnetic binary system consists of two charged spheres subject to electromagnetic interactions. Where the discussion in the previous chapter was quite technical and introduced a lot of field theory language, this chapter will focus more on the physical interpretation of that language in the context of the system under consideration. Compared to the effective field theory approach of gravitational binaries, which will be discussed in the next chapter, this chapter will be limited to a relatively simplified discussion. This means that we will ignore some complications such as divergences, and radiation reaction effects in this chapter. Those are discussed in either the previous or the next chapter, or both. This choice of simplification will serve the familiarity with the fundamentals of the effective theory approach, before applying it to the gravitational theory.

We will start the description of the system of two charged spheres by zooming in on the finite-size effects, which occur at the scale of the sphere's radii. Integrating out that scale gives a theory with an effective action that can be described on the scale of the radial separation between the two objects. In the section about the binding potential of the system, the potential field will be analysed and a diagrammatic description will generate Feynman diagrams to compute the potential terms of the system. In the last section of this chapter, we will integrate out the potential field such that the radiated power can be computed.

8.1 Finite-size effects

In this section we consider a system consisting of two charged spheres. The starting point is the point particle approximation. The action for a collection of point particles is given by

$$S = \sum_{i=1,2} \int d\lambda_i \left(m_i \sqrt{\frac{dx_i^\mu}{d\lambda_i} \frac{dx_{i\mu}}{d\lambda_i}} + e_i \frac{x_i^\mu}{d\lambda_i} A_\mu(x_i(\lambda_i)) \right) - \int d^4x \frac{1}{4} F_{\mu\nu} F^{\mu\nu}, \tag{8.1}$$

where e_i is the charge of particle i, and the world lines are parametrized in λ_i. To account for the finite-size effects, which occur at the sphere's radius scale, we need to add a term to this action. The requirement is that the added term(s) respect the symmetries of the theory: gauge invariance, Lorentz invariance, and world-line reparameterization invariance. Additionally, at a large enough distance from the source, only Maxwell's electrodynamics plays a role so the added terms for finite effects at the source radius scale should vanish there. Constructing the added terms from the vector potential A_μ, four-velocities of the world lines v^μ, and higher time derivatives of the world line x^μ, we find that at leading order, the added terms of lowest dimension are given by

$$S_{FS} = \int d\lambda \left(\frac{C_1}{\sqrt{v^2}} v^\mu F_{\mu\nu} v_\alpha F^{\alpha\nu} + C_2 \sqrt{v^2} F_{\mu\nu} F^{\mu\nu} \right), \tag{8.2}$$

where C_1 and C_2 are coefficients to be fixed and must scale as $1/R^3$, where R is the radial separation of the spheres, for dimensional reasons (Rothstein, 2016, pp. 3–4).

The finite-size effects could be caused by, for example, polarization or deformation due to an external field, or structural deformations of the sphere(s). Whether these effects are classical or quantum does not matter, only the strength of the effects will be recorded in the coefficients. Note that we have assumed the time scale for the deformations to be short in comparison to the external time scales, such as the period of the orbit (Rothstein, 2016, p. 4).

At this order, the system is still Gaussian and thus the path integral could be solved exactly (Rothstein, 2016, p. 5). However, the goal is to study how to solve non-Gaussian gravitational systems and therefore we will also look at approximate rather than exact solutions of this system.

8.2 Binding potential

Now we consider the action for sources coupled to the electromagnetic field:

$$S = \int d^4x \left(-\frac{1}{4} F_{\mu\nu} F^{\mu\nu} - \frac{1}{2} (\partial_\mu A^\mu)^2 + J_\mu A^\mu \right), \tag{8.3}$$

in which the second term accounts for the Feynman gauge, and the current from two particles traversing the worldlines $x_1^\mu(\tau)$ and $x_2^\mu(\tau)$ is given by (Rothstein, 2016, pp. 6, 13):

$$J^\mu(x) = e_1 \int d\tau v_1^\mu(\tau)\delta^{(4)}(x - x_1(\tau)) + e_2 \int d\tau v_2^\mu(\tau)\delta^{(4)}(x - x_2(\tau)). \tag{8.4}$$

Ignoring the finite-size corrections for a moment, we separate the scales of the potential modes and the radiation modes. We can then write the gauge field as

$$A_\mu(x) = \underbrace{\boldsymbol{A}_\mu}_{\text{potential field}} + \underbrace{\bar{A}_\mu}_{\text{radiation field}} . \tag{8.5}$$

The goal here is to make sure that there is no overlap between these fields, which is naturally satisfied. The underlying idea of this approach is based on the potential part being "off-shell", i.e. $k_\mu k^\mu \sim 1/r^2 > 0$, thus existing only on a very short time scale compared to the on-shell radiation field. One can think of this as the potential field fluctuating on a (relatively) static background radiation field. The next step then is to "integrate out" the potential field, leaving an effective action for the background radiation field. We have already seen the method of integrating out in the previous section because the classical limit of this process corresponds to performing the saddle point approximation. For this system the approximation looks as follows:

$$Z[J] = \int D\bar{A}D\boldsymbol{A}e^{iS(\bar{A},\boldsymbol{A},J)} = \int D\bar{A}e^{iS_{eff}(\bar{A},J)}, \tag{8.6}$$

in which S_{eff} is the effective action (Rothstein, 2016, pp. 16–17).

Before integrating out the potential field, we should consider the gauge invariance of the theory. In the background field formalism, it is possible to choose distinct gauges for $\bar{A}$ and $\boldsymbol{A}$. The preferred gauge within this formalism is automatically incorporated in the process of integrating out the potential field and constructing the effective action for the radiation field $\bar{A}$. The gauge fixing term for $\boldsymbol{A}$ is then fixed by covariantizing the typical gauge fixing term with respect to the background field. For a linear theory, such as we are considering now, this is not a problem since the gauge field does not transform under the gauge symmetry. However, for a non-linear theory such as General Relativity, the gauge fixing term will shift the action and can generate a non-gauge invariant effective action S_{eff} (Rothstein, 2016, p. 17).

Starting from the full action in which the source terms are included and the finite-size effects are neglected:

$$S = -\sum_i \int m_i d\tau_i - \frac{1}{4}\int d^4x F_{\mu\nu}F^{\mu\nu} - \frac{1}{2}\int d^4x(\partial_\mu A^\mu)^2 + \sum_i \int e_i v_\mu(x_i)A^\mu(x_i)d\tau_i. \tag{8.7}$$

Using the partial Fourier transform,

$$\boldsymbol{A}_\mu(t,\boldsymbol{x}) = \int [d^3k] e^{i\boldsymbol{k}\cdot\boldsymbol{x}} \boldsymbol{A}_{\boldsymbol{k}\mu}(t) \equiv \int_{\boldsymbol{k}} e^{i\boldsymbol{k}\cdot\boldsymbol{x}} \boldsymbol{A}_{\boldsymbol{k}\mu}(t), \tag{8.8}$$

and substituting the mode decomposition from equation 8.5 into the full action:

$$S = \underbrace{\frac{1}{2}\int d^4x (\bar{A}_\mu \Box \bar{A}^\mu)}_{\text{potential photon}} + \underbrace{\frac{1}{2}\int dt \int_{\boldsymbol{k}} (\boldsymbol{k}^2 \boldsymbol{A}^\mu_{\boldsymbol{k}} \boldsymbol{A}_{-\boldsymbol{k}\mu} + \partial_0 \boldsymbol{A}^\mu_{\boldsymbol{k}} \partial_0 \boldsymbol{A}^\mu_{-\boldsymbol{k}})}_{\text{corrections to instantaneity}}$$
$$+ \underbrace{\sum_i \int e_i \frac{dx_i^\mu}{dt_i}(t_i) \left(\bar{A}_\mu(x_i) + \int_{\boldsymbol{k}} e^{i\boldsymbol{k}\cdot\boldsymbol{x}_i(t_i)} \boldsymbol{A}_{\boldsymbol{k}\mu}(t_i) \right) dt_i}_{\text{interactions of the source with a photon}}. \tag{8.9}$$

The terms describing the kinetic energy of the point particles, and terms linear in the fluctuating field $\boldsymbol{A}_{\boldsymbol{k}\mu}(t_i)$ do not play a role in the next steps so these have been omitted (Rothstein, 2016, pp. 17–18).

Now we can analyse the scaling in v of each term in the effective action 8.9. The reference for the scaling of the fields is the kinetic term for the photon, which must be leading order to have a sensible perturbative expansion. The scaling of the fields is then as follows (Rothstein, 2016, pp. 18–19):

- Radiation field: Consider the term $\int d^4x (\bar{A}_\mu \Box \bar{A}^\mu)$, in which $\Box \sim v^2/r^2$, and the spatial integration generates a momentum conserving delta function $\sim r^4/v^4$. This gives a scaling of the radiation field of $\bar{A}_\mu \sim v/r$.
- Potential field: We consider the term $\int dt \int_{\boldsymbol{k}} \boldsymbol{k}^2 \boldsymbol{A}^\mu_{\boldsymbol{k}} \boldsymbol{A}_{-\boldsymbol{k}\mu}$ in which we have $dt \sim \frac{r}{v}$, and $k \sim \frac{1}{r}$, which gives $\boldsymbol{A}^2_{\boldsymbol{k}\mu}(t) \sim \frac{v}{r} r^3 r^2$. Thus the potential field scales as $\boldsymbol{A}_{\boldsymbol{k}\mu}(t) \sim v^{1/2} r^2$.

8.2.1 Diagrammatic approach

Inverting the term quadratic in the potential photon field gives the propagator,

$$\langle \boldsymbol{A}_{\boldsymbol{k}\mu}(t_1) \boldsymbol{A}_{\boldsymbol{q}\nu}(t_2) \rangle = (2\pi)^3 \delta(t_1 - t_2) \delta^3(\boldsymbol{k} + \boldsymbol{q}) \frac{i g_{\mu\nu}}{\boldsymbol{k}^2}. \tag{8.10}$$

That the propagator does not depend on the energy means that its Fourier transform is proportional to $\delta(t)$ and is thus instantaneous. The absence of an energy pole in this propagator also eliminates the possibility of overlap with the radiation field, for which $k_0 \sim |\boldsymbol{k}|$. Corrections to this instantaneity come from the temporal derivative terms, which are being suppressed by a factor v^2. The leading order interaction involves a temporal potential photon and generates the Coulomb potential. The coupling to non-temporal photons is suppressed by v (Rothstein, 2016, p. 19).

This is an example of what is called 'power counting' in effective field theory language. It is a generalized version of dimensional analysis in which you consider the scaling of each element in the terms of the action to determine the order at which the terms contribute to the theory (Cannella, 2011, p. 49). This allows us to integrate out the potential modes, which will eliminate the scale $1/r$ from the theory. The result will be a one body theory, since at the next scale, v/r, it is no longer possible to distinguish the two objects in the binary. At this next scale, the theory will couple to the radiation field. The approximate solution to the theory can be constructed by considering the Feynman diagrams order by order. We have already found the potential photon propagator, so now we extract the Feynman rules for two types of vertices from expanding the interaction term in the effective action:

$$\sum_i \int e_i \frac{dx_i^\mu}{dt_i}(t_i) \left(\int_{\boldsymbol{k}} e^{i\boldsymbol{k}\cdot\boldsymbol{x}_i(t_i)} \boldsymbol{A}_{\boldsymbol{k}\mu}(t_i) \right) dt_i \approx \sum_i e_i \left(\int_{\boldsymbol{k}} e^{i\boldsymbol{k}\cdot\boldsymbol{x}_i(t_i)} (\boldsymbol{A}_{\boldsymbol{k}0}(t_i) - v_a \boldsymbol{A}_{\boldsymbol{k}a}(t_i)) \right) dt_i. \tag{8.11}$$

In this expansion, it is possible to recognise a leading-order coupling to the temporal photon, and an order v vertex coupling to the spatial photon (Rothstein, 2016, pp. 19–20).

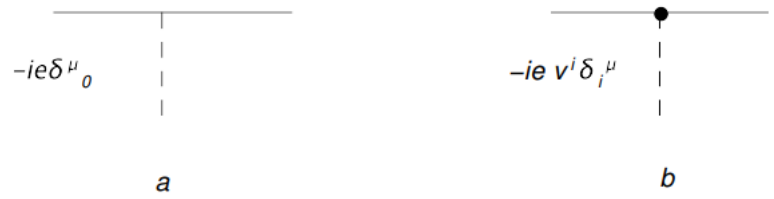

FIGURE 8.1: Feynman rules for the interaction of the source with a photon: (a) leading order in v, (b) $\mathcal{O}(v)$ interaction. Omitted are the explicit factors of $\int_{\boldsymbol{k}} e^{i\boldsymbol{k}\cdot\boldsymbol{x}_i(t_i)}$ associated with the potential $\boldsymbol{A}_{\boldsymbol{k}}$ at the vertex coupling to worldlines $x_i(t_i)$ (Rothstein, 2016, p. 20).

The last term, and last Feynman rule, we need to consider for this theory is coming from the term describing the corrections to instantaneity in equation 8.9. The leading order propagator for this term is given by

$$\langle \boldsymbol{A}_{\boldsymbol{k}\mu}(t_1) \boldsymbol{A}_{\boldsymbol{k}'\nu}(t_2) \rangle = i(2\pi)^3 g_{\mu\nu} \delta^3(\boldsymbol{k} - \boldsymbol{k}') \frac{d}{dt_1} \frac{d}{dt_2} \delta(t_1 - t_2) \frac{1}{\boldsymbol{k}^4}, \tag{8.12}$$

and depicted in figure 8.2 (Rothstein, 2016, p. 20).

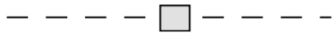

FIGURE 8.2: The box corresponds to the first correction to instantaneity. It can be thought of as the corrected propagator. Higher-order corrections to instantaneity, i.e. with n insertions of the box go as $\sim \frac{1}{(k_i^2)^n} \left(\frac{d}{dt_1} \frac{d}{dt_2} \right)^n \delta(t_1 - t_2)$ (Rothstein, 2016, p. 20).

Now that all the Feynman rules for this theory have been derived, we can see that only three diagrams can be constructed up to order v^2, they are depicted in figure 8.3.

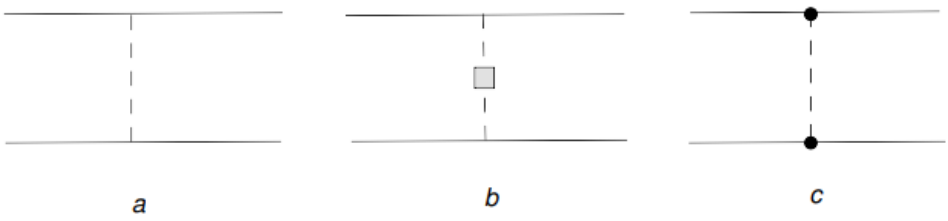

FIGURE 8.3: Feynman diagrams generating the potentials up to order v^2: (a) leading order Coulomb potential, (b) instantaneity correction, and (c) velocity dependent vertex correction (Rothstein, 2016, p. 21).

8.2.2 Calculating the potentials

The potentials for these first three diagrams can be calculated from the Feynman rules and the contributing diagrams. Doing this for diagram (a) in figure 8.3 results in the Coulomb potential (Rothstein, 2016, pp. 14, 20–22):

$$V_C = \frac{e_1 e_2}{4\pi|\boldsymbol{x}_1 - \boldsymbol{x}_2|}. \tag{8.13}$$

And the first relativistic correction is calculated from both diagrams (b) and (c) in figure 8.3, which results in the potential (Rothstein, 2016, p. 14):

$$V_{1PC} = -\frac{e_1 e_2}{8\pi r}\left(\boldsymbol{v}_1 \cdot \boldsymbol{v}_2 + \boldsymbol{v}_1 \cdot \frac{\boldsymbol{x}_1 - \boldsymbol{x}_2}{|\boldsymbol{x}_1 - \boldsymbol{x}_2|}\boldsymbol{v}_2 \cdot \frac{\boldsymbol{x}_1 - \boldsymbol{x}_2}{|\boldsymbol{x}_1 - \boldsymbol{x}_2|}\right). \tag{8.14}$$

8.3 Radiated power loss

After integrating out the potential field, the effective Lagrangian has the form

$$L = \sum_i V_i + L_{rad}(\bar{A}(x)), \tag{8.15}$$

where we have dropped the kinetic terms which do not play a role in this part. However, not all contributions of $1/r$ order have been eliminated yet, because there are still couplings between the potential and the worldlines at this scale. In order to remove these couplings, we have to apply the multipole expansion. We first consider the coupling of the radiation photon, which can be expanded as follows in the centre-of-mass frame:

$$\sum_i e_i v_\nu^i A^\nu(x_i) = \sum_i e_i (v_\nu^i A^\nu(t,0) - v_\nu^i (\boldsymbol{x}^i \cdot \boldsymbol{\partial}) A^\nu(t,0) + \cdots) \tag{8.16}$$

$$= Q A_0(t,0) + \boldsymbol{p} \cdot \boldsymbol{E}(t,0) + \cdots \tag{8.17}$$

Q represents the total charge, and $\boldsymbol{p}$ is the net dipole moment. The first order in v gives the electric dipole, and including higher orders in v would generate the magnetic dipole and electric quadrupole, etc. In this expansion the scale $1/r$ has been completely eliminated and the multipole moments belong to the composite object (Rothstein, 2016, pp. 22–23).

8.3.1 Diagrammatic approach

To calculate the power loss we consider the leading order diagram depicted in figure 8.4. Even though the diagram represents the situation in which the emitted graviton is re-absorbed by the system, it can be used to compute the radiated power via the optical theorem that we discussed in section 7.2.2. Instead of deriving the Feynman rules for this diagram, we can also calculate the contribution from the diagram by first identifying the Wick contraction from which the diagram arises, then calculating the diagram's amplitude, and performing the integral (Rothstein, 2016, p. 23).

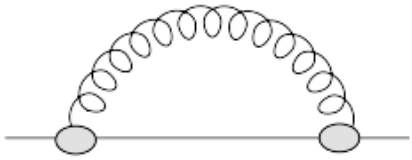

FIGURE 8.4: Feynman diagram responsible for the leading order power loss (Rothstein, 2016, p. 23).

The only possible Wick contraction in the dipole interaction is given by

$$-\frac{1}{2}\int dt_1 dt_2 p_i(t_1)p_j(t_2)\langle T\{\partial_i A_0(t_1,0)\partial_j A_0(t_2,0)+\partial_0 A_i(t_1,0)\partial_0 A_j(t_2,0)\}\rangle. \tag{8.18}$$

Where we can use the usual radiation photon propagator in the Feynman gauge:

$$\int [d^4x]e^{ik\cdot x}\langle T\{A_\mu(x)A_\nu(0)\}\rangle = \frac{-ig_{\mu\nu}}{k^2+i\epsilon}. \tag{8.19}$$

And we have rotational invariance which gives

$$\langle \partial_i A_0(t_1,0)\partial_j A_0(t_2,0)\rangle = i\frac{1}{3}\int \frac{[d^4k]\delta_{ij}\boldsymbol{k}^2}{k^2}e^{-ik_0\cdot(t_1-t_2)}. \tag{8.20}$$

Combining this gives the following amplitude:

$$iM = i\frac{1}{2}\int dt_1 dt_2 \int \frac{[d^4k]\left(-\frac{\boldsymbol{k}^2}{3}+k_0^2\right)}{k^2+i\epsilon}\boldsymbol{p}(t_1)\cdot\boldsymbol{p}(t_2)e^{-ik_0(t_1-t_2)} \tag{8.21}$$

$$= -\int dt_1 dt_2 \int \frac{[d^3k]\left(-\frac{\boldsymbol{k}^2}{3}+k^2\right)}{4k}\boldsymbol{p}(t_1)\cdot\boldsymbol{p}(t_2)e^{-ik(t_1-t_2)}, \tag{8.22}$$

which yields

$$\operatorname{Im} M = \frac{1}{6}\int dt_1 dt_2 \int [d^3k]|\boldsymbol{k}|\boldsymbol{p}(t_1)\cdot\boldsymbol{p}(t_2)e^{-i|\boldsymbol{k}|(t_1-t_2)}. \tag{8.23}$$

The last steps in calculating the dipole radiation consist of weighing this result by the energy, and using that

$$\operatorname{Re}\ln(Z[J]) = -\frac{\Gamma T}{2}, \tag{8.24}$$

where Γ is the width of the state, corresponding to a decay rate Γ^{-1}, and T is the observation time. The dipole radiation formula is then given by

$$\langle P\rangle = \frac{1}{6\pi T}\int dt\ddot{\boldsymbol{p}}(t)\cdot\ddot{\boldsymbol{p}}(t), \tag{8.25}$$

with

$$\boldsymbol{p_i} = \sum_i e_i\boldsymbol{x}_i \tag{8.26}$$

giving the dipole moment (Rothstein, 2016, pp. 9, 15, 23–24).

Chapter 9

Gravitational Binary Inspiral

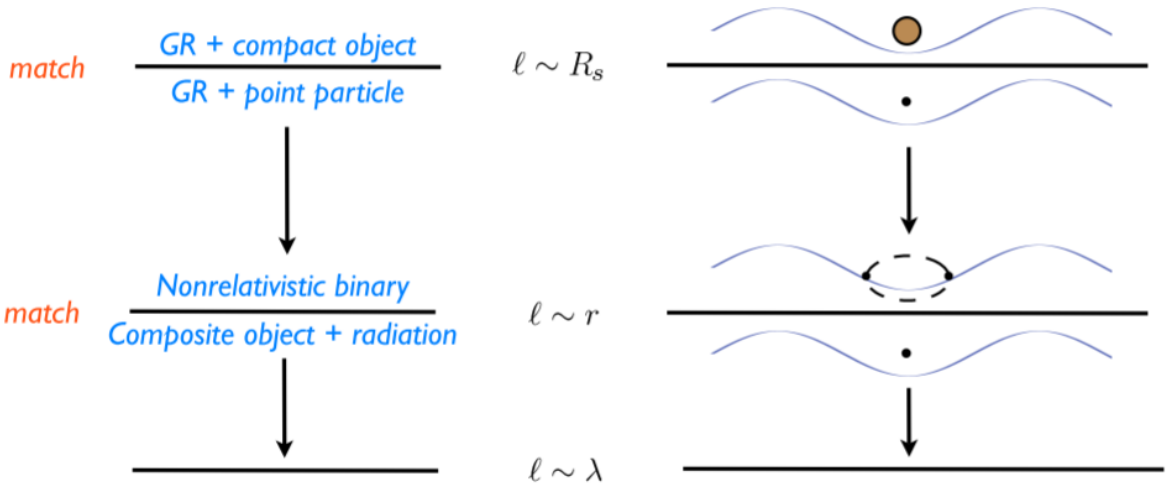

FIGURE 9.1: Graphical representation of the step-like construction of a tower of effective field theories for the binary problem in General Relativity. From top to bottom, the characteristic values of the length scale l are: the size of the compact object R_s, the orbital radius r, and the radiation wavelenght λ (Cannella, 2011, p. 46).

The full effective theory approach for General Relativity includes a version of all the steps described above for the scalar and electrodynamic theories, however, in the gravitational situation, there are some extra complications which we will discuss in this section. The complete set of steps to take is as follows:

- **Parameterization of ignorance.** In this step the degrees of freedom at the source radius scale R_s are dealt with. Some finite-size effects beyond the minimal coupling are included in the point-particle action, which could be for extended objects for example tidal and dissipative effects. When these effects vary on distances of order $|\boldsymbol{k}|^{-1}$, the finite-size effects entering in the action are of power $|\boldsymbol{k}|R_s$ (Porto, 2016, p. 25).
- **Conservative dynamics.** These are the (off-shell) potential modes that we have also seen

in the scalar field theory, which occur at the orbit scale. For small velocities, these interactions can be treated as instantaneous, plus time derivatives yielding velocity corrections as perturbations. The equations of motions can be extracted in this step from the binding potential energy. The finite-size effects for compact objects scale as powers of $R_s/r \simeq v^2$, which can be seen from the virial theorem combined with the fact that the potential modes vary on a scale $|\boldsymbol{k}| \simeq 1/r$ as probes for the internal structure of the objects (Porto, 2016, p. 25).

- **Radiated power.** At the scale of radiation the multipole expansion comes in to describe the point-like sources in the binary system. The multipole expansion for a binary inspiral consists of a series of ($l \geq 2$) multipole moments, (I^L, J^L), scaling as $I^L \sim Mr^l$.The expansion parameter is given by $|\boldsymbol{k}|r$, with $|\boldsymbol{k}|^{-1} \sim \lambda_{rad}$. The multipoles are a function of the dynamical variables from the two steps above, like positions, velocities, and spins. And the changes in energy of the system and gravitational wave amplitude are expressed in terms of derivatives of these multipoles (Porto, 2016, p. 26).

- **Hereditary effects.** From this step the non-linear contributions start to become more prominent. The hereditary effects are included, which account for the interaction of the emitted gravitational wave with the static potential, thus an interaction between the effects from the λ_{rad}- and the r-scale in figure 9.1. These interaction effects are also referred to as the 'tail effects', and contribute to the radiated power loss. In this step, the time-dependent contributions arising from non-linear self-interactions in the radiation field, a memory effect, also contributes (Porto, 2016, p. 26).

- **Radiation-reaction.** This step accounts for the effect of the back-reaction of gravitational waves on the motion of the binary system. It includes a non-linear coupling that causes a subtle interplay between different regions/scales with both conservative and dissipative contributions. They are incorporated in the EFT framework by using appropriated retarded Green's functions (Porto, 2016, p. 26).

The first three steps have been described for the spin-0 and spin-1 fields already. We will briefly discuss these in the spin-2 field, for the gravitational binary inspiral. The first step, the parameterization of ignorance, is similar to the process of taking the finite-size effects into account in section 8.1, and we will call it the "worldline effective theory". The steps concerning the conservative dynamics and the radiated power are part of what is often referred to as "non-relativistic General Relativity" and have been discussed in the contexts of both the scalar and Maxwell theory. The last two steps, which take into account hereditary effects and radiation-reaction, have not yet been discussed and will be introduced briefly at the end of this chapter.

9.1 Worldline effective theory

9.1.1 Point-like source approximation

Similar to the procedure in the Maxwell case, we start by integrating out the finite-size effect on the R_s scale. We start systematically doing this, by splitting the metric field as

$$g_{\mu\nu} = \eta_{\mu\nu} + \frac{h_{\mu\nu}}{M_{Pl}}. \tag{9.1}$$

The cut-off scale, M_{Pl} here, is the Planck mass at which quantum gravity is expected. We can ignore contributions from that scale since they are negligible in the classical regime of the binary dynamics. The Planck mass relates to Newton's constant according to the relation $\frac{1}{M_{Pl}^2} = 32\pi G$ (Cannella, 2011, pp. 51–52). This shows that an expansion of the metric field in powers of $\frac{1}{M_{Pl}}$ is equivalent to an expansion in powers of G, thus this process of integrating out the finite-size effects of the compact objects of the binary at scale R_s is what we have referred to as the post-Minkowskian expansion in section 6.1.

Inserting this expansion of the metric into the Einstein-Hilbert action that we saw in equation 2.33, which we can write as

$$S_{EH} = -2M_{Pl}^2 \int \sqrt{g(x)} R(x) d^4x, \tag{9.2}$$

we get the following expansion (Cannella, 2011, pp. 51–53):

$$S_{EH} = \int d^4x \left[(\partial h)^2 + \frac{h(\partial h)^2}{M_{Pl}} + \frac{h^2(\partial h)^2}{M_{Pl}^2} + \cdots \right]. \tag{9.3}$$

The first term corresponds to the free propagation of a graviton, and the higher-order terms introduce gravitational self-interactions. Equation 9.3 can be solved iteratively in powers of $\frac{R_s}{r} \ll 1$ to obtain an expression for $h_{\mu\nu}$. In the effective theory, the limit $R_s \to 0$ is taken and the effects from the scale $r < R_s$ are incorporated in the boundary conditions. Each compact object, which is in our case a black hole or a neutron star, can then be described as a localized source (Porto, 2016, p. 27). The interaction of the gravitational field with a point particle is given by the minimal coupling, in the expansion around the Minkowski space from equation 9.1 this is given by

$$S_{pp} = -m \int \left[\left(\eta_{\mu\nu} + \frac{h_{\mu\nu}}{M_{Pl}} \right) dx^\mu dx^\nu \right]^{1/2} = -m \int d\bar{\tau} \sqrt{1 + \frac{h_{\mu\nu} v^\mu v^\nu}{M_{Pl}}} \tag{9.4}$$

$$= -m \int d\bar{\tau} - \frac{m}{2M_{Pl}} \int d\bar{\tau} h_{\mu\nu} v^\mu v^\nu - \frac{m}{8M_{Pl}^2} \int d\bar{\tau} (h_{\mu\nu} v^\mu v^\nu)^2 + \cdots, \tag{9.5}$$

where $d\bar{\tau}^2 = \eta_{\mu\nu} dx^\mu dx^\nu$ and $v^\mu \equiv dx^\mu / d\tau$. We can consider these point-like matter sources

to be static, because they have a three momentum $\boldsymbol{p} \sim mv$ with v the orbital velocity, while the gravitons will have an approximate three-momentum of $\boldsymbol{k} \sim \hbar$. Thus, the recoil of the macroscopic object in our point-particle description due to the graviton is negligible and we can consider the compact objects of the binary systems as static sources of gravitons. The Feynman representations corresponding to the vertices in equation 9.5 are presented in figure 9.2. In the diagrams, the continuous lines represent the compact objects, the arrows describe the flow of time of the particle worldlines, and each curly line represents a factor $h_{\mu\nu}v^\mu v^\nu$.

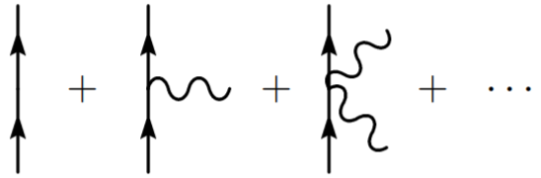

FIGURE 9.2: Diagrammatic representation of the terms in equation 9.5 that represent the interaction between a static point-particle source and (a) graviton(s) (Cannella, 2011, p. 54).

Another way of writing the action terms from equation 9.4 is in terms of the stress-energy tensor for a point particle, $T^{\mu\nu}_{pp}$, given by

$$T^{\mu\nu}_{pp}(x) = m \int d\sigma \frac{u^\mu u^\nu}{\sqrt{u^2}} \frac{\delta^4(x - x(\sigma))}{\sqrt{g(x)}} + \cdots , \tag{9.6}$$

where at higher-order gravitational non-linear effects will show up. The terms of the action that describe the coupling between the point-particle and the gravitational field are then given by

$$-\frac{1}{2M_{Pl}} \int d^4x T^{\mu\nu}_{pp}(x) h_{\mu\nu}(x) \to -\frac{m}{2M_{Pl}} \int dt h_{00}(t, 0) + \cdots , \tag{9.7}$$

where, for the moment, we only have retained the h_{00}-polarization, and we can take the static limit and evaluate the expression at the origin to compute the metric for an isolated object. This point-like approximation leads to divergences due to the non-linear structure of the field equations. These can be removed by counter-terms proportional to higher-order derivatives of the metric. At the same time, these counter-terms will be the terms in which the finite-size effects of the objects are incorporated (Porto, 2016, p. 27). However, Birkhoff's theorem shows that as long as the spherical symmetry of a mass distribution is maintained, the Schwarzschild metric is a solution despite possible time variations in the mass distribution (Johansen and Ravndal, 2006, p. 538). As a consequence, the counter-terms and the non-linear worldline couplings do not contribute to the computation of the classical one-point function.

9.1.2 Gauge fixing

To get rid of redundant degrees of freedom due to the coordinate invariance discussed in section 2.2.1, we need to add a gauge fixing term to the action. An example of a suitable gauge is the harmonic gauge, $\Gamma_\mu = 0$, with

$$\Gamma_\mu = \partial_\alpha h^\alpha_\mu - \frac{1}{2}\partial_\mu h^\alpha_\alpha. \tag{9.8}$$

At the action-level this means that we have to add the term

$$S_{GF} = \int d^4x \Gamma_\mu \Gamma^\mu. \tag{9.9}$$

As a result, there is a unique solution to the Feynman propagator given by:

$$\Delta_{F\alpha\beta\mu\nu} = P_{\alpha\beta\mu\nu}\Delta_F(t - t', \boldsymbol{x} - \boldsymbol{x}'), \tag{9.10}$$

in which Δ_F is the Feynman propagator that was defined in equation 7.7, and

$$P_{\alpha\beta\mu\nu} = \frac{1}{2}(\eta_{\alpha\mu}\eta_{\nu\beta} + \eta_{\alpha\nu}\eta_{\mu\beta} - \eta_{\alpha\beta}\eta_{\mu\nu}). \tag{9.11}$$

is responsible for the tensorial structure necessary to compute the contributions from the diagrams later (Porto, 2016, p. 28).

9.1.3 Non-linearities

At this point, we add the non-linearities as we have also done in section 7.1.3 for the scalar situation. These occur for the gravitational situation at higher orders in G, coming from both the Einstein-Hilbert action and the coupling to the source. The worldline non-linearities in equation 9.6 do not contribute to the metric of an isolated object at the classical level. These will only be important later on in the binary problem, so we can keep using equation 9.7 for now. What is different from the scalar situation, is that the non-linearities in General Relativity involve derivatives, as can be seen in equation 9.3. These derivatives add extra factors of k^2 to the vertices, improving the situation for the IR divergences, but worsening the UV problem (Porto, 2016, p. 28).

To incorporate the gravitational non-linearities, we first rewrite the perturbation of the metric term as

$$\frac{h_{\mu\nu}}{M_{Pl}}(k_0, \boldsymbol{k}) = -\frac{i}{2M_{Pl}^2}P_{\mu\nu\alpha\beta}\frac{i}{k_0^2 - \boldsymbol{k}^2}\mathcal{T}^{\alpha\beta}(k_0, \boldsymbol{k}), \tag{9.12}$$

where $\mathcal{T}^{\alpha\beta}(x)$ is introduced as the pseudo stress-energy tensor, which is an extension of the stress-energy tensor that incorporates the energy-momentum of gravity. At leading order in G

it is given by

$$\mathcal{T}^{\mu\nu}_{(1)}(k_0, \boldsymbol{k}) = m(2\pi)\delta(k_0)e^{-i\boldsymbol{k}\cdot\boldsymbol{x}(\tau)}u^\mu u^\nu, \tag{9.13}$$

and it can be computed at higher orders by using the background field method. This method starts by splitting up the metric perturbation into the following components:

$$h_{\mu\nu} = \underbrace{\mathcal{H}_{\mu\nu}}_{\text{background}} + \underbrace{H_{\mu\nu}}_{\text{perturbation}} . \tag{9.14}$$

Even though the method looks similar to the procedure we have seen for integrating out the potential field on the radiation scale, there is no radiation in the static limit that we are still considering. It can be considered here to be a trick to integrate out the perturbation. The expansion of the metric perturbation yields the path integral

$$e^{iS_{eff}[\mathcal{H}_{\mu\nu}]} \equiv e^{-\frac{i}{2M_{Pl}}\int T^{\mu\nu}_{pp}(x)\mathcal{H}_{\mu\nu}(x)} \int DH_{\mu\nu} \exp\Bigg[iS_{EH}[\mathcal{H}_{\mu\nu} + H_\mu\nu] + iS^{(\mathcal{H})}_{GF}[H_{\mu\nu}] - \frac{i}{2M_{Pl}}\int T^{\mu\nu}_{pp}(x)H_{\mu\nu}(x)\Bigg]. \tag{9.15}$$

To ensure invariance under coordinate transformations, we need to adapt the gauge fixing term from equation 9.8 to

$$\Gamma^{(\mathcal{H})}_\mu = \nabla^{(\mathcal{H})}_\alpha H^\alpha_\mu - \frac{1}{2}\nabla^{(\mathcal{H})}_\mu H^\alpha_\alpha, \tag{9.16}$$

where $\nabla^{(\mathcal{H})}$ is the covariant derivative compatible with the $\mathcal{H}_{\mu\nu}$-metric. This also ensures conservation of the pseudo stress-energy tensor, including the self-energy in the gravitational field, as described by the Ward identity:

$$\partial_\alpha \mathcal{T}^{\alpha\beta}(x) = 0. \tag{9.17}$$

This allows us to compute the contribution at order G^2, which corresponds to the diagram in figure 9.3:

$$\mathcal{T}^{\alpha\beta}_{(2)}(k) = (2\pi)\delta(k_0)\frac{m^2}{32M^2_{Pl}}[-7(\eta^{\alpha\beta}k^2 - k^\alpha k^\beta) + k^2 v^\alpha v^\beta]\int_{\boldsymbol{q}} \frac{1}{\boldsymbol{q}^2(\boldsymbol{q}^2 + \boldsymbol{k}^2)} \tag{9.18}$$

$$= (2\pi)\delta(k_0)\frac{m^2}{16M^2_{Pl}|\boldsymbol{k}|}\left[-\frac{7}{32}(\eta^{\alpha\beta}k^2 - k^\alpha k^\beta) + \frac{1}{32}k^2 v^\alpha v^\beta\right], \tag{9.19}$$

where $v^\mu = (1, 0)$. With this result, and equation 9.12, we can compute the next order of the curved spacetime metric:

$$g_{00} = 1 - \frac{2Gm}{r} + 2\left(\frac{Gm}{r}\right)^2 + \cdots \tag{9.20}$$

$$g_{ij} = -\delta_{ij}\left[1 + \frac{2Gm}{r} + 5\left(\frac{Gm}{r}\right)^2 + \cdots\right]. \tag{9.21}$$

This result corresponds to Schwarzschild's solution in harmonic coordinates as a series expansion in powers of R_s/r (Porto, 2016, pp. 28–29).

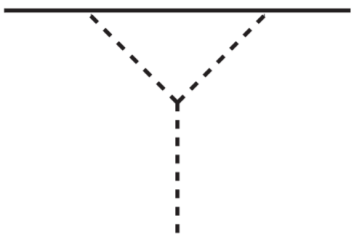

FIGURE 9.3: Feynman diagram to compute the $\mathcal{O}(G^2)$ pseudo stress-energy tensor contribution (Porto, 2016, p. 31).

9.1.4 Divergences

Some of the integrals we have encountered so far, and even more that occur at higher orders, run into divergences. There are different types of divergences: power-law divergences, and logarithmic divergences. Both will be briefly discussed in relation to examples of diagrams that introduce these types of divergences, and the results of solving the divergences are given for those diagrams. However, for a more extensive discussion of the full procedures of dealing with divergences, it is recommended to take a look at the references, such as (Porto, 2016, pp. 30–34).

Starting with the power-law divergences, which occur, for example, when the ∂^2 from the cubic vertex in figure 9.3 hits the propagator. A diagram of such a situation is given in figure 9.4, and contributions from these types of diagrams are set to zero in the procedure called 'dimensional regularisation'. The divergent part of the integral corresponding to the diagram in figure 9.4 is given by

$$A^{ij}(\boldsymbol{k}) \equiv \int_{\boldsymbol{q}} \frac{\boldsymbol{q}^i \boldsymbol{q}^j}{\boldsymbol{q}^2(\boldsymbol{k}+\boldsymbol{q})^2}, \tag{9.22}$$

which runs into problems for $i = j$, when the numerator cancels out of the propagator. Setting the trace of the integral to zero will still leave other contributions from the integral which we

therefore need to compute. The result of the dimensional regularisation of the integral is:

$$A^{ij}(\boldsymbol{k}) = \int_{\boldsymbol{q}} \frac{\boldsymbol{q}^i \boldsymbol{q}^j}{\boldsymbol{q}^2(\boldsymbol{k}+\boldsymbol{q})^2} = \frac{1}{64|\boldsymbol{k}|}(3\boldsymbol{k}^i\boldsymbol{k}^j - \boldsymbol{k}^2\delta^{ij}), \tag{9.23}$$

the full computation of which can be found in (Porto, 2016, p. 30).

FIGURE 9.4: Diagram corresponding to the power-law divergence at $\mathcal{O}(G^2)$ (Porto, 2016, p. 30).

Another type of divergence is the logarithmic divergence, such as occur in the diagrams in figure 9.5. To regularize these we need to consider the responsible integrals in d spacetime dimensions. The relevant scalar integral is given by

$$I_0(\boldsymbol{k}) = \int \frac{d^{d-1}\boldsymbol{q}}{(2\pi)^{d-1}} \frac{d^{d-1}\boldsymbol{p}}{(2\pi)^{d-1}} \frac{1}{\boldsymbol{q}^2\boldsymbol{p}^2(\boldsymbol{q}+\boldsymbol{p}+\boldsymbol{k})^2}. \tag{9.24}$$

Analytic continuation of this integral in d and expanding around $\epsilon \simeq 0$ for $\epsilon \equiv 4 - d$, as is explained in (Porto, 2016, pp. 31–32), yields the result

$$I_0(\boldsymbol{k}) = \frac{1}{32\pi^2}\left[\frac{1}{\epsilon} + \log(4\pi) - \gamma_E + 3 - \log\frac{\boldsymbol{k}^2}{\mu^2}\right] + \mathcal{O}(\epsilon), \tag{9.25}$$

where $\gamma_E \simeq 0.572$ is the Euler-Mascheroni constant, and μ is the renormalization scale.

FIGURE 9.5: Feynman diagrams contributing at $\mathcal{O}(G^3)$ (Porto, 2016, p. 31).

In some cases, there remain poles after dimensional regularization. These poles can be removed by adding counter-terms, which absorb the divergences. This is part of the renormalization of the theory, and there are several renormalization schemes available. In (Porto, 2016, pp. 32–34) the minimal subtraction bar ($\bar{MS}$) scheme is explained, also concerning the renormalization group flow in which the coefficients of the counter-terms are chosen as functions of the parameter $\boldsymbol{k}$.

9.1.5 Effective action

To integrate out the first and smallest scale of our system, R_s, this involves adding the finite-size effects to the point-particle action, according to the procedure discussed in section 8.1. In the gravitational case we split the metric as

$$g_{\mu\nu} = \underbrace{g^S_{\mu\nu}}_{\text{short-distance}} + \underbrace{g^L_{\mu\nu}}_{\text{long-distance}} , \tag{9.26}$$

where the short and long distances are taken as compared to the scale R_s. The effective theory will consist of the long-wavelength metric field, $g^L_{\mu\nu}$, and the centre-of-mass of the compact object, $x^\mu_{cm}(\sigma)$. The effective action describing this theory, $S_{eff}[x_{cm}, g^L_{\mu\nu}]$, is constructed by integrating out the short-distance modes in the saddle-point approximation that we saw in equation 7.2. For a compact object in our binary problem we have

$$\exp\left\{iS_{EH}[g^L_{\mu\nu}(x)] + iS_{eff}[x^\alpha_{cm}(\sigma), g^L_{\mu\nu}(x)]\right\} = \int Dg^S_{\mu\nu}(x) D\delta x^\alpha_p(\sigma_p) \exp\left\{iS_{EH}[g_{\mu\nu}(x)] + iS_{int}[x^\alpha_p(\sigma_p), g^S_{\mu\nu}(x)]\right\}, \tag{9.27}$$

where $S_{int}[x^\alpha_p, g^S_{\mu\nu}]$ describes the dynamics of the internal degrees of freedom which depends on the short-distance field $g^S_{\mu\nu}$ and the positions of all the constituents of the object $x^\mu_p(\sigma_p)$. The constituents' positions are integrated out by the integral over the displacement with respect to the centre-of-mass, $\delta x^\alpha_p \equiv x^\alpha_p - x^\alpha_{cm}$ (Porto, 2016, p. 34).

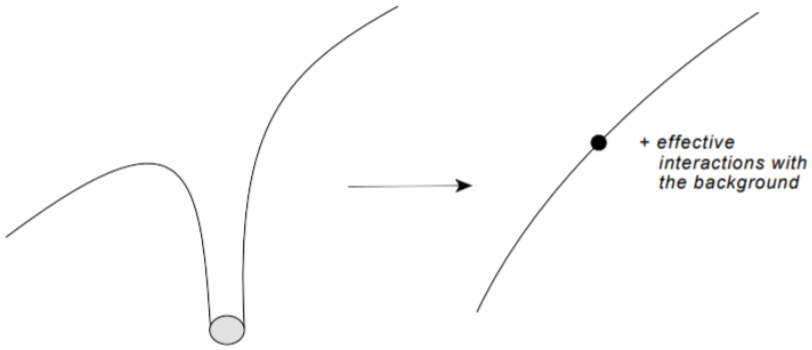

FIGURE 9.6: The idea behind the worldline effective theory: the full space-time geometry of the object is replaced by a point particle together with some effective action interactions with its slowly varying background (Kol and Smolkin, 2012, p. 4).

The exact form of the effective action is unknown, but we do know that it must satisfy the symmetries of the long-distance physical system: diffeomorphism and reparameterization invariance. Therefore, we construct an effective action consisting of all the terms respecting these

symmetries (Porto, 2016, pp. 34–35):

$$S_{eff}[x_{cm}, g^L_{\mu\nu}] = \int d^4x d\sigma \delta^4(x - x_{cm}(\sigma)) \Bigg(- m\sqrt{g^L_{\mu\nu}(x) u^\mu_{cm}(\sigma) u^\nu_{cm}(\sigma)} + C_R \int R^L[g^L_{\mu\nu}] \sqrt{g^L_{\mu\nu}(x) u^\mu_{cm}(\sigma) u^\nu_{cm}(\sigma)} + C_V \int R^L_{\mu\nu}[g^L_{\mu\nu}] \frac{u^\mu_{cm}(\sigma) u^\nu_{cm}(\sigma)}{\sqrt{g^L_{\mu\nu}(x) u^\mu_{cm}(\sigma) u^\nu_{cm}(\sigma)}} + \cdots \Bigg). \quad (9.28)$$

Due to Birkhoff's theorem, the coefficients C_R and C_V can be set to zero, which means that the terms containing the Ricci tensor $R_{\mu\nu}$ are dropped. This is allowed because $R_{\mu\nu} = 0$ in the vacuum Einstein field equations. After a suitable redefinition, the terms which do not occur in the equations of motions and are referred to as 'redundant' are removed, because they do not alter the physical prediction of the theory (Goldberger, 2007, pp. 41–43). Higher powers of the Riemann tensor $R_{\mu\nu\alpha\beta}$ do occur through its components of the electric and magnetic type parity given by

$$E_{\mu\nu} = R_{\mu\nu\alpha\beta} v^\alpha v^\beta, \quad (9.29)$$

$$B_{\mu\nu} = \epsilon_{\mu\nu\beta\rho} R^{\alpha\beta}{}_{\nu\sigma} v^\rho v^\sigma, \quad (9.30)$$

respectively. This allows us to rewrite the effective action from equation 9.28 as

$$S_{eff}[x, g_{\mu\nu}] = c_E \int d\tau E_{\mu\nu} E^{\mu\nu} + c_B \int d\tau B_{\mu\nu} B^{\mu\nu} + \cdots . \quad (9.31)$$

Where we have dropped the sub- and superscripts of x_{cm} and $g^L_{\mu\nu}$, and included reparameterization invariance by switching to the proper time. The terms in this effective action encode the finite-size effects of the objects, here given by the electric and magnetic quadrupole moments. The coefficients c_E and c_B can be computed by matching (Cannella, 2011, p. 52). Conceptually, the procedure of matching consists of two stages: (1) calculating a convenient observable in the full theory and expanding the result in the low energy limit, and (2) comparing this result with the prediction of the effective theory and fixing the coefficients on which the operators of the effective theory depend (Cannella, 2011, p. 46). Fixing c_E and c_B involves splitting the components of the quadrupole moments into background and response components, corresponding to the short-distance and long-wavelength modes respectively. The results of the matching procedure, as performed in (Porto, 2016, pp. 36–39), (Goldberger and Rothstein, 2006a) and (Goldberger, 2007), show that both coefficients scale as $M^2_{Pl} R^5_s$. Considering the scaling of the full first term contribution:

$$\frac{c_{E/B}}{M^2_{Pl}} \int (\partial_i \partial_j H_{00})^2 dt \sim c_{E/B} \frac{G^2 m^2}{r^6} \frac{r}{v} \sim \left(\frac{R_s}{r}\right)^6 \frac{L}{v^2} \sim L v^{10}, \quad (9.32)$$

where it was used that for a gravitationally bound system $\frac{H_{00}}{M_{Pl}} \sim \frac{Gm}{r}$, and derivatives add extra factors of $1/r$ (Porto, 2016, p. 44). This means that the quadrupole moments do not contribute to the binary dynamics until the 5PN order (Cannella, 2011, p. 52).

It should be noted here that it has been shown that for this matching procedure the differences between neutron stars and black holes become relevant. In fact, it has been shown that the coefficients c_E and c_B from equation 9.31 vanish for black holes (Kol and Smolkin, 2012). The first non-zero terms include time derivatives, such as $\dot{E}_{\mu\nu}\dot{E}^{\mu\nu}$, thus also altering the scaling of these effects in the effective action (Porto, 2016, p. 44).

9.2 Non-relativistic General Relativity

The next two steps in the procedure are considering the conservative dynamics and the radiated power. We have seen these steps in sections 7.1 and 7.2 for the scalar theory, and in sections 8.2 and 8.3 for Maxwell's theory of electrodynamics. In the gravitational situation, these two steps are part of the non-relativistic General Relativity (NRGR) formalism, which emphasises the small-velocity approximation that is considered. The procedure is very similar to what we have seen so far, only with the addition of gauge fixing issues, tensor structure, and more complicated non-linear interactions.

The decomposition of the metric perturbation into potential and radiation modes is as follows:

$$h_{\mu\nu} = \underbrace{H_{\mu\nu}}_{\text{potential}} + \underbrace{\bar{h}_{\mu\nu}}_{\text{radiation}} , \tag{9.33}$$

where the following scaling applies

$$(k_0, \boldsymbol{k})_{pot} \sim (v/r, 1/r), \ (k_0, \boldsymbol{k})_{rad} \sim (v/r, v/r). \tag{9.34}$$

The potential modes appear off-shell and mediate the binding forces between the objects in the binary. Integrating out the $H_{\mu\nu}$ field in the background radiation modes, which appear as the on-shell propagating degrees of freedom, will give the non-relativistic General Relativity theory that we are looking for. The non-linear coupling between these modes complicates the procedure, but as we will see, the effective field theory framework can deal with this by systematically separating the relevant scales (Porto, 2016, p. 40). We will discuss both the binding potential and the gravitational wave radiation in the following sections.

9.2.1 Binding potential

To compute the binding potential of the gravitational binary system, we consider the real part of the functional $W[\boldsymbol{x}_a]$, because the potential modes are off-shell:

$$\mathrm{Re}\, W[\boldsymbol{x}_a] = \int dt(K[\boldsymbol{x}_a] - V[\boldsymbol{x}_a]), \tag{9.35}$$

in which $K[\boldsymbol{x}_a]$ is the kinetic part of the effective action, and $V[\boldsymbol{x}_a]$ is the binding potential we are looking to compute. $W[\boldsymbol{x}_a]$ is obtained through the integral from which we have to integrate out the potential modes:

$$e^{iW[\boldsymbol{x}_a]} = \int DH_{\mu\nu} \exp\left\{iS_{EH}[H_{\mu\nu}] + iS^{pp}_{eff}[\boldsymbol{x}_a(t), H_{\mu\nu}] + iS_{GF}[H_{\mu\nu}]\right\}, \tag{9.36}$$

where $(a = 1, 2)$, S_{GF} is the gauge fixing term that we have already seen in equation 9.1.2, and the point particle action $S^{pp}_{eff}[\boldsymbol{x}_a(t), H_{\mu\nu}]$ contains the point particle coupling to the gravitational field plus the terms that have been established when the R_s scale was integrated out. At zero-th order in G, the effective point-particle action is given by the kinetic part of the effective action,

$$W_{(0)}[\boldsymbol{x}_a] \to S^{pp}_{eff}[\boldsymbol{x}_a, \eta_{\mu\nu}] \equiv \int dt K[\boldsymbol{x}_a], \tag{9.37}$$

which still has to be expanded in powers of v. Computing higher orders of $W[\boldsymbol{x}_a]$ is done by solving for $H_{\mu\nu}$ perturbatively and plugging it back into the action. To integrate out the potential modes, we use the quasi-instantaneous Green's function

$$\langle T\{H_{\mu\nu}(t_1, \boldsymbol{x}_1)H_{\alpha\beta}(t_1, \boldsymbol{x}_2)\}\rangle = -iP_{\mu\nu\alpha\beta}\Bigg[\delta(t_1 - t_2)\int_{\boldsymbol{k}} \frac{1}{\boldsymbol{k}^2} e^{i\boldsymbol{k}\cdot(\boldsymbol{x}_1 - \boldsymbol{x}_2)} + \frac{d}{dt_1 dt_2}\delta(t_1 - t_2)\int_{\boldsymbol{k}} \frac{1}{\boldsymbol{k}^4} e^{i\boldsymbol{k}\cdot(\boldsymbol{x}_1 - \boldsymbol{x}_2)} + \cdots\Bigg]. \tag{9.38}$$

To get an expansion in the velocity for slowly moving sources, we can expand the denominator in powers of $\frac{k_0}{|\boldsymbol{k}|} \sim \frac{v/r}{1/r} \ll 1$, resulting in the propagator and velocity corrections represented in figure 7.1. From the leading order term in equation 9.38 the scaling can be determined:

$$\langle T\{H_{\mu\nu}(t, \boldsymbol{k})H_{\alpha\beta}(0, \boldsymbol{q})\}\rangle \sim \frac{1}{\boldsymbol{k}^2}\delta(t)\delta^3(\boldsymbol{k} + \boldsymbol{q}) \sim \left(\frac{1}{r}\right)^{-2}\left(\frac{r}{v}\right)^{-1}\left(\frac{1}{r}\right)^{-3} \sim r^4 v \tag{9.39}$$

$$[H_{\mu\nu}(t, \boldsymbol{k})] \sim r^2\sqrt{v}. \tag{9.40}$$

Using the virial theorem $v^2 \sim \frac{Gm}{r}$, scaling of the Planck mass $\frac{1}{M_{Pl}^2} \sim G$ and the orbital angular momentum $L = mvr$, we can see that the following scaling applies the source coupling:

$$\frac{m}{M_{Pl}} \sim \sqrt{Lv}. \tag{9.41}$$

Recalling the the point-particle action from the combination of equations 9.7 and 9.6:

$$S^{pp}_{eff}[\boldsymbol{x}_a, H_{\mu\nu}] = -\frac{m}{2M_{Pl}} \int dt \frac{v^\mu v^\nu}{\sqrt{v^\alpha v_\alpha}} H_{\mu\nu} + \cdots , \tag{9.42}$$

we can derive the scaling of the leading order interaction term, where we note that it is sufficient to consider $v^\mu = (1, \boldsymbol{v}^i)$ (Porto, 2016, pp. 40–41):

$$\left[\frac{m}{2M_{Pl}} \int H_{00} dt\right] \sim \sqrt{Lv} \left(\frac{r}{v}\right) \left(\frac{1}{r}\right)^{-3} (r^2\sqrt{v}) \sim \sqrt{L} \tag{9.43}$$

The diagram at first order in G consists of two of these interactions, which together introduce a propagating graviton that is described by the propagator in equation 9.10. We now have all the tools to compute the potential corresponding to the diagram in figure 9.7.

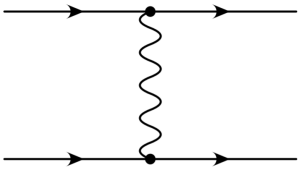

FIGURE 9.7: First diagram contributing to the computation of the potential, corresponding to the Newton potential (Cannella, 2011, p. 54).

$$W_{(1)}[\boldsymbol{x}_a, \boldsymbol{x}_b] = \left(-\frac{m_1}{2M_{Pl}} \int dt \frac{v_a^\mu v_a^\nu}{\sqrt{v_a^\alpha v_{a\alpha}}} H_{\mu\nu}\right) \left(-\frac{m_2}{2M_{Pl}} \int dt' \frac{v_b^\rho v_b^\sigma}{\sqrt{v_b^\beta v_{b\beta}}} H_{\rho\sigma}\right) \tag{9.44}$$

$$= \frac{m_1 m_2}{4M_{Pl}^2} \left(\int dt \int dt'\right) \frac{1}{\sqrt{v_a^\alpha v_{a\alpha}}\sqrt{v_b^\beta v_{b\beta}}} v_a^\mu v_a^\nu \Delta_{F\mu\nu\rho\sigma} v_b^\rho v_b^\sigma . \tag{9.45}$$

The contraction with the tensorial structure of the Feynman propagator is given by

$$v_a^\mu v_a^\nu P_{\mu\nu\rho\sigma} v_b^\rho v_b^\sigma = \frac{1}{2} v_a^\mu v_a^\nu [\eta_{\rho\mu}\eta_{\sigma\nu} + \eta_{\rho\nu}\eta_{\sigma\mu} - \eta_{\mu\nu}\eta_{\rho\sigma}] v_b^\rho v_b^\sigma \tag{9.46}$$

$$= \frac{1}{2}[(v_a \cdot v_b)^2 + (v_a \cdot v_b)^2 - (v_a \cdot v_a)(v_b \cdot v_b)] \tag{9.47}$$

$$= \frac{1}{2}[2(v_a \cdot v_b)^2 - v_a^2 v_b^2] = \frac{1}{2}[2(v_a \cdot v_b)^2 - 1]. \tag{9.48}$$

But since we are not yet interested in the higher-order contributions in v, we only get a factor $\frac{-1}{2}$ from this propagator now. Similarly the factors $\frac{1}{\sqrt{v_i^\alpha v_{i\alpha}}}$ can be dropped for now:

$$W_{(1)}[\boldsymbol{x}_a, \boldsymbol{x}_b] \to -\int dt V_N[\boldsymbol{x}_a, \boldsymbol{x}_b] \tag{9.49}$$

$$V_N = -\frac{m_1 m_2}{8M_{Pl}^2} \int_{\boldsymbol{p}} \frac{e^{-i\boldsymbol{p}\cdot(\boldsymbol{x}_a - \boldsymbol{x}_b)}}{\boldsymbol{p}^2} = -\frac{m_1 m_2}{8M_{Pl}^2} \frac{1}{4\pi|\boldsymbol{x}_a - \boldsymbol{x}_b|} = -\frac{Gm_1 m_2}{r} \tag{9.50}$$

Note that this computation is analogous to the computation in equation 7.14 that we did in the scalar theory, and that from the scaling derived in equation 9.43 we can see that this contribution scales as $\sim L$.

The same procedure can be followed to compute the contributions that scale as $\sim Lv^2$ at 1PN order. The contributing diagrams are shown in figure 9.8. Diagram (a) includes the first correction at order v^2 from the graviton propagator in equation 9.38, which can be expanded in a similar way as the propagator in 7.1. The diagrams (b) and (c) contribute to the 1PN order because they include velocity corrections from the point-particle action in equation 9.42. The leading order term in the point-particle action has a coupling of $-\frac{m}{2M_{Pl}}h_{00}$ in the Lagrangian, the two terms in the Lagrangians have couplings $-\frac{m}{M_{Pl}}h_{0i}v^i$ and $-\frac{m}{2M_{Pl}}\left(h_{ij}v^iv^j+\frac{1}{2}h_{00}v^2\right)$ (Porto, 2016, p. 128). This gives the diagrams with either two sources with an $\mathcal{O}(v)$-correction, or one of the sources having an $\mathcal{O}(v^2)$-correction. It is straightforward to see that diagrams (a), (b) and (c) all have a scaling of $\sim Lv^2$, since they all include a v^2 correction with respect to the diagram corresponding to the Newtonian potential. The potentials of these diagrams are given by (Porto, 2016, p. 42):

$$V_{9.8(a)} = -\frac{1}{2}\frac{Gm_1m_2}{r}\left(\boldsymbol{v}_1\cdot\boldsymbol{v}_2-\frac{(\boldsymbol{v}_1\cdot\boldsymbol{r})(\boldsymbol{v}_2\cdot\boldsymbol{r})}{r^2}\right), \tag{9.51}$$

$$V_{9.8(b)} = 4\frac{Gm_1m_2}{r}\boldsymbol{v}_1\cdot\boldsymbol{v}_2, \tag{9.52}$$

$$V_{9.8(c)} = -\frac{3}{2}\frac{Gm_1m_2}{r}\boldsymbol{v}_1^2. \tag{9.53}$$

Before calculating the potential corresponding to diagram (d) in figure 9.8, we first show that it contributes to the 1PN order by power counting. The term in the point-particle Lagrangian corresponding to this diagram has a coupling $\frac{m}{8M_{Pl}^2}h_{00}h_{00}$, and thus we consider the scaling of the two propagators coupling to a source:

$$\left[\frac{m}{8M_{Pl}^2}\int H_{00}^2dt\right] \sim m\left(\frac{v^2r}{m}\right)\left(\frac{r}{v}\right)\left(\frac{1}{r}\right)^{-6}(r^4v) \sim v^2. \tag{9.54}$$

Which gives a total scaling of $\sim Lv^2$ for the diagram, where the couplings between the propagators to the source, $\sim \sqrt{L}$, have also been included. For the computation of the 'seagull diagram', diagram (d) in figure 9.8, we have two propagators connecting the two sources:

$$\mathrm{Re}\,W_{9.8(d)}[\boldsymbol{x}_a] = \frac{1}{2!}\left(\frac{-im_2}{2M_{Pl}}\right)^2\frac{im_1}{8M_{Pl}^2}\int dt_1dt_2d\tilde{t}_2\langle T\{H_{00}(t_2,\boldsymbol{x}_2(t_2))H_{00}(\tilde{t}_2,\boldsymbol{x}_2(\tilde{t}_2)H_{00}^2(t_1,\boldsymbol{x}_1(t_1))\}\rangle \tag{9.55}$$

$$= -\frac{m_1^2m_2}{32M_{Pl}^4}\int dt_1dt_2d\tilde{t}_2\delta(t_1-t_2)\delta(t_1-\tilde{t}_2)(-P_{0000})^2\int_{\boldsymbol{p},\boldsymbol{q}}\frac{e^{i\boldsymbol{p}\cdot(\boldsymbol{x}_2(t_2)-\boldsymbol{x}_1(t_1))}}{\boldsymbol{p}^2}\frac{e^{i\boldsymbol{q}\cdot(\boldsymbol{x}_2(\tilde{t}_2-\boldsymbol{x}_1(t_1))}}{\boldsymbol{q}^2}, \tag{9.56}$$

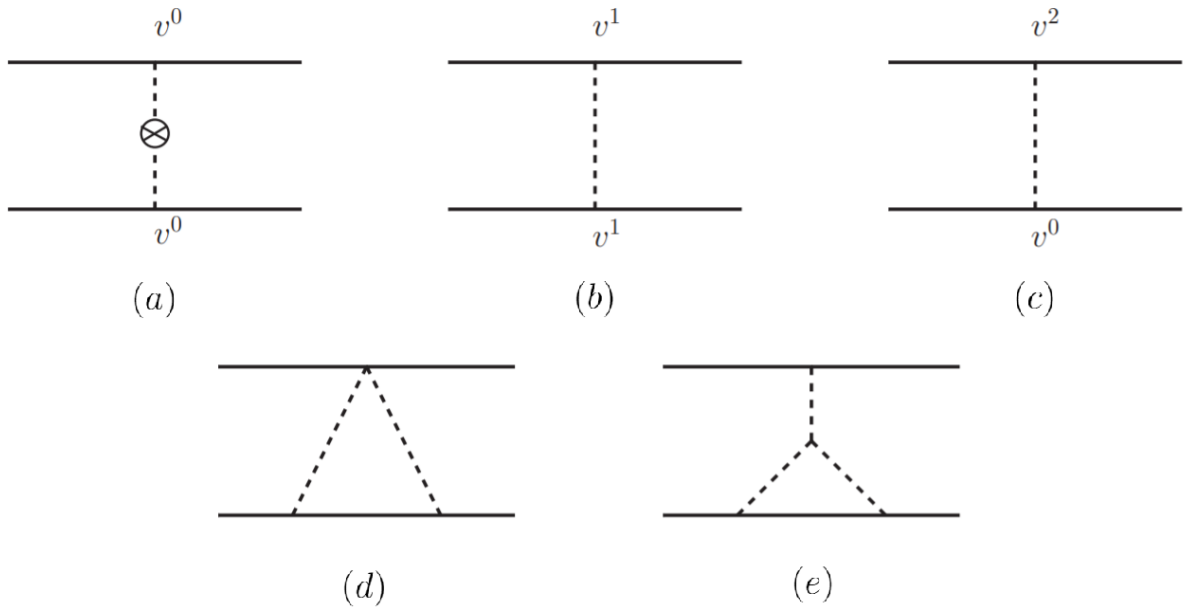

FIGURE 9.8: Feynman diagrams contributing at 1PN order. (a) corresponds to a correction to non-instantaneity, (b) and (c) correspond to different velocity corrections introduced by higher-order terms in the point-particle action in equation 9.42, (d) corresponds to a non-linear contrubtion from the point-particle source, (e) corresponds to the self-interction term of the graviton in the Einstein-Hilbert action (Porto, 2016, p. 42).

where we have used Wick contractions. This allows us to extract

$$V_{9.8(d)}[\boldsymbol{x}_a] = -\frac{m_1^2 m_2}{(4\pi)^2 128 M_{Pl}^4} \frac{1}{|\boldsymbol{x}_1(t) - \boldsymbol{x}_2(t)|^2} = -\frac{G^2 m_1^2 m_2}{2r^2} \tag{9.57}$$

as the potential corresponding to the diagram (Porto, 2016, p. 42).

The last diagram contributing to the 1PN order includes the three-graviton vertex. The vertex corresponds to

$$\begin{aligned}\langle T\{H_{00}(t_1,\boldsymbol{p}_1)H_{00}(t_2,\boldsymbol{p}_2)H_{00}(t_3,\boldsymbol{p}_3)\}\rangle = \\ \frac{i}{4M_{Pl}}\delta(t_1-t_2)\delta(t_1-t_3)\left(\frac{-i}{\boldsymbol{p}_1^2}\right)\left(\frac{-i}{\boldsymbol{p}_2^2}\right)\left(\frac{-i}{\boldsymbol{p}_3^2}\right)(\boldsymbol{p}_1^2+\boldsymbol{p}_2^2+\boldsymbol{p}_3^2)\delta^3(\boldsymbol{p}_1+\boldsymbol{p}_2+\boldsymbol{p}_3).\end{aligned} \tag{9.58}$$

To which we can apply our power counting method:

$$\left[\frac{1}{M_{Pl}}\int dt\delta^3(\boldsymbol{k})\boldsymbol{k}^2\left(d^3\boldsymbol{k}H_{\mu\nu}(t,\boldsymbol{k})\right)^3\right] \sim \frac{1}{M_{Pl}}\left(\frac{r}{v}\right)r^3\frac{1}{r^2}\left(\frac{M_{Pl}v^2}{\sqrt{L}}\right)^3 \sim \frac{v^2}{\sqrt{L}}, \tag{9.59}$$

which gives a total scaling for diagram (c) in figure 9.8 of $\frac{(\sqrt{L})^3 v^2}{\sqrt{L}} \sim Lv^2$. The situation in which the vertex, with a $\boldsymbol{p}_i^2$ part, cancels the propagator and causes a divergence like the one in figure

9.4 and thus can be set to zero by dimensional regularization. The only surviving term, without a scale-less integral, then gives (Porto, 2016, p. 43):

$$V_{9.8(e)}[\boldsymbol{x}_a] = \frac{G^2 m_1^2 m_2}{r^2}. \tag{9.60}$$

Adding up all the potential contributions from the diagrams in figure 9.8, including factors due to symmetries for diagrams (c), (d), and (e), we find the Einstein-Infeld-Hoffmann Lagrangian:

$$L_{EIH} = \frac{1}{8}\sum_{a=1,2} m_a \boldsymbol{v}_a^4 + \frac{G m_1 m_2}{2r}\left[3(\boldsymbol{v}_1^2 + \boldsymbol{v}_2^2) - 7(\boldsymbol{v}_1 \cdot \boldsymbol{v}_2) - \frac{(\boldsymbol{v}_1 \cdot \boldsymbol{r})(\boldsymbol{v}_2 \cdot \boldsymbol{r})}{r^2}\right] - \frac{G^2 m_1 m_2 (m_1 + m_2)}{2r^2}. \tag{9.61}$$

At higher orders in the post-Newtonian expansion, it will become increasingly difficult to compute the contributions to the Lagrangian. The reason for this is that other components than H_{00} will start to become relevant for the self-interaction vertex. To make the computations easier, a spacetime decomposition can be introduced to reduce the number of and simplify the Feynman diagrams at each order. Splitting the spacetime metric up into a scalar, vector, and (3-)metric is known as the 'Kaluza-Klein' decomposition:

$$g_{\mu\nu} dx^\mu dx^\nu = e^{2\phi}(dx^0 - \boldsymbol{A}_i d\boldsymbol{x}^i)^2 - e^{-2\phi}\gamma_{ij} d\boldsymbol{x}^i d\boldsymbol{x}^j. \tag{9.62}$$

In this decomposition, the Einstein-Hilbert action takes the form

$$S_{EH} = -2M_{Pl}^2 \int d^4x \sqrt{\gamma}\left[R^{(3)}[\gamma] + 2\gamma^{ij}\partial_i\phi\partial_j\phi + e^{4\phi}F_{ij}F^{ij}\right], \tag{9.63}$$

where $F_{ij} \equiv \partial_i \boldsymbol{A}_j - \partial_j \boldsymbol{A}_i$ (Porto, 2016, p. 43). The coupling to point-like sources in terms of $(\phi, \boldsymbol{A}_i, \gamma_{ij})$ can be obtained from equation 9.62. There is no scalar cubic coupling, because ϕ always couples to the vector and tensor perturbations, which always come with extra factors of v. This means that in this decomposition, diagram (e) in figure 9.8 does not contribute to the 1PN order but enters at 2PN order (Foffa and Sturani, 2014, pp. 11–12). The last term in the Einstein-Infeld-Hoffmann Lagrangian, in equation 9.61, is in the Kaluza-Klein decomposition accounted for by diagram (d) from figure 9.8, instead of both diagrams (d) and (e) from that figure. Although this approach has proved to be helpful in the conservative dynamics, it does not provide much of an advantage for the radiation modes because the physical modes are encoded in γ_{ij} (Porto, 2016, p. 43).

9.2.2 Radiated power loss

We start constructing the long-wavelength effective theory by turning on the radiation field $\bar{h}_{\mu\nu}$. The potential modes now have to be integrated out in a non-trivial background,

$$g_{\mu\nu} = \bar{g}_{\mu\nu} + \frac{H_{\mu\nu}}{M_{Pl}}, \;\; \bar{g}_{\mu\nu} + \frac{\bar{h}_{\mu\nu}}{M_{Pl}}. \tag{9.64}$$

The effective action for the radiation theory, $S^{rad}_{eff}[\boldsymbol{x}_a, \bar{g}_{\mu\nu}]$, is obtained from

$$e^{iW[\boldsymbol{x}_a]} = \int D\bar{h}_{\mu\nu} \exp\left\{iS_{EH}[\bar{g}_{\mu\nu}] + S^{rad}_{eff}[\boldsymbol{x}_a, \bar{g}_{\mu\nu}] + iS_{GF}[\bar{h}_{\mu\nu}]\right\} \tag{9.65}$$

$$= \int DH_{\mu\nu} D\bar{h}_{\mu\nu} \exp\left\{iS_{EH}[g_{\mu\nu}] + S^{pp}_{eff}[\boldsymbol{x}_a, g_{\mu\nu}] + iS^{(\bar{h})}_{GF}[\bar{h}_{\mu\nu}]\right\}. \tag{9.66}$$

where we have to integrate out the radiation modes to obtain $W[\boldsymbol{x}_a]$ (Porto, 2016, p. 45). Then by using the optical theorem from section 7.2.2, the total radiated power can be obtained. The gauge fixing term can be determined in a similar way as in section 9.1.2.

Analogous to the steps take in section 9.1.5, we will construct an effective action that satisfies the symmetries of General Relativity at the gravitational wavelength scale. This means that the description of the two objects in the binary system will be replaced by a single point-like object endowed with a series of multipole moments. This takes the following form (Ross, 2012, pp. 31–32):

$$S^{rad}_{eff}[\boldsymbol{x}_a, \bar{h}_{\mu\nu}] = \int dt\sqrt{\bar{g}_{00}} \left[-M(t) + \sum_{l=2} \left(\frac{1}{l!} I^L(t) \nabla_{L-2} E_{i_{l-1} i_l} - \frac{2l}{(2l+1)!} J^L(t) \nabla_{L-2} B_{i_{l-1} i_l}\right)\right]. \tag{9.67}$$

The centre-of-mass of the binary is placed at the origin and at rest with respect to distant observers, such that the integration variable $\sqrt{\bar{g}_{00}}dt = d\tau$ is the proper time. The binding energy of the system is represented by the first term containing M. The electric and magnetic multipole $(l \geq 2)$ moments, (I^L, J^L), are $SO(3)$ symmetric and traceless tensors (Porto, 2016, p. 45).

Applying the optical theorem, performing the integral using Feynman's boundary conditions, and incorporating the gauge fixing term is in the gravitational context similar to what we have seen in the scalar case. Therefore, we can now write down the total power (Porto, 2016, p. 46):

$$P = \frac{G}{T} \int_0^\infty \frac{d\omega}{\pi} \left[\frac{\omega^6}{5} |I^{ij}(\omega)|^2 + \frac{16}{45} \omega^6 |J^{ij}(\omega)|^2 + \frac{\omega^8}{189} |I^{ijk}(\omega)|^2 + \cdots\right]. \tag{9.68}$$

To link this result to a diagrammatic description, we recall that the power can be computed by integrating the energy of the emitted gravitons over the differential rate of radiation, like we have done in equation 7.61 for the scalar case. The differential rate of radiation per polarization

is given by

$$d\Gamma_h(\boldsymbol{k}) = \frac{1}{T}\frac{d^3\boldsymbol{k}}{(2\pi)^3 2|\boldsymbol{k}|}|\mathcal{A}_h(|\boldsymbol{k}|,\boldsymbol{k})|^2, \tag{9.69}$$

where the the gravitational wave amplitude for polarizations $h = \pm 2$ can be represented by the diagram in figure 9.9.

$i\mathcal{A}_h(\omega,\boldsymbol{k}) =$ 

FIGURE 9.9: The double line represents the constitutents of the binary system, separated by a distance much smaller than the scale of radiation λ (Porto, 2016, p. 46).

Computing this amplitude as a derivative expansion from equation 9.67 yields

$i\mathcal{A}_h(\omega,\boldsymbol{k}) =$ 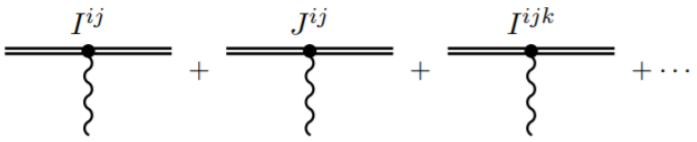

$$= \frac{i}{4M_{\rm Pl}}\epsilon^*_{ij}(\boldsymbol{k},h)\left[\omega^2 I^{ij}(\omega) + \frac{4}{3}\omega\,\boldsymbol{k}^l\epsilon^{ikl}J^{jk}(\omega) - \frac{i}{3}\omega^2\boldsymbol{k}^l I^{ijl}(\omega) + \cdots\right]$$

FIGURE 9.10: Expanded form of the gravitational wave amplitude from figure 9.9, based on equation 9.67 (Porto, 2016, p. 46).

where $\omega = |\boldsymbol{k}|$, and $\epsilon_{ij}(\boldsymbol{k}, h = \pm 2)$ is the polarization tensor. The combination of these results allows us to write the power of the gravitational waves, analogous to the expression in equation 7.61:

$$P|_{h=\pm 2} = \int_{\boldsymbol{k}} |\boldsymbol{k}| d\Gamma_h(\boldsymbol{k}). \tag{9.70}$$

Summing over the polarizations in this expression yields the result from equation 9.68 (Porto, 2016, p. 46).

Diagrammatic approach

We can associate a diagrammatic description to the effective radial action in equation 9.67. We need to find the propagator for the radiation gravitons and their couplings to the potential modes and world lines of matter particles. The couplings are described by the functional integral in equation 9.65, from which the potential modes have been integrated out to give a theory depending on the radiation only.

We follow similar steps as that we have seen before, starting with the propagator to asses the scaling of radiation gravitons $\bar{h}_{\mu\nu}$:

$$\langle T\{\bar{h}_{\mu\nu}(x)\bar{h}_{\alpha\beta}(0)\}\rangle = \int \frac{d^4k}{(2\pi)^4}\frac{i}{k^2+i\epsilon}e^{ik\cdot x}P_{\mu\nu\alpha\beta}, \tag{9.71}$$

where $P_{\mu\nu\alpha\beta}$ provides the tensor structure, which we have already seen in equation 9.11. Considering that $k^\mu \sim \frac{v}{r}$, since the momentum of the radiation scales with the inverse of the wavelength, we can derive that the radiation modes should scale as (Cannella, 2011, pp. 68–69):

$$\bar{h}_{\mu\nu} \sim \frac{v}{r}. \tag{9.72}$$

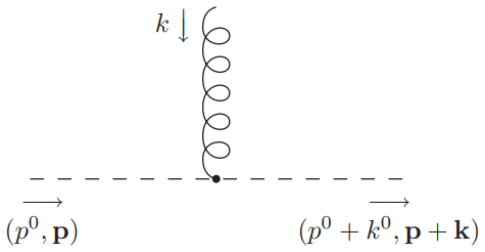

FIGURE 9.11: Three-graviton vertex where a radiation graviton (curly line) interactions with two potential gravitons (dashed lines). The transfer of momentum is indicated (Cannella, 2011, p. 69).

Now consider the situation in which a radiation graviton transfers momentum to a potential graviton. Such an interaction is represented in figure 9.11. The potential mode after the interaction has a three-momentum of $\boldsymbol{p}+\boldsymbol{k}$, corresponding to a propagator with the scaling

$$\sim \frac{1}{(\boldsymbol{p}+\boldsymbol{k})^2} = \frac{1}{\boldsymbol{p}^2}[1+2\boldsymbol{p}\cdot\boldsymbol{k}+\cdots]. \tag{9.73}$$

The scaling of the individual momenta is $|\boldsymbol{p}| \sim \frac{1}{r}$ and $|\boldsymbol{k}| \sim \frac{v}{r}$, resulting in an infinite number of powers of v in the scaling of the combined propagator. Thus, to allow a proper application of the power counting procedure, we need to make sure that radiation gravitons do not transmit momentum to the potential gravitons. This can be done by multipole-expanding the radiation field at the level of the action:

$$\bar{h}_{\mu\nu}(x^0,\boldsymbol{x}) = \bar{h}_{\mu\nu}(x^0,\boldsymbol{x}) + \delta\boldsymbol{x}^i\partial_i\bar{h}_{\mu\nu}(x^0,\boldsymbol{x}) + \frac{1}{2}\delta\boldsymbol{x}^i\boldsymbol{x}^j\partial_i\partial_j\bar{h}_{\mu\nu}(x^0,\boldsymbol{x}) + \cdots, \tag{9.74}$$

where $\boldsymbol{x}$ can be chosen at the centre-of-mass. This expansion avoids transfer of momentum between radiation and potential modes by applying a redefinition of the radiation field, which is in the expanded form only a function of time. This means that the couplings between radiation field and potential field or matter are not Fourier expanded, and terms like those in equation 9.73 will not appear (Cannella, 2011, pp. 69–70).

The next step is to consider the coupling between the radiation field and the particle world-lines, this is given by

$$-\sum_a \frac{m_a}{2M_{Pl}} \int d\tau_a^0 \bar{h}_{\mu\nu}(v_a^\mu v_a^\nu) \simeq -\sum_a \frac{m_a}{2M_{Pl}} \int dx_a^0 \left\{ \bar{h}_{00} + 2\bar{h}_{0s}v_a^8 + \bar{h}_{rs}v_a^r v_a^s + \frac{1}{2}v_a^2 \bar{h}_{00} \right\}, \quad (9.75)$$

where $\bar{h}_{\mu\nu} \equiv \bar{h}_{\mu\nu}(x^0, \boldsymbol{x})$, and only terms up to order $\mathcal{O}(v^2)$ in the velocity expansion have been kept. The diagrammatic description of this coupling is given in figure 9.12.

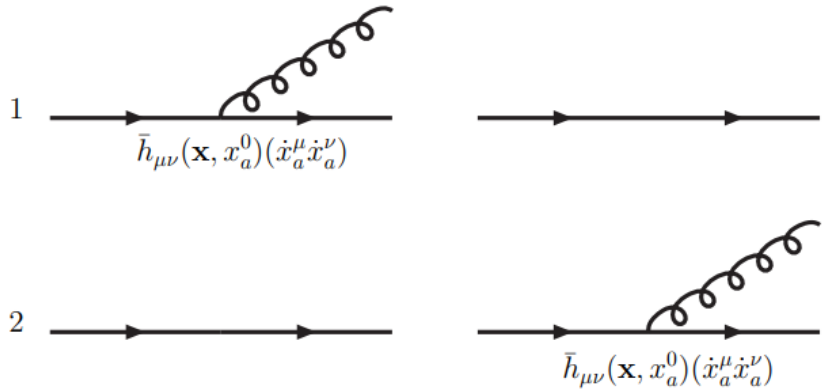

FIGURE 9.12: Diagrammatic representation of the coupling between a radiation graviton to the particle world-lines (Cannella, 2011, p. 70).

For each of the polarizations in equation 9.75 we can perform the multipole-expansion from equation 9.74. For the polarization $\bar{h}_{00}$ this yields:

$$-\sum_a \frac{m_a}{2M_{Pl}} \int dx_a^0 \left(1 + \frac{1}{2}v^2\right) \bar{h}_{00} \simeq$$
$$-\sum_a \frac{m_a}{2M_{Pl}} \int dx_a^0 \left\{ \bar{h}_{00} + \delta \boldsymbol{x}_a^i \partial_i \bar{h}_{00} + \frac{1}{2}\delta \boldsymbol{x}_a^i \delta \boldsymbol{x}_a^j \partial_i \partial_j \bar{h}_{00} + \frac{1}{2}v_a^2 \bar{h}_{00} \right\}, \quad (9.76)$$

where implicitly the choice $\boldsymbol{x} = \boldsymbol{x}_{cm} = 0$ has been made. The leading order is the coupling between the radiation field and the mass monopole. However, from taking $\boldsymbol{k}^2 = k_0^2 = 0$ in equation 9.70 we know that the mass monopole does not lead to the emission of radiation. The first term does therefore not contribute to the power, and $\bar{h}_{00}$ is not a physical degree of freedom in General Relativity (Cannella, 2011, pp. 70–71). The second term on the right hand side of equation 9.76 has order v with respect to the leading order. This term is zero when the sum over the masses is taken due to the choice of the centre-of-mass at the origin of the coordinate system. The terms of order v^2 in equation 9.76 cannot be made to vanish and we will get back to these later (Cannella, 2011, p. 71).

For the polarizations $\bar{h}_{0i}$ we have

$$-\sum_a \frac{m_a}{2M_{Pl}} \int dx_a^0 2\bar{h}_{0s} v_a^s \simeq -\sum_a \frac{m_a}{2M_{Pl}} \int dx_a^0 2 \left\{ \bar{h}_{0s} v_a^s + \delta \boldsymbol{x}_a^i \partial_i \bar{h}_{0s} v_a^s \right\}. \tag{9.77}$$

Following a similar argumentation as for the $\bar{h}_{00}$-polarization, we can write the first term at first order in v as

$$2\bar{h}_{0s} \boldsymbol{P}_{cm}^s = 0, \tag{9.78}$$

in which the total linear momentum $\boldsymbol{P}_{cm} = \sum_a m_a v_a$ of the system has been defined. That the term results in a contribution of zero is a consequence of the choice for the centre-of-mass frame. The fact that all terms in the coupling of order v vanish, the second term in equation 9.76 and the first term in equation 9.77, proves that there is no gravitational dipole radiation. The second term on the right side of equation 9.77 is of order v^2 and does not vanish (Cannella, 2011, p. 71).

The last term we need to consider from equation 9.75 is the one with the $\bar{h}_{rs}$-polarization:

$$-\sum_a \frac{m_a}{2M_{Pl}} \int dx_a^0 \bar{h}_{rs} v_a^r v_a^s, \tag{9.79}$$

which only has a non-vanishing contribution of order v^2 (Cannella, 2011, p. 71).

The $\mathcal{O}(v^2)$ Lagrangian expressing the coupling between radiation and point particles can now be constructed from the non-vanishing terms in equations 9.76, 9.77, and 9.79:

$$-\sum_a \frac{m_a}{2M_{Pl}} \int dx_a^0 \left\{ \frac{1}{2} v_a^2 \bar{h}_{00} + \frac{1}{2} \delta \boldsymbol{x}_a^i \delta \boldsymbol{x}_a^j \partial_i \partial_j \bar{h}_{00} + \delta \boldsymbol{x}_a^i \partial_i \bar{h}_{0s} v_a^s + \bar{h}_{rs} v_a^r v_a^s \right\}. \tag{9.80}$$

There are two problems with this Lagrangian. The first is that it is not gauge invariant under infinitesimal coordinate transformations, and the second is that the polarizations $\bar{h}_{00}$ and $\bar{h}_{0i}$ appear to be sourced by the Lagrangian but, as we saw in section 2.2.3, they can be removed by fixing a suitable gauge and are therefore un-physical. The problems turn out to be related and can be solved by considering the scaling of the couplings from radiation to potential modes, given in figure 9.13.

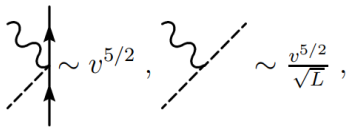

FIGURE 9.13: Scaling of coupling of radiation to potential modes (Cannella, 2011, p. 72).

With these scaling rules, one can interpret the three Feynman diagrams representing the radiation at $\mathcal{O}(v^2)$, given in figure 9.14.

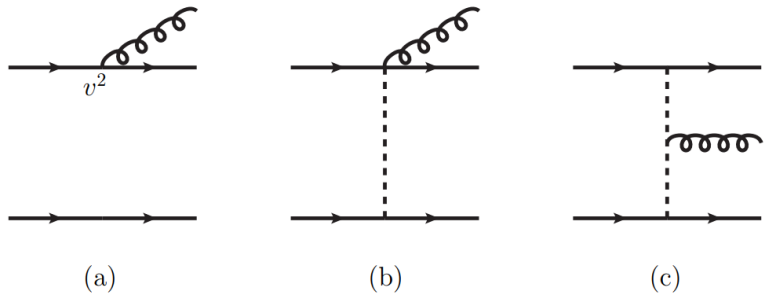

FIGURE 9.14: Feynman diagrams representing the radiation sector at first non-trivial order. The continuous lines with arrows are world lines of point particles, the dashed lines correspond to potential modes, and the curly lines represent the radiation modes (Cannella, 2011, p. 71). Diagram (a) is the multipole expansion carried out to order v^2, diagrams (b) and (c) are needed to ensure gauge invariance of the radiation graviton couplings (Goldberger and Rothstein, 2006a, p. 11).

The diagrams (b) and (c) include a coupling of radiation to potential modes. With the scaling from figure 9.13, and other scaling rules from non-relativistic General Relativity summarised in table 9.1, you can see that each diagram in figure 9.14 scales as $\sqrt{L}v^{5/2}$.

$\boldsymbol{k}$	$H^{\boldsymbol{k}}_{\mu\nu}$	$\bar{h}_{\mu\nu}$	$\frac{m}{M_{Pl}}$
$\frac{1}{r}$	$r^2\sqrt{v}$	$\frac{v}{r}$	$\sqrt{Lv}$

TABLE 9.1: Power counting rules in non-relativistic General Relativity (Goldberger and Rothstein, 2006a, p. 6).

We will not go through the details of all the diagrams, since diagram (a) has been discussed to some extent in the discussion of figure 9.12, and diagram (b) is similar to the seagull diagram from figure 9.8(d). The discussion of the diagrams can also be found in, for example, (Cannella, 2011, pp. 72–74), (Goldberger and Rothstein, 2006a, pp. 10–11) and (Porto, 2016, pp. 49–52). The combined result of contributions from the three diagrams is given by

$$L_{v^2}[\bar{h}] = -\frac{1}{2M_{Pl}}\bar{h}_{00}\left[\frac{1}{2}\sum_a m_a \boldsymbol{v}_a^2 - \frac{Gm_1m_2}{|\boldsymbol{x}_1-\boldsymbol{x}_2|}\right] - \frac{1}{2M_{Pl}}\epsilon_{ijk}\boldsymbol{L}_k\partial_j\bar{h}_{0i} + \frac{1}{M_{Pl}}\sum_a m_a \boldsymbol{x}_a^i \boldsymbol{x}_a^j R_{0i0j}. \tag{9.81}$$

The first term in this Lagrangian is the coupling of $\bar{h}_{00}$ to the Newtonian energy of the binary system. It can be considered as a correction to the kinetic and gravitational energy. The second term is a coupling of the graviton $\bar{h}_{0i}$ to the total angular momentum, $\boldsymbol{L} = \sum_a \boldsymbol{x}_a \times m_a \boldsymbol{v}_a$. Since both the mass monopole, represented by the kinetic and gravitational energy and the angular momentum are conserved at this order, $\bar{h}_{00}$ and $\bar{h}_{0i}$ do not represent physical contributions to the radiation. The last term in the expression, however, does give a physical contribution. This term is the coupling of the source moment $\sum_a m_a \boldsymbol{x}_a^i \boldsymbol{x}_a^j$ to the Riemann tensor of the radiation

field:

$$R_{0i0j} = \frac{1}{2}(\partial_0^2 \bar{h}_{ij} + \partial_i \partial_j \bar{h}_{00} - \partial_0 \partial_i \bar{h}_{0j} - \partial_0 \partial_j \bar{h}_{0i}). \tag{9.82}$$

It shows that $R_{00} = R_{0i0j} = 0$ for all on-shell graviton matrix elements, and that the radiation only couples to

$$Q^{ij} = \sum_a m_a \left(\boldsymbol{x}_a^i \boldsymbol{x}_a^j - \frac{1}{3} \boldsymbol{x}_a^2 \delta_{ij} \right), \tag{9.83}$$

which is the traceless quadrupole moment of the source (Cannella, 2011, pp. 73–74).

9.3 Other effects

There are some other complicating effects that we have left out of the discussion so far. Generally, these effects become relevant for higher-order corrections, thus the discussion above provides a good description up to those orders. To give an idea of what these effects are, we briefly discuss the concept of tail effects in this section. For the other effects, there are some good resources available:

- Gravitational radiation-reaction: this incorporates the back-reaction effects of the radiation on the dynamics of the binary which have been neglected by using the 'in-out' boundary conditions in the optical theorem. Including these effects requires incorporating causal propagation in non-relativistic General Relativity, i.e. using the 'in-in' formalism. More information in (Porto, 2016, pp. 60–62) and (Galley and Leibovich, 2012).
- Spinning extended objects: the discussion in this project is mainly about non-spinning extended objects. Only in the 1PN diagrams (b) and (b) in figure 9.8, we included some v-contributions due to the spin of objects. The derivation of these contributions and other effects due to the spin of objects in the binary can be found in (Porto, 2016, pp. 68–86).

9.3.1 Tail effects

The tail effects originate from the gravitational interactions with the background geometry far away from the binary, which can be approximated by a Schwarzschild spacetime with total mass or energy M. At leading order in G, the gravitational potential is given by the Newtonian approximation

$$V_N(\boldsymbol{k}) = -\frac{GM}{\boldsymbol{k}^2} + \mathcal{O}(G^2), \tag{9.84}$$

which varies on scales of order $|\boldsymbol{k}| \simeq \lambda_{rad}^{-1} \ll \frac{1}{r}$. The gravitational tails can be parametrized in powers of the ratio $\eta \equiv \frac{\mathcal{R}_s}{\lambda_{rad}}$, with $\mathcal{R}_s \equiv 2GM$ the gravitational radius of the system. For post-Newtonian sources, we have $\eta \sim v^3$, which means that the first tail effects enter at 1.5PN order beyond the leading effects for binary inspirals (Porto, 2016, p. 52).

Conceptually, tails are disturbances that cannot keep up with the rest of the wave. Where electromagnetic waves satisfy Huygens' principle that the total disturbance of a wave is confined to a single expanding wavefront defined by the speed of the light, gravitational waves do not satisfy this principle. This means that 'tails' arising from the interaction of the wave with the curved spacetime background of the source can bounce around indefinitely (Kennefick, 2017, pp. 206–207). For example, consider the spacetime diagram in figure 9.15. At a spacetime point S in the diagram, the source emits a gravitational wave which propagates to R, where a part of the wave is reflected because of the curved spacetime. A while later, the source emits another gravitational signal at point S'. At a point P both the signals from S' and R arrive, which means that spacetime point P can be affected not just by the source at the moment that it intersects with the past light-cone of P, but also by other moments in the past of the source, through reflections such as occurred at R. The gravitational signal coming from point R is then referred to as the 'tail' of source S.

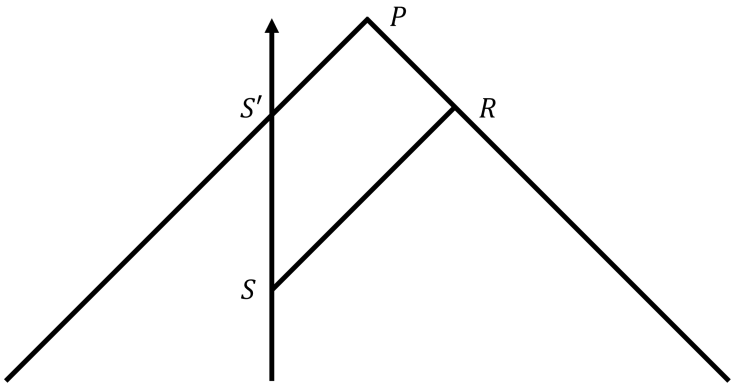

FIGURE 9.15: Spacetime diagram in the rest-frame of source S, with time represented vertically, and one space-dimension horizontally. Spacetime event P is affected by both the source directly, from point S', and indirectly, through its tail coming from spacetime point R.

This makes the calculations much more complicated since sources can be surrounded by echoes of the original disturbance. Even a tail itself might have a tail, which is then called the 'tail-of-the-tail' at $\mathcal{O}(\eta^2)$. However, understanding of these effects allows for them to be computed and shows that the effects are small throughout the inspiral, in the post-Newtonian regime they are of order $\eta^2 \log(\omega r) \sim v^6 \log(v)$ (Porto, 2016, pp. 55–57).

Chapter 10

Discussion of Part II

Binary systems in three different situations were discussed in this part: scalar theory, electromagnetic theory, and General Relativity. In all of them, we followed the same principles of the effective field theory approach. The assumption in all systems was that there was a separation of scales possible, for the gravitational case, this is given by the source radius R_s, the separation of the objects r, and the wavelength of the emitted signal λ. This separation ensured the decoupling of different terms in the theories, which in turn allowed us to integrate out the lowest scales and describe the physics as those scales in an effective action contribution.

We can note that the expansion around the Minkowski space of the spacetime metric,

$$g_{\mu\nu} = \eta_{\mu\nu} + \frac{h_{\mu\nu}}{M_{Pl}}, \tag{10.1}$$

looks similar to the weak field approximation of linearized gravity,

$$g_{\mu\nu} = \eta_{\mu\nu} + h_{\mu\nu}. \tag{10.2}$$

The difference is the cut-off scale M_{Pl} that is present in the effective field theory decomposition. This is a very important aspect of the effective field theory approach to gravitational dynamics because it represents the breaking down of the theory at the Planck scale, at which quantum gravity effects are expected to dominate.

In all three cases, we encountered a 'tower of effective field theories', because two scales had to be integrated out. First, the finite-size effects were integrated out which resulted in an effective point particle action. The charged spheres and massive objects thereby were reduced to point particles, which has the advantage of reducing the number of variables of the theory drastically. The next step was to integrate out the off-shell potential modes. The point particles in the theory would act as sources and be able to exchange scalar particles in the scalar theory, photons in the electromagnetic situation, and gravitons in the gravitational situation. However, these virtual particles exchanged in the interactions are acting instantaneously. Higher orders in the approximation would therefore add velocity corrections to the theory.

The expanded terms in the action can be associated with Feynman rules, which can then be interpreted in a diagrammatic representation. For the theory of General Relativity, there are also self-interaction terms present. The Feynman diagrams which can be constructed from this set of rules are ordered by the power counting procedure to determine the different ways in which the terms from the action contribute to the observables. This adds some conceptual grip on the procedures and supports the physical understanding of the theory.

The on-shell modes of the effective theory are responsible for the radiation. Through the optical theorem, the imaginary part of the functional W associated with a radiation diagram of the system can be used to compute the emitted power of the gravitational waves. One of the challenges in this computation is to find the multipole moments that contribute to each order by a matching procedure. The diagrammatic description of the expansion has shown that, in gravity, there exists no monopole radiation, due to the conservation of mass, and no dipole radiation, due to the conservation of momentum.

Some more complications that occur in the effective field theory approach of General Relativity were conceptually discussed but not fully calculated or explicitly solved. Divergences can be dealt with by dimensional regularization or renormalizing the effective theory. Every time that a scale is integrated out the gauge has to be fixed to remove redundancies introduced by coordinate invariance and symmetries of the long-range theory are satisfied. The compact object in a gravitational binary can have a spin that needs to be taken into account in the effective theory. The radiation provides feedback on the system itself, called the radiation reaction.

Although the method still is quite complicated, it is clear that there are a lot of tools available and the systematic approach is very rigorous when applied correctly. Which can be viewed as confusing initially, the mixing of all different expansions discussed in section 6.1 into the 'post-Newtonian' framework, is very useful to combine the results from different approaches into one description. This is also the reason that it is hard to consider the results of the effective field theory approach to gravitational binary systems in isolation because it is often combined with results from other approaches that generate post-Newtonian descriptions. The most important of those other approaches is the Arnowitt-Deser-Misner-Hamiltonian method (ADM) (Arnowitt, Deser, and Misner, 1959). Collectively, the approaches have been able to describe binary system consisting of non-spinning objects up to 4PN order, and consisting of spinning objects up to 3PN order. The effective field theory approach has been instrumental in including finite-size effects for the spinning objects, which could not be obtained with the other methods (Porto, 2016, p. 4).

The post-Newtonian results will be of great importance in the next part of this thesis, about the Effective One Body approach. That approach takes the post-Newtonian description rewritten it in the center-of-mass frame and coordinates close to Hamiltonian coordinates, modified due to shifts to eliminate the accelerations (Blümlein et al., 2020, p. 6). In this new description, the

symmetric mass ratio $\nu \equiv \frac{\mu}{M} = \frac{m_1 m_2}{(m_1+m_2)^2}$ plays a big role since this parameter will be used to generalise the test-mass analytic description.

Part III

Effective One Body Approach

Chapter 11

Effective One Body Basics

The Effective One Body (EOB) approach to a binary system can be understood as a generalisation of the test particle limit. For two objects with gravitational interaction, the test particle limit describes the situation of a large difference in mass between the two objects. The effect of the object with the smaller mass on the object with the bigger mass can be neglected. This means that the dynamics of the system can be described by the lighter object moving in a background in which the heavier object is stationary. This simplifies the situation enormously, and that is why a generalisation of this situation to situations in which the mass difference is smaller is highly interesting. In the case of General Relativity, it is looking for an external spacetime geometry, $g_{\mu\nu}^{ext}$, such that the geodesic dynamics of a test particle of mass μ equivalent to the original dynamics (Damour and Nagar, 2009, pp. 6–7).

First, the ingredients of the Effective One Body approach will be discussed. It will be mainly framed in the gravitational context because that is the context of origin for the approach. However, a test particle limit does not only exist for a system of objects with masses subject to gravitational interaction, it also exists for systems with charges subject to electromagnetic interactions. We have discussed the analogy between electrodynamics and gravitational dynamics, and we will extend this analogy to study the Effective One Body approach in chapter 12 of this part. Then we will finish this part with a chapter on the Effective One Body approach in the gravitational dynamics of binary systems.

11.1 Ingredients

The Effective One Body approach comprises three ingredients (Damour and Nagar, 2009, p. 2):

- a description of the conservative (Hamiltonian) part of the dynamics of two objects;
- an expression of the radiation reaction part of the dynamics;
- a description of the waveform emitted by a coalescing binary system.

Each one of these ingredients can be found in the high-order post-Newtonian results from approaches such as the effective field theory approach that was discussed in the previous part of this thesis. The key difference between those results on themselves, compared to the Effective One Body result, is that the post-Newtonian result is given in its original expanded form. The Effective One Body approach, however, presents those terms in a resummed form, thus as a non-polynomial function of v. This allows the Effective One Body approach to incorporate some non-perturbative features of the exact result (Damour and Nagar, 2009, pp. 2–3).

The consequence of this approach is that the analytic solution can be extended to apply much longer into the inspiral. While the post-Newtonian description on itself can only describe the binary inspiral for non-relativistic situations, which means approximately up to the last stable orbit of the inspiral stage, the analytic description constructed in the Effective One Body approach is successful in describing also the late inspiral, plunge, merger and ring-down stages of the coalescence (Damour and Nagar, 2009, pp. 3–5).

Chapter 12

Case: Classical Electrodynamics

In this chapter, we will discuss a binary system consisting of two charges with electromagnetic interaction, instead of two masses with gravitational interaction. The electromagnetic field equations are linear, and therefore less involved than the Einstein field equations of General Relativity considered in the next chapter (Kunze and Spohn, 2001, p. 322). The relevance of this case in the understanding of the coalescence of binary systems in gravity is supported by the fact that approaches to describe the gravitational dynamics are inspired by results from quantum electrodynamics. The work of Brezin, Itzykson, and Zinn-Justin on including recoil effects in the relativistic Balmer formula had especially been inspiring in the development of the one-body description for gravity (Brezin, Itzykson, and Zinn-Justin, 1970). In this chapter, we will discuss the approach of an effective one-body description of a two-body system in classical electrodynamics. This discussion is mainly based on an article written by Alessandra Buonanno (Buonanno, 2000).

The discussion starts with an explanation of the two-body description of the system, based on a general description of the laws governing the particles. Towards the end of the first section of this chapter, we will derive the radial action variable and discuss the energy levels, which will play a big role in the process of mapping and matching the effective one-body description to the two-body description. The second section then starts with the discussion of the effective one-body description and distinguishes three different methods to perform the mapping to the two-body description, first with an effective scalar potential, then with an effective vector potential, and finally with an effective metric. The chapter will conclude with a discussion of the effective description and the different ways of matching the different descriptions to each other.

12.1 Two-body description

The first step in describing the dynamics of a system consisting of two charges, is to write down the electromagnetic field equations, also called Maxwell's laws (Kunze and Spohn, 2001,

p. 322):

$$\frac{1}{c}\frac{\partial}{\partial t}\boldsymbol{B}(x,t) = -\nabla \times \boldsymbol{E}(x,t), \tag{12.1}$$

$$\frac{1}{c}\frac{\partial}{\partial t}\boldsymbol{E}(x,t) = \nabla \times \boldsymbol{B}(x,t) - \frac{1}{c}\boldsymbol{j}(x,t), \tag{12.2}$$

$$\nabla \cdot \boldsymbol{E}(x,t) = \rho(x,t), \tag{12.3}$$

$$\nabla \cdot \boldsymbol{B}(x,t) = 0. \tag{12.4}$$

The equations of motions of the system are given by the Lorentz force equations for both particles:

$$\frac{d}{dt}(m_1\gamma_1\boldsymbol{v}_1(t)) = e_1\left(\boldsymbol{E}_\psi(\boldsymbol{q}_1(t),t) + \frac{1}{c}\boldsymbol{v}_1(t)\times\boldsymbol{B}_\psi(\boldsymbol{q}_1(t),t)\right), \tag{12.5}$$

$$\frac{d}{dt}(m_2\gamma_2\boldsymbol{v}_2(t)) = e_2\left(\boldsymbol{E}_\psi(\boldsymbol{q}_2(t),t) + \frac{1}{c}\boldsymbol{v}_2(t)\times\boldsymbol{B}_\psi(\boldsymbol{q}_2(t),t)\right), \tag{12.6}$$

where m_i is particle i's mass, $\gamma_i = \frac{1}{\sqrt{1-\left(\frac{v_i^2}{c^2}\right)}}$ the relativistic factor, $\boldsymbol{q}_i(t)$ the position of particle i, $\boldsymbol{v}_i = \dot{\boldsymbol{q}}_i(t)$ the velocity, and e_i is particle i's charge (Kunze and Spohn, 2001, pp. 322–323).

The rigid charge distribution of the particles is described by the form factor ψ, for which we assume the following characteristics (Kunze and Spohn, 2001, p. 323):

$$\text{Smooth} \quad 0 \le \psi \in C_0^\infty(\mathbb{R}^3), \tag{12.7}$$

$$\text{Radial} \quad \psi(\boldsymbol{x}) = \psi_r(|\boldsymbol{x}|), \tag{12.8}$$

$$\text{Compactly supported} \quad \psi(\boldsymbol{x}) = 0 \text{ for } |\boldsymbol{x}| \ge R_\psi, \tag{12.9}$$

$$\text{Normalized} \quad \int d\boldsymbol{x}\psi(\boldsymbol{x}) = 1. \tag{12.10}$$

To define the charge and current densities as follows:

$$\rho(\boldsymbol{x},t) = e_1\psi(\boldsymbol{x}-\boldsymbol{q}_1(t)) + e_2\psi(\boldsymbol{x}-\boldsymbol{q}_2(t)), \tag{12.11}$$

$$\boldsymbol{j}(\boldsymbol{x},t) = e_1\psi(\boldsymbol{x}-\boldsymbol{q}_1(t))\boldsymbol{v}_1 + e_2\psi(\boldsymbol{x}-\boldsymbol{q}_2(t))\boldsymbol{v}_2. \tag{12.12}$$

These equations determine the source terms in the Maxwell equations. The combination of Maxwell equations, equations of motion, and the charge and current densities together are often referred to as the "Abraham model" (Kunze and Spohn, 2001, p. 323).

We can use an approximation for non-relativistic situations, in the gravitational situation given by the post-Newtonian expansion. In the electromagnetic context, the expansion in $\frac{1}{c^2}$ is referred to as post-Coulombian (PC). The 0PC terms are called the 'Coulomb terms' and are of order $(v^2/c^2)^0$, the 1PC terms are called the 'Darwin-terms' and are of order $(v^2/c^2)^1$, and so on.

Starting at 1.5PC order, charges will lose energy through multipole radiation, thus extending the expansion is not merely an addition of extra terms anymore, and dissipative contributions will be appearing (Kunze and Spohn, 2001, p. 324). Descriptions including these terms are non-conservative.

Limited to the conservative part of the dynamics of the bound states of two charged particles, the electromagnetic system up to 2PC order can be described by the following Lagrangian (Buonanno, 2000, p. 5):

$$\mathcal{L}(\mathbf{q_1}, \mathbf{q}_2, \dot{\mathbf{q}}_1, \dot{\mathbf{q}}_2) = \mathcal{L}_0 + \frac{1}{c^2}\mathcal{L}_2 + \frac{1}{c^4}\mathcal{L}_4, \tag{12.13}$$

in which

$$\mathcal{L}_0 = \frac{1}{2}m_1\dot{\mathbf{q}}_1^2 + \frac{1}{2}m_2\dot{\mathbf{q}}_2^2 - \frac{e_1e_2}{q}, \tag{12.14}$$

$$\mathcal{L}_2 = \frac{1}{8}m_1\dot{\mathbf{q}}_1^4 + \frac{1}{8}m_2\dot{\mathbf{q}}_2^4 + \frac{e_1e_2}{2q}[\dot{\mathbf{q}}_1\cdot\dot{\mathbf{q}}_2 + (\mathbf{n}\cdot\dot{\mathbf{q}}_1)(\mathbf{n}\cdot\dot{\mathbf{q}}_2)], \tag{12.15}$$

$$\begin{aligned}\mathcal{L}_4 = &\frac{1}{16}m_1\dot{\mathbf{q}}_1^6 + \frac{1}{16}m_1\dot{\mathbf{q}}_2^6 - \frac{e_1e_2}{8q}\Bigg\{\dot{\mathbf{q}}_1^2\dot{\mathbf{q}}_2^2 - 2(\dot{\mathbf{q}}_1\cdot\dot{\mathbf{q}}_2)^2 + 3(\mathbf{n}\cdot\dot{\mathbf{q}}_1)^2(\mathbf{n}\cdot\dot{\mathbf{q}}_2)^2 \\ &- (\mathbf{n}\cdot\dot{\mathbf{q}}_1)^2\dot{\mathbf{q}}_2^2 - (\mathbf{n}\cdot\dot{\mathbf{q}}_2)^2\dot{\mathbf{q}}_1^2 + \frac{e_1e_2}{m_2q}[\dot{\mathbf{q}}_1^2 - 2(\mathbf{n}\cdot\dot{\mathbf{q}}_1)^2] + \frac{e_1e_2}{m_1q}[\dot{\mathbf{q}}_2^2 - 2(\mathbf{n}\cdot\dot{\mathbf{q}}_2)^2] \\ &- \frac{2(e_1e_2)^2}{m_1m_2q^2}\Bigg\},\end{aligned} \tag{12.16}$$

where $\mathbf{q} = \mathbf{q}_1 - \mathbf{q}_2$ and $\mathbf{n} = \mathbf{q}/q$.

Applying the Legendre transform to arrive at the Hamiltonian description, the expressions

$$M = m_1 + m_2, \quad \mu = \frac{m_1m_2}{M}, \quad \nu = \frac{\mu}{M}, \tag{12.17}$$

can be used to rewrite the expression. Note that the parameter ν can take all values in between the test mass limit, for $\nu = 0$, and the equal mass case, for $\nu = 1/4$ (Buonanno, 2000, p. 5).

The next step to simplify the Hamiltonian is limiting the case to the dynamics of bound states in two-body dynamics, which means to take $e_1e_2 < 0$ and pose that coupling constant $\alpha = -e_1e_2 > 0$. Considering the centre-of-mass frame in which $\boldsymbol{P} = \boldsymbol{p}_1 = -\boldsymbol{p}_2$, we can introduce the following reduced variables (Buonanno, 2000, p. 6)

$$\hat{\mathcal{H}} = \frac{\mathcal{H}}{\mu}, \quad \boldsymbol{p} = \frac{\boldsymbol{P}}{\mu}, \quad \hat{t} = \frac{\mu t}{\alpha}, \quad r = \frac{\mu q}{\alpha}. \tag{12.18}$$

After which the Hamiltonian can be rewritten in the following form (Buonanno, 2000, p. 6):

$$\begin{aligned}\hat{\mathcal{H}}(\boldsymbol{r},\boldsymbol{p}) = \frac{1}{2}\boldsymbol{p}^2 - \frac{1}{r} - \frac{1}{8c^2}(1-3\nu)\boldsymbol{p}^4 - \frac{1}{2c^2}\frac{\nu}{r}[\boldsymbol{p}^2 + (\boldsymbol{n}\cdot\boldsymbol{p})^2] \\ - \frac{1}{8c^2}\frac{1}{r}[3\nu^2(\boldsymbol{n}\cdot\boldsymbol{p})^4 + \nu(3\nu-2)\boldsymbol{p}^4 + 2\nu(\nu-1)\boldsymbol{p}^2(\boldsymbol{n}\cdot\boldsymbol{p})^2] \\ + \frac{1}{16c^4}(1-5\nu+5\nu^2)\boldsymbol{p}^6 + \frac{1}{4c^4}\frac{\nu}{r^2}\boldsymbol{p}^2 + \frac{1}{4c^4}\frac{\nu}{r^3}. \quad (12.19)\end{aligned}$$

In this Hamiltonian, we can identify the symmetries for time translations and space rotations. They are corresponding to the following two conserved quantities:

$$\text{centre-of-mass non-relativistic energy:} \quad \hat{\mathcal{H}}(\boldsymbol{r},\boldsymbol{p}) = \hat{\mathcal{E}}^{NR} = \frac{\mathcal{E}^{NR}_{c.m.}}{\mu}, \quad (12.20)$$

$$\text{angular momentum:} \quad \boldsymbol{r}\times\boldsymbol{p} = \boldsymbol{j} = \frac{\boldsymbol{\mathcal{J}}_{c.m.}}{\alpha}. \quad (12.21)$$

From now on we will drop the centre-of-mass subscripts, thus define $\mathcal{E}^{NR} \equiv \mathcal{E}^{NR}_{c.m.}$ and $\boldsymbol{\mathcal{J}} \equiv \boldsymbol{\mathcal{J}}$ (Buonanno, 2000, p. 6).

12.1.1 Energy levels and reduced radial action

Using the Hamilton-Jacobi formalism, we can evaluate the energy levels of the system, in which the two-body description can be summarized in a coordinate invariant manner. To do so, we first introduce the reduced Hamilton principal-function $\hat{S}$, defined by

$$\frac{\partial\hat{S}}{\partial\boldsymbol{r}} = \boldsymbol{p}. \quad (12.22)$$

Restricting the description to the planar motion, and separating the time and angular coordinates, we can write the reduced Hamilton principal function as follows:

$$\hat{S} = -\hat{\mathcal{E}}^{NR}\hat{t} + j\phi + \hat{S}_r(r,\hat{\mathcal{E}}^{NR},j). \quad (12.23)$$

Solving the Hamilton-Jacobi equation $\hat{\mathcal{H}}(\boldsymbol{r},\boldsymbol{p}) = \hat{\mathcal{E}}^{NR}$ with respect to $(d\hat{S}_r/dr) = p_r = \boldsymbol{n}\cdot\boldsymbol{p}$ yields

$$\hat{S}_r(r,\hat{\mathcal{E}}^{NR},j) = \int dr\sqrt{\mathcal{R}(r,\hat{\mathcal{E}}^{NR},j)}, \quad (12.24)$$

where we have used that $\boldsymbol{p}^2 = (\boldsymbol{n}\cdot\boldsymbol{p})^2 + \frac{j^2}{r^2}$, and $\mathcal{R}$ is a polynomial of the fifth order in $1/r$. Neglecting terms $\mathcal{O}(c^{-6})$, the effective potential for the radial motion is given by:

$$\mathcal{R}(r,\hat{\mathcal{E}}^{NR},j) = A + \frac{2B}{r} + \frac{C}{r^2} + \frac{D_1}{r^3} + \frac{D_2}{r^4} + \frac{D_3}{r^5}, \quad (12.25)$$

with

$$A = 2\hat{\mathcal{E}}^{NR} + \frac{1}{c^2}(1-3\nu)(\hat{\mathcal{E}}^{NR})^2 + \frac{1}{c^4}\nu(4\nu-1)(\hat{\mathcal{E}}^{NR})^3, \tag{12.26}$$

$$B = 1 + \frac{1}{c^2}(1-\nu)\hat{\mathcal{E}}^{NR} + \frac{1}{c^4}\frac{\nu}{2}(2\nu-1)(\hat{\mathcal{E}}^{NR})^2, \tag{12.27}$$

$$C = -j^2 + \frac{1}{c^2}(1+\nu), \tag{12.28}$$

$$D_1 = -\frac{1}{c^2}\nu j^2 - \frac{1}{c^4}\nu^2 j^2 \hat{\mathcal{E}}^{NR} + \frac{1}{c^4}\frac{\nu}{2}(4\nu-1), \tag{12.29}$$

$$D_2 = -\frac{3}{c^4}\nu^2 j^2, \tag{12.30}$$

$$D_3 = \frac{3}{4c^4}\nu^2 j^4. \tag{12.31}$$

For our purposes, we will consider

$$i_r^{real}(\hat{\mathcal{E}}^{NR}, j) = \frac{2}{2\pi}\int_{r_{min}}^{r_{max}} dr\sqrt{\mathcal{R}(r, \hat{\mathcal{E}}^{NR}, j)}, \tag{12.32}$$

which is the reduced radial action variable (Buonanno, 2000, pp. 6–7).

By performing a complex contour integral, Damour and Schäfer have shown that

$$\mathcal{I}(A,B,C,D_1,D_2,D_3) = \frac{B}{\sqrt{-A}} - \sqrt{-C}\Bigg\{1 - \frac{1}{2}\frac{B}{C^2}\left[D_1 - \frac{3}{2}\frac{D_2 B}{C} + \frac{15}{8}\frac{D_1^2 B}{C^2}\right] - \frac{1}{4}\frac{A}{C^2}\left[D_2 - \frac{3}{4}\frac{D_1^2}{C}\right] + \frac{3}{4}\frac{B}{C^3}\left[A - \frac{5}{3}\frac{B^2}{C}\right]D_3\Bigg\} + \cdots, \tag{12.33}$$

where the higher-order terms contain combinations of the D_i-coefficients which yield higher orders in $1/c$ (Damour and Schäfer, 1988, p. 144). Inserting the expressions from equations 12.26-12.31, we find an expression for the radial action variable $\mathcal{I}_R^{real} = \alpha i_r^{real}$ (Buonanno, 2000, p. 7):

$$\mathcal{I}_R^{real}(\mathcal{E}^{NR}, \mathcal{J}) = \frac{\alpha\mu^{1/2}}{\sqrt{-2\mathcal{E}^{NR}}}\left[1 - \frac{1}{4}(\nu-3)\frac{\mathcal{E}^{NR}}{\mu c^2} - \frac{1}{32}(5-6\nu-3\nu^3)\left(\frac{\mathcal{E}^{NR}}{\mu c^2}\right)^2\right] - \mathcal{J} + \frac{\alpha^2}{c^2\mathcal{J}}\left(\frac{1}{2} - \frac{\nu}{2}\frac{\mathcal{E}^{NR}}{\mu c^2}\right) + \frac{1}{8}(1-6\nu)\frac{\alpha^4}{c^4\mathcal{J}^3}. \tag{12.34}$$

Solving this equation in terms of the relativistic energy, $\mathcal{E}^R = \mathcal{E}^{NR} + Mc^2$, will lead to the description of the energy levels:

$$\mathcal{E}^R(\mathcal{N},\mathcal{J}) = Mc^2 - \frac{1}{2}\frac{\alpha^2\mu}{\mathcal{N}^2} + \frac{1}{c^2}\alpha^4\mu\left[-\frac{1}{2}\frac{1}{\mathcal{J}\mathcal{N}^3} + \frac{1}{8}(3-\nu)\frac{1}{\mathcal{N}^4}\right] + \frac{1}{c^4}\alpha^6\mu\left[-\frac{3}{8}\frac{1}{\mathcal{J}^2\mathcal{N}^4} + \frac{1}{16}(-5+3\nu-\nu^2)\frac{1}{\mathcal{N}^6} + \frac{1}{4}(3-2\nu)\frac{1}{\mathcal{J}\mathcal{N}^5} + \frac{1}{8}(6\nu-1)\frac{1}{\mathcal{J}^3\mathcal{N}^3}\right], \quad (12.35)$$

in which we have introduced the Delaunay action variable $\mathcal{N} = \mathcal{I}_R^{real} + \mathcal{J}$. At 0PC order this describes the degeneracy of the energy levels in the Coulomb problem. Identifying $\mathcal{N}/\hbar$ with the principal quantum-number n, and $\mathcal{J}/\hbar$ with the total angular momentum quantum-number l, the 1PC order describes the correct bound-state energies of the singlet sates of the positronium in the classical limit, with $e_1 = -e_2$, $m_1 = m_2$, and $\mathcal{J}/\hbar \gg 1$. Due to the dipole-type interactions that enter at 1.5PC order and have not been included in this description, equation 12.35 does not provide the correct descriptions for 2PC order energy levels. The dipole radiation reaction effects can be postponed to the 2.5PC quadrupole order by choosing $e_1/m_1 = e_2/m_2$ (Buonanno, 2000, pp. 7–8). We will not make the choice to restrict ourselves to the $e_1/m_1 = e_2/m_2$ case in our discussion, since we will only look at the conservative part of the bound state dynamics and will not encounter the problems which arise at the radiation scale.

12.2 Effective one-body description

The goal is to map the two-body dynamics to an effective dynamics of a test particle in an external electromagnetic field. When we associate the mass m_0 and charge e_0 to the test particle, we can describe its effective action with

$$S_{eff} = \int\left(-m_0 c ds_0 + \frac{1}{c}e_0 A^\mu_{eff}(z)dz^\mu\right) \quad (12.36)$$

where $A^\mu_{eff} = (\Phi_{eff}, \boldsymbol{A}_{eff})$ is the effective electromagnetic field potential. Then, after performing a Legendre transform, the effective Hamiltonian must satisfy

$$\frac{(\mathcal{H}_{eff} - e_0\Phi_{eff})^2}{c^2} = m_0^2c^2 + \left(\boldsymbol{p} - \frac{e_0}{c}\boldsymbol{A}_{eff}\right)^2. \quad (12.37)$$

Now the effective electromagnetic field can be constructed by expanding in the dimensionless parameter $\frac{\alpha_0}{m_0c^2R}$ in which we have a coupling constant $\alpha_0 = e_0^2$, and $\frac{\alpha_0}{m_0c^2}$ is the classical charge

radius of m_0. This yields

$$\Phi_{eff}(R) = \frac{e_0\phi_0}{R}\left[1 + \phi_1\frac{\alpha_0}{m_0c^2R} + \phi_2\left(\frac{\alpha_0}{m_0c^2R}\right)^2 + ...\right], \tag{12.38}$$

$$\boldsymbol{A}_{eff}(R) = \frac{e_0\boldsymbol{a}}{cR}\left[a_0 + a_1\frac{\alpha_0}{m_0c^2R} + ...\right], \tag{12.39}$$

in which we have introduced the dimensionless parameters $\phi_0, \phi_1, \phi_2, a_0, a_1$, and a vector with the dimension of a velocity, $\boldsymbol{a}$. These will be fixed by matching the two-body description to the effective one-body description (Buonanno, 2000, p. 8).

$$\frac{\mathcal{E}_0^{NR}}{m_0c^2} = \frac{\mathcal{E}^{NR}}{\mu c^2}\left[1 + \alpha_1\frac{\mathcal{E}^{NR}}{\mu c^2} + \alpha_2\left(\frac{\mathcal{E}^{NR}}{\mu c^2}\right)^2\right] \tag{12.40}$$

where α_1, α_2 will be fixed by matching (Buonanno, 2000, p. 10).

There are three ways to map the two descriptions to each other, differing from one another by choice of effective electromagnetic field and spacetime metric.

12.2.1 Effective scalar potential

The first mapping is by expanding in the scalar potential, while taking the vector potential equal to zero.

$$\Phi_{eff}(R) = \frac{e_0\phi_0}{R}\left[1 + \phi_1\frac{\alpha_0}{m_0c^2R} + \phi_2\left(\frac{\alpha_0}{m_0c^2R}\right)^2 + ...\right], \tag{12.41}$$

$$\boldsymbol{A}_{eff}(R) = 0. \tag{12.42}$$

This results in the following derivative of the radial Hamilton principal-function:

$$\frac{dS_R^0}{dR} = 2m_0\mathcal{E}_0^{NR} - 2m_0e_0\Phi_{eff} - \frac{\mathcal{J}_0^2}{R^2} + \frac{(\mathcal{E}_0^{NR})^2}{c^2} + \frac{e_0^2\Phi_{eff}^2}{c^2} - \frac{2e_0\mathcal{E}_0^{NR}\Phi_{eff}}{c^2} \tag{12.43}$$

in which $\mathcal{E}_0^{eff} = \mathcal{E}_0^R - m_0c^2$ is the non-relativistic energy. Plugged into the integral for the effective radial action variable, this yields:

$$\begin{aligned}\mathcal{I}_0^{eff}(\mathcal{E}_\prime^{\mathcal{NR}}, \mathcal{J}_\prime) = \frac{\alpha_0 m_0^{1/2}}{\sqrt{-2\mathcal{E}_0^{NR}}}&\left[-\phi_0 - \frac{3\phi_0}{4}\frac{\mathcal{E}_0^{NR}}{m_0c^2} + \frac{5\phi_0}{32}\left(\frac{\mathcal{E}_0^{NR}}{m_0c^2}\right)^2\right] \\ &- \mathcal{J}_0 + \frac{\alpha_0^2}{\mathcal{J}_0c^2}\left[\frac{\phi_0^2}{2} - \phi_0\phi_1 - \phi_0\phi_1\frac{\mathcal{E}_0^{NR}}{m_0c^2}\right] \\ &+ \frac{1}{8}\frac{\alpha_0^4}{\mathcal{J}_0^3c^4}[\phi_0^4 - 12\phi_0^3\phi_1 + 8\phi_0^2\phi_2 + 4\phi_0^2\phi_1^2].\end{aligned} \tag{12.44}$$

Identifying this equation with the result from equation 12.34, assuming that $m_0 = \mu$ and using the relation between the adiabatic invariants $\mathcal{N} = \mathcal{N}_0,\ \mathcal{J} = \mathcal{J}_0$, and the mapping from equation 12.40, we can derive the value or expressions for the unknown parameters. In particular, at 0PC order, we have:

$$-\phi_0\alpha_0 = \alpha \tag{12.45}$$

where it is then natural to take $\phi_0 = -1$, yielding that $e_0^2 = \alpha_0 = \alpha = -e_1e_2$. At 1PC order we have the equations:

$$-\phi_0\alpha_0(2\alpha_1 - 3) = \alpha(\nu - 3), \quad \alpha_0^2(\phi_0^2 - 2\phi_0\alpha_1) = \alpha^2, \tag{12.46}$$

Filling in the values found from 0PC order, these result in: $\alpha_1 = \frac{\nu}{2}$ and $\phi_1 = 0$.

For 2PC order we have the equations:

$$-\phi_0\alpha_0(5 - 12\alpha_1 - 12\alpha_1^2 - 16\alpha_2) = \alpha(5 - 6\nu - 3\nu^2), \tag{12.47}$$

$$\alpha_0^4(\phi_0^4 + 4\phi_0^2\phi_1^2 - 12\phi_0^3\phi_1 + 8\phi_0^2\phi_2) = \alpha^4(1 - 6\nu), \tag{12.48}$$

$$\phi_0\phi_1\alpha_0^2 = \frac{\nu}{2}\alpha^2. \tag{12.49}$$

which yield $\alpha_2 = 0$ and $\phi_2 = \frac{-3\nu}{4}$, but leave the last equation inconsistent. This inconsistency can be solved by introducing another parameter. Suppose that the coefficients in the effective scalar potential depend on an external parameter E_{ext} with the dimension of energy.

$$\phi_0(E_{ext}) = \phi_0^{(0)} + \phi_0^{(2)}\frac{E_{ext}}{m_0c^2} + \phi_0^{(4)}\left(\frac{E_{ext}}{m_0c^2}\right)^2, \tag{12.50}$$

$$\phi_1(E_{ext}) = \phi_1^{(0)} + \phi_1^{(2)}\frac{E_{ext}}{m_0c^2}, \tag{12.51}$$

$$\phi_2(E_{ext}) = \phi_2^{(0)}. \tag{12.52}$$

For the matching between the 'real' description and the effective description to work, the external parameter should be set equal to the effective non-relativistic energy, $E_{ext} \equiv \mathcal{E}_0^{NR}$.

What this external parameter then does, is reshuffle the $\frac{1}{c^2}$ expansion such that the parameter-equations for the 1PC and 2PC orders are modified. This introduces many different solutions to the constraint equations. The simplest one incorporates the requirement that the energy-dependence only start to play a role from the 2PC order, and it is given by:

$$\phi_0^{(0)} = -1, \quad \phi_0^{(2)} = 0, \quad \phi_0^{(4)} = 0, \tag{12.53}$$

$$\phi_1^{(0)} = 0, \quad \phi_1^{(2)} = -\frac{\nu}{2}, \quad \phi_1^{(4)} = -\frac{3}{4}\nu, \tag{12.54}$$

$$\alpha_1 = \frac{\nu}{2}, \quad \alpha_2 = 0. \tag{12.55}$$

These parameters define the mapping from the two-body description to an effective one-body description for a body of test mass $m_0 = \mu$ moving in an external scalar potential given by:

$$\Phi_{eff}(R, E_{ext}) = -\frac{e_0}{R}\left[1 - \frac{\nu}{2}\left(\frac{E_{ext}}{m_0c^2}\right)\left(\frac{\alpha_0}{m_0c^2R}\right) - \frac{3\nu}{4}\left(\frac{\alpha_0}{m_0c^2R}\right)^2\right] \tag{12.56}$$

in which the external energy parameter is equal to the non relativistic energy, $E_{ext} \equiv \mathcal{E}_0^{NR}$.

The energy levels are related by the fomula

$$\frac{\mathcal{E}_0^{NR}}{m_0c^2} = \frac{\mathcal{E}^{NR}}{\mu c^2}\left[1 + \frac{\nu}{2}\frac{\mathcal{E}^{NR}}{\mu c^2}\right] \tag{12.57}$$

giving the following relation between the real total relativistic energy $\mathcal{E}$ and the effective relativistic energy $\mathcal{E}_0$:

$$\frac{\mathcal{E}_0}{m_0c^2} \equiv \frac{\mathcal{E}^2 - m_1^2c^4 - m_2^2c^4}{2m_1m_2c^4} \tag{12.58}$$

This result is very interesting because for the limit $m_1 \ll m_2$ the effective energy of the effective particle equals the energy of the particle 1 in the rest frame of particle 2, and likewise the other way around.

Despite these good qualities, the result is unsatisfactory due to the dependence on the energy of the effective scalar potential. It obscures the nature of the mapping and complicates the possibility of incorporating radiation reaction effects (Buonanno, 2000, p. 12).

12.2.2 Effective vector potential

Now exploring the possibility of expanding the vector potential, while the scalar potential Φ_{eff} is independent of any external parameter:

$$\boldsymbol{A}_{eff} = \frac{e_0(\boldsymbol{J}_{ext} \times \boldsymbol{R})}{m_0cR^3}\left[a_0 + a_1\frac{\alpha_0}{m_0c^2R} + ...\right] \tag{12.59}$$

where $\boldsymbol{J}_{ext}$ is an external vector supposed to be perpendicular to the plane of motion. To solve the inconsistency in the constraint equations, we apply the Hamilton-Jacobi framework, and restrict the situation to $\theta = \pi/2$, resulting in

$$\boldsymbol{p} = \frac{\partial S_{eff}}{\partial \boldsymbol{R}} = \hat{\boldsymbol{e}}_R\frac{\partial S_{eff}}{\partial R} + \hat{\boldsymbol{e}}_\phi\frac{1}{R}\frac{\partial S_{eff}}{\partial \phi} \tag{12.60}$$

in which $\hat{\boldsymbol{e}}_R$ and $\hat{\boldsymbol{e}}_\phi$ are vectors of an orthonormal basis. For the particular choice of $\boldsymbol{J}_{ext}$, we now have:

$$\boldsymbol{A}_{eff} = \frac{e_0J_{ext}\hat{\boldsymbol{e}}_\phi}{m_0cR^3}\left[a_0 + a_1\frac{\alpha_0}{m0c^2R} + ...\right] \tag{12.61}$$

where $J_{ext} = |\boldsymbol{J}_{ext}|$. Using $\frac{\partial S_{eff}}{\partial \phi} = \mathcal{J}_0$, we get

$$\boldsymbol{p}\cdot\boldsymbol{A}_{eff} = \frac{e_0 J_{ext}\mathcal{J}_0}{m_0 c R^3}\left[a_0 + a_1\frac{\alpha_0}{m_0 c^2 R} + ...\right], \quad \boldsymbol{A}^2_{eff} = \frac{e_0^2 J_{ext}^2 a_0^2}{m_0^2 c^2 R^4} + ... \tag{12.62}$$

Note that with this special choice for the vector potential, $\boldsymbol{p}\cdot\boldsymbol{A}_{eff}$ does not depend on $\boldsymbol{p}_R$. Plugging this into the Hamilton-Jacobi equation, equation 12.37, with $\mathcal{H}_{eff} = \mathcal{E}_0^{NR} + m_0^2 c^2$ we obtain:

$$\begin{aligned}\frac{dS_R^0}{dR} = 2m_0\mathcal{E}_0^{NR} - 2m_0 e_0\Phi_{eff} - \frac{\mathcal{J}_0^2}{R^2} + \frac{(\mathcal{E}_0^{NR})^2}{c^2} + \frac{e_0^2\Phi_{eff}^2}{c^2} - \frac{2e_0\mathcal{E}_0^{NR}\Phi_{eff}}{c^2} \\ + \frac{2\mathcal{J}_0 J_{ext}}{R^2}\left[a_0\frac{\alpha_0}{m_0 c^2 R} + a_1\left(\frac{\alpha_0}{m_0 c^2 R}\right)^2\right] - \frac{J_{ext}^2}{R^2}a_0^2\left(\frac{\alpha_0}{m_0 c^2 R}\right)^2\end{aligned} \tag{12.63}$$

where Φ_{eff} is given by the expression in equation 12.38, which is the expansion of the scalar potential. Evaluating the radial action variable yields

$$\begin{aligned}\mathcal{I}_R^{eff}(\mathcal{E}_0^{NR}, \mathcal{J}_0, J_{ext}) = \frac{\alpha_0 m_0^{1/2}}{\sqrt{-2\mathcal{E}_0^{NR}}}\left[-\phi_0 - \frac{3\phi_0}{4}\frac{\mathcal{E}_0^{NR}}{m_0 c^2} + \frac{5\phi_0}{32}\left(\frac{\mathcal{E}_0^{NR}}{m_0 c^2}\right)^2\right] - \mathcal{J}_0 \\ + \frac{\alpha_0^2}{\mathcal{J}_0 c^2}\left[\frac{\phi_0^2}{2} - \phi_0\phi_1 - \phi_0 a_0\frac{J_{ext}}{\mathcal{J}_0}\frac{\mathcal{E}_0^{NR}}{m_0 c^2}\left(-\phi_0\phi_1 - \phi_0 a_0\frac{J_{ext}}{\mathcal{J}_0} + a_1\frac{J_{ext}}{\mathcal{J}_0} + a_0^2\frac{J_{ext}^2}{\mathcal{J}_0^2}\right)\right] \\ + \frac{1}{8}\frac{\alpha_0^4}{\mathcal{J}_0^3 c^4}\left[\phi_0^4 - 12\phi_0^3\phi_1 + 8\phi_0^2\phi_2 + 4\phi_0^2\phi_1^2 + 24\phi_0^2\phi_1 a_0\frac{J_{ext}}{\mathcal{J}_0} - 12\phi_0^3 a_1\frac{J_{ext}}{\mathcal{J}_0} + 24\phi_0^2 a_0^2\frac{J_{ext}^2}{\mathcal{J}_0^2}\right].\end{aligned} \tag{12.64}$$

The constraint equations to be satisfied, give the same result for the 0PC order as in the case for the scalar potential: $-\phi_0\alpha_0 = \alpha$, and we pose $\phi_0 = -1$. At 1PC order, we get

$$-\phi_0\alpha_0(2\alpha_1 - 3) = \alpha(\nu - 3), \quad \alpha_0^2\left(\phi_0^2 - 2\phi_0\phi_1 - 2\phi_0 a_0\frac{J_{ext}}{\mathcal{J}_0}\right) = \alpha^2. \tag{12.65}$$

The first of these yields, together with the result from 0PC, that $\alpha_1 = \nu/2$. And for the second of these 1PC constraints, we assume that either the Coulomb potential does not have a correction at 1PC order ($\phi_1 = 0$), or that the vector potential only enters at the next Coulombian order

($a_0 = 0$). The 2PC order constraints are

$$-\phi_0\alpha_0(5 - 12\alpha_1 - 12\alpha_1^2 + 16\alpha_2) = \alpha(5 - 6\nu - 3\nu^2), \tag{12.66}$$

$$\begin{aligned}\alpha_0^2\Bigg(&\phi_0^4 + 4\phi_0^2\phi_1^2 - 12\phi_0^3\phi_1 + 8\phi_0^2\phi_2 + 24\phi_0^2\phi_1 a_0\frac{J_{ext}}{\mathcal{J}_0} \\ &-12\phi_0^3 a_0\frac{J_{ext}}{\mathcal{J}_0} + 24\phi_0^2 a_0^2\frac{J_{ext}^2}{\mathcal{J}_0^2} + 12\phi_0^2 a_1\frac{J_{ext}}{\mathcal{J}_0}\Bigg) = \alpha^4(1 - 6\nu),\end{aligned} \tag{12.67}$$

$$\alpha_0^2\left(\phi_0\phi_1 + \phi_0 a_0\frac{J_{ext}}{\mathcal{J}_0} - a_0^2\frac{J_{ext}^2}{\mathcal{J}_0^2}\right) = \nu\frac{\alpha^2}{2}. \tag{12.68}$$

Plugging the results from the 0PC and 1PC order into the 2PC constraints, and assuming that the external vector J_{ext} coincides with the constant of motion $\mathcal{J}_0$, we end up with the rather simple solution: $\phi_2 = 0$, $a_1 = -\frac{\nu}{2}$, and $\alpha_2 = 0$.

We can conclude from this that it is possible to reduce the two-body description at 2PC order to the description of one test particle moving in an effective electromagnetic field described by a Coulomb potential $\Phi_{eff}(R) = -\frac{e_0}{R}$ and a vector potential dependent on the external vector $\boldsymbol{J}_{ext}(\equiv \boldsymbol{\mathcal{J}}_0)$

$$\boldsymbol{A}_{eff}(R, J_{ext}) = -\frac{\nu}{2}\frac{e_0\alpha_0}{m_0^2c^3}\frac{(\boldsymbol{J}_{ext} \wedge \boldsymbol{R})}{R^4} \tag{12.69}$$

Though this mapping is quite satisfactory because it still satisfies equation 12.58, the fact that it depends on an external parameter is not desirable.

12.2.3 Effective metric

To find an effective description that does not depend on an external parameter, such as the energy or angular momentum of the test particle, especially relevant for incorporating radiation reaction effects, we now relax the assumption that the test mass is moving in flat spacetime. In this section, we describe an effective spacetime metric that can be viewed as an effective way of describing the global exchange of energy between the two charged particles in the two-body description.

We start from the most general spherical symmetric metric in the Schwarzschild gauge:

$$ds_{eff}^2 = -A(R)c^2dt^2 + B(R)dR^2 + R^2(d\theta^2 + \sin\theta^2 d\phi^2), \tag{12.70}$$

where the coefficients $A(R)$ and $B(R)$ are given as expansion in the dimensionless parameter $\frac{\alpha_0}{m_0c^2R}$ as follows:

$$A(R) = 1 + A_1\frac{\alpha_0}{m_0c^2R} + A_2\left(\frac{\alpha_0}{m_0c^2R}\right)^2 + A_3\left(\frac{\alpha_0}{m_0c^2R}\right)^3 + ..., \tag{12.71}$$

$$B(R) = 1 + B_1\frac{\alpha_0}{m_0c^2R} + B_2\left(\frac{\alpha_0}{m_0c^2R}\right)^2 + ... \tag{12.72}$$

Reducing the two-body description to a one-body description can be done by assuming that in the effective metric description only the scalar potential Φ_{eff} is non-zero, thus using equations 12.41 and 12.42. By using the derivative of the Hamilton principal-function, it is now possible to write down the radial action variable for the effective metric situation (Buonanno, 2000, p. 16):

$$\mathcal{I}_R^{eff}(\mathcal{E}_0^{NR}, \mathcal{J}_0) = \frac{\alpha_0 m_0^{1/2}}{\sqrt{-2\mathcal{E}_0^{NR}}}\left[\mathcal{A} + \mathcal{B}\frac{\mathcal{E}_I^{\mathcal{NR}}}{m_0c^2} + \mathcal{C}\left(\frac{\mathcal{E}_I^{\mathcal{NR}}}{m_0c^2}\right)^2\right] - \mathcal{J}_0 + \frac{\alpha_0^2}{\mathcal{J}_0c^2}\left[\mathcal{D} + \mathcal{E}\frac{\mathcal{E}_I^{\mathcal{NR}}}{m_0c^2}\right] + \frac{\alpha_0^4}{\mathcal{J}_0^3c^4}\mathcal{F}, \tag{12.73}$$

where the coefficients are given by (Buonanno, 2000, p. 16):

$$\mathcal{A} = -\phi_0 - \frac{1}{2}A_1, \tag{12.74}$$

$$\mathcal{B} = -\frac{3}{4}\phi_0 + \left(B_1 - \frac{7}{8}A_1\right), \tag{12.75}$$

$$\mathcal{C} = \frac{5}{32}\phi_0 + \left(\frac{B_1}{4} - \frac{19}{64}A_1\right), \tag{12.76}$$

$$\mathcal{D} = \phi_0\left(-\phi_1 - \frac{B_1}{2} + A_1\right) + \frac{1}{2}\phi_0^2 - \frac{1}{4}A_1B_1 + \frac{A_1^2}{2} - \frac{A_2}{2}, \tag{12.77}$$

$$\mathcal{E} = \phi_0\left(-\phi_1 - \frac{B_1}{2} + A_1\right) + A_1^2 + -A_2 - \frac{1}{2}A_1B_1 - \frac{B_1^2}{8} + \frac{B_2}{2}, \tag{12.78}$$

$$\begin{aligned}\mathcal{F} =& \frac{1}{64}(24A_1^4 - 48A_1^2A_2 + 8A_2^2 + 16A_1A_3 - 8A_1^3B_1 + 8A_1A_2B_1 - A_1^2B_1^2 + 4A_1^2B_2) \\ &+ \frac{\phi_0}{16}(-16\phi_1A_1^2 + 24A_1^3 + 8\phi_2A_1 + 8\phi_1A_2 - 32A_1A_2 + 8A_3 + 4\phi_1A_1B_1 \\ &- 8A_1^2B_1 + 4A_2B_1 - A_1B_1^2 + 4A_1B_2) + \frac{\phi_0^3}{4}(-6\phi_1 + 4A_1 - B_1) + \frac{\phi_0^4}{8} \\ &+ \frac{\phi_0^2}{16}(8\phi_1^2 - 40\phi_1A_1 + 32A_1^2 + 16\phi_2 - 20A_2 + 8\phi_1B_1 - 10A_1B_1 - B_1^2 + 4B_2).\end{aligned} \tag{12.79}$$

If you let $\phi_0 \to 0$ and take $\alpha_0 = Gm_1m_2$ in this expression, with G Newton's constant, the result coincides with the expression for the radial action variable in pure General Relativity (Buonanno, 2000, p. 16).

Equate the two-body radial action variable from equation 12.34, and the effective metric one-body radial action variable from equation 12.73, while assuming that $\mathcal{J}_0 = \mathcal{J}$, $m_0 = \mu$, and the mapping between energy levels of the two descriptions from equation 12.40. Then the result is that at 0PC order the constraint is given by $\alpha_0(\phi_0 - A_1/2) = \alpha$ which is fulfilled for taking $A_1 = 0$ and $\phi_0 = -1$. For 1PC order you can then derive the following constraint equations (Buonanno, 2000, p. 16):

$$-2\phi_0\alpha_0(2\alpha_1 - 3_+\alpha_0(7A_1 - 8B_1 - 2A_1\alpha_1) = 2\alpha(\nu - 3), \tag{12.80}$$

$$2\alpha_0^2(\phi_0^2 + \phi_0(2A_1 - B_1 - 2\phi_1)) + \alpha_0^2(2A_1^2 - 2A_2 - A_1B_1) = 2\alpha^2. \tag{12.81}$$

Pose that $\phi_1 = 0$, $A_2 = 0$, and $B_1 = 0$ to ensure that the scalar potential and the effective metric do not differ from the Coulomb potential and the flat spacetime metric. This implies $\alpha_1 = \nu/2$ from the first 1PC constraint, and automatically satisfies the second one (Buonanno, 2000, p. 17).

For 2PC order the values found above can be inserted into the constraint equations, and setting $\phi_2 = 0$ imposes the lack of corrections to the Coulomb potential at this order. This then yields the simple and unique solution with $\alpha_2 = 0$, $A_3 = \nu$, and $B_2 = -\nu$. Hence, introducing the effective metric approach allows for a mapping between the two-body description and one-body description without the introduction of external parameters. There is also no requirement to modify the Coulomb scalar potential because $\Phi_{eff}(R) = -e_0/R$ holds up. To conclude this mapping, the external spacetime metric is given by (Buonanno, 2000, p. 17):

$$A(R) = 1 + \nu\left(\frac{\alpha_0}{m_0c^2R}\right)^3, \quad B(R) = 1 - \nu\left(\frac{\alpha_0}{m_0c^2R}\right)^2. \tag{12.82}$$

Chapter 13

Gravitational Binary Inspiral

Now we go back to the gravitational binary problem. The Effective One Body approach in the gravitational context is based on four tools: resummation methods, flexibility of analytical approaches, extraction of the non-perturbative information contained in numerical simulations, and qualitative understanding of the physical features determining the waveform (Damour and Nagar, 2009, p. 6). The resummation methods will be explained in section 13.1, where the multiplicative multipole decomposition, explained in section 13.1.2, is a way of including qualitative understanding of the physical features of the waveform. The flexibility of analytical approaches is used in creating the mapping between the two-body and one-body descriptions, as we have seen in the previous chapter, and we will see again in sections 13.2 and 13.3 for the gravitational case. Lastly, the extraction of non-perturbative information from numerical relativity will not be discussed in detail, but those are key in the description of the merger stage of the waveform. For the part that we will discuss now, we will first briefly discuss the two resummation methods. After that, we take the post-Newtonian description, as can be found by applying the effective field theory approach, as a starting point to construct the one-body description.

In this section, keep in mind that the main goal of the Effective One Body approach is to extend the analytical representation of the gravitational waveform templates to stages beyond the reach of the post-Newtonian expansion. The post-Newtonian expanded results yield accurate descriptions of the motion and radiation for binary systems in their early inspiralling stage, thus as long as the expansion parameter $\frac{GM}{c^2R}$ is significantly smaller than $\sim \frac{1}{6}$. This boundary corresponds to the last stable orbit, represented by a distance between the two objects of $R \sim \frac{6GM}{c^2}$. After this last stable orbit, the orbital motion is expected to become dynamically unstable, which is the beginning of the plunge-stage of the coalescence (Damour and Nagar, 2009, pp. 5–6). The simplified and condensed description of the one-body formalism is constructed in the stage in which the post-Newtonian description is valid, and then extended to the stages in which the post-Newtonian description breaks down, where the one-body description is tuned by using results from perturbation theory and numerical relativity.

13.1 Resummation methods

To improve the convergence properties of the post-Newtonian expansions, two resummation methods are applied systematically. In the following sections, we will conceptually discuss these resummation methods and their results.

13.1.1 Padé approximants

The first resummation method uses Padé approximants. This method is discussed in the article written by Thibault Damour, Bala R. Iyer, and B.S. Sathyaprakash (Damour, Iyer, and Sathyaprakash, 1998). It takes as input the Taylor-expanded, or PN-expanded, results for the energy and radiation flux, as given in equations 6.5 and 6.6. Without the Padé approximants procedure, these expansions are used to construct approximate waveforms through a standard map, that we will call T. This map takes the successive Taylor coefficients, represented by E_{T_n} and F_{T_n}, and inserts them into an integral, such as the one in equation 6.8 to construct the waveform $h_n^T(t, \lambda_k)$, depending on the time t and the parameters of the signal λ_k, with $k = 1, \ldots, n_\lambda$:

$$(E_{T_n}, F_{T_n}) \xrightarrow{T} h_n^T(t, \lambda_k). \tag{13.1}$$

Alternatively, the Padé approximants approach inserts two extra steps in the mapping procedure, using newly introduced energy-type and flux-type functions, represented by $e(v)$ and $f(v)$. Let us denote this alternative map with P, and consider the four-stage procedure

$$(E_{T_n}, F_{T_n}) \to (e_{T_n}, f_{T_n}) \to (e_{P_n}, f_{P_n}) \to (E[e_{P_n}], F[e_{P_n}, f_{P_n}]) \to h_n^P(t, \lambda_k). \tag{13.2}$$

In their paper, Damour, Iyer, and Sathyaprakash show that the templates $h_n^P(t, \lambda_k)$ perform "better" in several ways than the templates $h_n^T(t, \lambda_k)$. The criteria for assessing the quality of the templates come from comparing the templates with the exact waveforms, which are available through exact results for $E(v)$ and very accurate numerical results for $F(v)$ in the test mass limit (Damour, Iyer, and Sathyaprakash, 1998, pp. 1–4).

The test mass limit is not only used to confirm the robustness of the $h_n^P(t, \lambda_k)$ templates, it also plays a large role in the construction of the Padé approximations $e(v)$ and $f(v)$. These are initially defined in the test mass limit, in which $\eta = 0$ and then extended to cases for which η is nonzero. The full derivation of the energy-type and flux-type functions is explained in (Damour, Iyer, and Sathyaprakash, 1998, pp. 6–13, 18–20). The basis for constructing these functions is the calculation of the Padé approximants to the truncated Taylor series expansions E_{T_n} and F_{T_n}, which are the Taylor expansions for the energy and radiation flux capped at order n. In general, for a truncated Taylor series $S_n(v) = a_0 + a_1 v + \cdots + a_n v^n$, the Padé approximant is defined by two integers m, k, such that $m + k = n$. If $T_n[\cdots]$ denotes the operation of Taylor

expanding a function up to and including order v^n, the Padé approximant of S_n is defined by

$$P_k^m(v) = \frac{N_m(v)}{D_k(v)}, \tag{13.3}$$

with the constraint that

$$T_n[P_m^k(v)] \equiv S_n(v). \tag{13.4}$$

N_m and D_k are polynomials in v of order m and k respectively, and the normalization of $D_k(v)$ such that $D_k(0) = 1$ assures that the Padé approximants are uniquely defined. Furthermore, in many cases the Padé approximants are most useful when they are near diagonal. This is the case for P_m^m if $n = 2m$ is even, and P_m^{m+1} or P_{m+1}^m if $n = 2m + 1$ is odd (Damour, Iyer, and Sathyaprakash, 1998, pp. 18–19).

An example of a diagonal Padé approximant for the truncated Taylor series expansion given by

$$S_2(v) = a_0 + a_1 v + a_2 v^2, \tag{13.5}$$

is given by

$$P_1^1(v) = \frac{c_0}{1 + \frac{c_1 v}{1 + c_2 v}} = c_0 \frac{1 + c_2 v}{1 + (c_1 + c_2)v}, \tag{13.6}$$

where the coefficients c_0, c_1, c_2 have to be determined by comparison to the Taylor expanded form (Damour, Iyer, and Sathyaprakash, 1998, p. 19).

13.1.2 Multiplicative decomposition of the metric multipolar waveform

The second resummation method specifically addresses the multipolar expansion and is explained in full detail in (Damour, Iyer, and Nagar, 2009). One of the characteristic features of this resummation method is that is uses a multiplicative decomposition of the complex multipolar waveform h_{lm}. The post-Newtonian multipolar expansion, on the other hand, is additive, which means that it has the structure of $h_{lm} = h_{lm}^N + h_{lm}^{1PN} + h_{lm}^{1.5PN} + \cdots$. The factors that the multipolar waveform is decomposed into are: (i) the "Newtonian" waveform, (ii) a relativistic correction coming from an "effective source", (iii) leading-order tail effects linked to propagation on a Schwarzschild background, (iv) a residual tail dephasing, (v) residual relativistic amplitude corrections. This yields the (l, m) multipolar waveform emitted by a circular nonspinning compact binary given by (Damour, Iyer, and Nagar, 2009, pp. 1–5):

$$h_{lm}^{(\epsilon)} = \underbrace{\frac{GM\nu}{c^2 R} n_{lm}^{(\epsilon)} c_{l+\epsilon}(\nu) x^{(l+\epsilon)/2} Y^{l-\epsilon,-m}\left(\frac{\pi}{n}, \Phi\right)}_{\text{Newtonian contribution: } h_{lm}^{(N,\epsilon)}} \underbrace{\hat{S}_{eff}^{(\epsilon)} T_{lm} e^{i\delta_{lm}} \rho_{lm}^l}_{\text{other factors: } \hat{h}_{lm}^{(\epsilon)}}. \tag{13.7}$$

ϵ denotes the parity of the multipolar waveform, for the circular case we have: even ($\epsilon = 0$, or $l + m$ =even) for mass-generated multipoles, and odd ($\epsilon = 1$, or $l + m$ =odd) for current-generated ones, $x \equiv (GM\Omega/c^3)^{2/3}$, and $Y^{lm}(\theta, \phi)$ are the usual scalar spherical harmonics. The two factors, $n_{lm}^{(\epsilon)}$ and $c_{l+\epsilon}(\nu)$ are numerical factors (Damour, Iyer, and Nagar, 2009, pp. 1–6). The first part of the multipolar waveform is called "Newtonian" because it is equal to the first term, corresponding to the 0-th post-Newtonian order, in the additive decomposition of the multipolar expansion of the waveform.

The "other factors" $\hat{h}_{lm}^{(\epsilon)} \equiv \hat{S}_{eff}^{(\epsilon)} T_{lm} e^{i\delta_{lm}} \rho_{lm}^{l}$ represents a resummed version of all the post-Newtonian corrections. $\hat{h}_{lm}^{(\epsilon)}$ itself and all its constituting factors have a structure $\hat{h}_{lm}^{(\epsilon)} = 1 + \mathcal{O}(x)$ (Damour and Nagar, 2009, p. 20). These four factors form a decomposition of the post-Newtonian-correction factor $\hat{h}_{lm}^{(\epsilon)} = 1 + h_1 x + h_{1.5} x^{3/2} + \cdots$, and this is the first step of the resummation method. The choice for these four factors is based on physical intuition of the main physical effects entering the final waveform. The motivation for the first factor, the source term $\hat{S}_{eff}^{(\epsilon)}$, is based on the form of the equation satisfied by each partial wave in the test-mass limit. This factor is a linear combination of terms linear in the stress-energy tensor $T_{\mu\nu}$ of a test-particle of mass μ moving around a hole of mass M. The second factor, the tail factor T_{lm}, is motivated by thinking about the structure of the transfer function relating the far-zone gravitational wave amplitude to the near zone one. The remaining two factors, $e^{i\delta_{lm}}$ and ρ_{lm}^{l}, can be identified as the phase and the l-th root of the modulus of the waveform respectively (Damour and Nagar, 2008, pp. 6–7).

13.2 Conservative dynamics

To give an idea of the construction of an effective one-body description, we will consider the procedure for the 2PN order, which is very similar to what we have seen in the previous chapter. The Hamiltonian that describes the conservative part of the equations of motion, in the centre-of-mass frame with the relative motion as a parameter, is given by (Damour and Nagar, 2009, p. 6):

$$H_{2PN}^{relative}(\boldsymbol{q}, \boldsymbol{p}) = H_0(\boldsymbol{q}, \boldsymbol{p}) + \frac{1}{c^2} H_2(\boldsymbol{q}, \boldsymbol{p}) + \frac{1}{c^4} H_4(\boldsymbol{q}, \boldsymbol{p}), \tag{13.8}$$

where

$$H_0(\boldsymbol{q},\boldsymbol{p}) = \frac{\boldsymbol{p}^2}{2\mu} + \frac{GM\mu}{|\boldsymbol{q}|}, \tag{13.9}$$

$$H_2(\boldsymbol{q},\boldsymbol{p}) = \frac{\boldsymbol{p}^4}{8\mu^3}(3\nu-1) - \frac{GM}{2\mu|\boldsymbol{q}|}\left[(3+\nu)\boldsymbol{p}^2 + \nu\left(\frac{\boldsymbol{q}\cdot\boldsymbol{p}}{GM|\boldsymbol{q}|}\right)^2\right] + \frac{\mu}{2}\left(\frac{GM}{|\boldsymbol{q}|}\right)^2, \tag{13.10}$$

$$\begin{aligned} H_4(\boldsymbol{q},\boldsymbol{p}) = {} & \frac{\boldsymbol{p}^6}{16\mu^5}(1-5\nu+5\nu^2) + \frac{GM}{8|\boldsymbol{q}|}\left[\frac{\boldsymbol{p}^4}{\mu^3}(5-20\nu-3\nu^3) - \frac{2\nu^2}{\mu}\left(\frac{\boldsymbol{p}(\boldsymbol{q}\cdot\boldsymbol{p})}{GM|\boldsymbol{q}|}\right)^2\right. \\ & \left. - 3\nu^2\left(\frac{\boldsymbol{q}\cdot\boldsymbol{p}}{GM|\boldsymbol{q}|}\right)^4\right] + \frac{1}{2}\left[\frac{\boldsymbol{p}^2}{\mu}(5+8\nu) + 3\nu\mu\left(\frac{\boldsymbol{q}\cdot\boldsymbol{p}}{GM|\boldsymbol{q}|}\right)^2\right]\left(\frac{GM}{|\boldsymbol{q}|}\right)^2 \\ & - \frac{\mu}{4}(1-3\nu)\left(\frac{GM}{|\boldsymbol{q}|}\right)^3, \end{aligned} \tag{13.11}$$

with $\mu = \frac{m_1 m_2}{M}$ the reduced mass, $M = m_1 + m_2$, and $\nu = \frac{\mu}{M}$ the symmetric mass ratio (Schäfer and Jaranowski, 2018, p. 45). The Newtonian approximation, H_0, can be thought of as a test particle of mass μ orbiting around an external mass GM. The goal of the Effective One Body approach will be to look for an external spacetime geometry $g^{ext}_{\mu\nu}(x^\lambda, GM)$ such that the geodesic dynamics of a test particle of mass μ within $g^{ext}_{\mu\nu}(x^\lambda, GM)$ is equivalent to the dynamics described by equation 13.8 (Damour and Nagar, 2009, pp. 6–7).

The relation between the two descriptions will be considered through a 'dictionary'. Instead of thinking about the classical Hamiltonian, $H(\boldsymbol{q},\boldsymbol{p})$, we will think in a way that is more related to quantum mechanics, in terms of quantized energy levels $E(n,l)$ of the quantum bound states of the Hamiltonian operator $H(\hat{\boldsymbol{q}},\hat{\boldsymbol{p}}$. The energy levels will depend on the integer-valued quantum numbers n and l. l parameterizes the total orbital angular momentum, $\boldsymbol{L}^2 = l(l+1)\hbar^2$, and n is the principal quantum number. These two are related through $n = l + n_r + 1$, where n_r denotes the number of nodes in the radial wave function. There is no magnetic quantum number m for the energy levels due to the spherical symmetry of the system. The non-relativistic Newton interaction in equation 13.9 can be associated with the energy levels given by

$$E_0(n,l) = -\frac{1}{2}\mu\left(\frac{GM\mu}{n\hbar}\right)^2, \tag{13.12}$$

which depends only on n. For the 2PN description of the system in equation 13.8, we can write the energy levels as

$$E^{relative}_{2PN}(n,l) = -\frac{1}{2}\mu\frac{\alpha^2}{n^2}\left[1 + \frac{\alpha^2}{c^2}\left(\frac{c_{11}}{nl} + \frac{c_{20}}{n^2}\right) + \frac{\alpha^4}{c^4}\left(\frac{c_{13}}{nl^3} + \frac{c_{22}}{n^2l^2} + \frac{c_{31}}{n^3l} + \frac{c_{40}}{n^4}\right)\right], \tag{13.13}$$

where $\alpha \equiv GM\mu/\hbar$, and we have assumed the quasi-classical limit where n and l are large. The dimensionless coefficients c_{pq} are functions of the symmetric mass ratio $\nu \equiv \mu/M$. The Hamiltonian expressed in terms of the action variables $J = l\hbar = \frac{1}{2\pi}\oint p_\phi d\phi$, and $N = n\hbar =$

$I_r + J$, with $I_r = \frac{1}{2\pi} \oint p_r dr$, applying to the classical limit, is called the 'Delaunay Hamiltonian' (Damour and Nagar, 2009, p. 7).

So far, the description has still been for a two-body system, but now we start constructing the one-body system. We describe an effective, spherically symmetric metric

$$g^{ext}_{\mu\nu} dx^\mu dx^\nu = -A(R)c^2 dT^2 + B(R)dR^2 + R^2(d\theta^2 + \sin^2\theta d\phi^2). \tag{13.14}$$

Like in the previous chapter, the metric functions $A(R)$ and $B(R)$ are a priori unknown and constructed in the form of expansions in GM/c^2R:

$$A(R) = 1 + a_1 \frac{GM}{c^2 R} + a_2 \left(\frac{GM}{c^2 R}\right)^2 + a_3 \left(\frac{GM}{c^2 R}\right)^3 + \cdots, \tag{13.15}$$

$$B(R) = 1 + b_1 \frac{GM}{c^2 R} + b_2 \left(\frac{GM}{c^2 R}\right)^2 + \cdots, \tag{13.16}$$

in which the dimensionless coefficients a_n, b_n depend on ν. The Newtonian limit, in which $H_2 = H_4 = 0$, fixes the first of the coefficients: $a_1 = -2$. We can separate the following variables in the effective action:

$$S_{eff} = -\mathcal{E}_{eff} t + J_{eff}\phi + S_{eff}(R), \tag{13.17}$$

to solve the effective Hamilton-Jacobi equation

$$g^{\mu\nu}_{eff} \frac{\partial S_{eff}}{\partial x^\nu} \frac{\partial S_{eff}}{\partial x^\mu} + \mu^2 c^2 = 0. \tag{13.18}$$

To compute the Delaunay Hamiltonian, $\mathcal{E}_{eff}(N_{eff}, J_{eff})$, we set

$$N_{eff} = n_{eff}\hbar = J_{eff} + I^{eff}_R, \tag{13.19}$$

$$J_{eff} = l_{eff}\hbar, \tag{13.20}$$

$$I^{eff}_R = \frac{1}{2\pi} \oint p^{eff}_R dR, \tag{13.21}$$

$$P^{eff}_R = \frac{\partial S_{eff}(R)}{dR}, \tag{13.22}$$

such that we get:

$$\mathcal{E}_{eff}(n_{eff}, l_{eff}) = \mu c^2 - \frac{1}{2}\mu \frac{\alpha^2}{n^2_{eff}} \left[1 + \frac{\alpha^2}{c^2}\left(\frac{c^{eff}_{11}}{n_{eff} l_{eff}} + \frac{c^{eff}_{20}}{n^2_{eff}}\right) + \frac{\alpha^4}{c^4}\left(\frac{c^{eff}_{13}}{n_{eff} l^3_{eff}} + \frac{c^{eff}_{22}}{n^2_{eff} l^2_{eff}} + \frac{c^{eff}_{31}}{n^3_{eff} l_{eff}} + \frac{c^{eff}_{40}}{n^4_{eff}}\right)\right]. \tag{13.23}$$

In this description, the dimensionless coefficients c_{pq}^{eff} are functions of the unknown coefficients a_n, b_n from the metric functions in equations 13.15 and 13.16 (Damour and Nagar, 2009, p. 8).

We want to define a 'dictionary' that maps the two-body description in equation 13.13 to the effective one-body description in equation 13.23. It is natural to identify $n = n_{eff}$ and $l = l_{eff}$. One then needs a rule to relate the two energies $E_{real}^{relative}$ and $\mathcal{E}_{eff}$. Buonanno and Damour suggest to first write down a general map between the energy levels of the following form (Buonanno and Damour, 1999, p. 15):

$$\frac{\mathcal{E}_{eff}}{\mu c^2} - 1 = f\left(\frac{E_{real}^{relative}}{\mu c^2}\right) = \frac{E_{real}^{relative}}{\mu c^2}\left(1 + \alpha_1 \frac{E_{real}^{relative}}{\mu c^2} + \alpha_2 \left(\frac{E_{real}^{relative}}{\mu c^2}\right)^2 + \cdots\right). \tag{13.24}$$

This map is represented in figure 13.1. Note that it cannot be directly identified, without some function f, due to the difference in rest-mass contribution (Damour and Nagar, 2009, pp. 8–9).

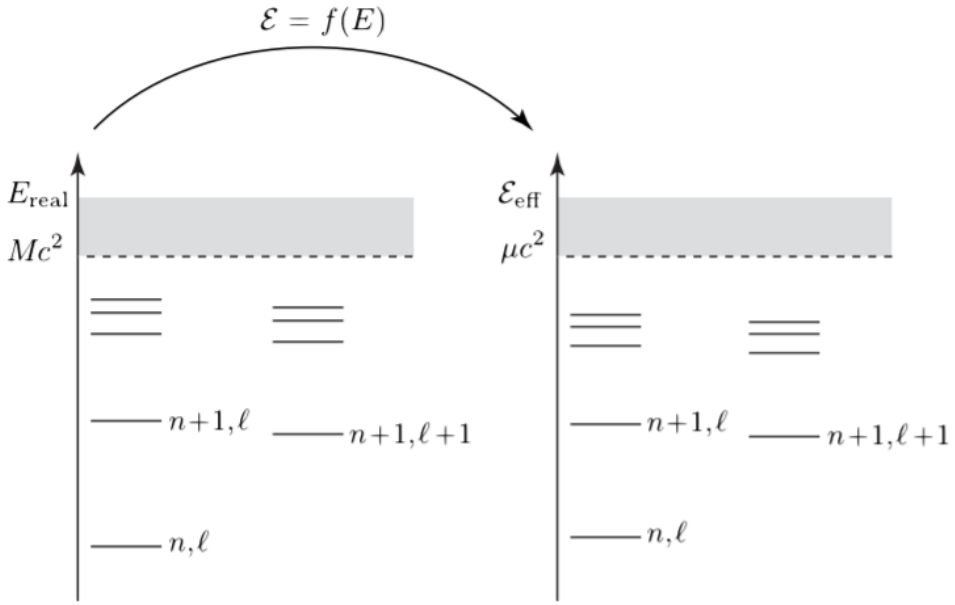

FIGURE 13.1: Schematic representation of the correspondence between energy levels of the real and effective conservative dynamics. n denotes the 'principal quantum number' ($n = n_r + l + 1$, with $n_r = 0, 1, \ldots$ denoting the number of nodes in the radial function), while l denotes the (relative) orbital angular momentum ($\boldsymbol{L}^2 = l(l+1)\hbar^2$) (Damour and Nagar, 2009, p. 9).

We can see that identifying $\mathcal{E}_{eff}(n,l)/\mu c^2$ to $f(E_{real}^{relative}/\mu c^2)$ yields six equations relating the six coefficients $c_{pq}^{eff}(a_2, a_3, b_1, b_2)$ to the six coefficients $c_{pq}(\nu)$ and to the two energy coefficients α_1 and α_2. A natural choice is to let the linearized effective metric coincide with the linearized Schwarzschild metric with mass $M = m_1 + m_2$, which is done by choosing $b_1 = +2$. This leaves

a unique solution for the remaining five coefficients (Damour and Nagar, 2009, p. 9):

$$a_2 = 0, \quad a_3 = 2\nu, \quad b_2 = 4 - 6\nu, \quad \alpha_1 = \frac{\nu}{2}, \quad \alpha_2 = 0. \tag{13.25}$$

At 2PN order, the metric component $A(R)$ is given by the simple expression

$$A_{2PN}(R) = 1 - 2\frac{GM}{c^2 R} + 2\nu\left(\frac{GM}{c^2 R}\right)^3. \tag{13.26}$$

In the test-mass limit, for $\nu \to 0$, equation 13.26 yields the Schwarzschild time-time metric coefficient:

$$g_{00}^{Schw} = 1 - 2\frac{GM}{c^2 R}. \tag{13.27}$$

This shows that the symmetric mass ratio ν has the role of a deformation parameter in equation 13.26 connecting the known test-mass result to the non-trivial 2PN order result for other mass ratios (Damour and Nagar, 2009, p. 9).

The simplicity of the one-body description becomes clear when you realise that the ν-dependent terms in the 2PN Hamiltonian from equation 13.8 are all condensed into the $2\nu\left(\frac{GM}{c^2R}\right)^3$-contribution in $A(R)$, together with another simple contribution in the radial metric component: $(A(R)B(R))_{2PN} = 1-6\nu\left(\frac{GM}{c^2R}\right)^2$. This rate of simplification increases for higher PN-orders. For example, including the 3PN-order contributions will add eleven new ν-dependent coefficients to the centre-of-mass frame Hamiltonian, but only adds three additional terms in the effective one-body description: (1) an additional contribution to $A(R)$, (2) an additional contribution to $B(R)$, and (3) a $\mathcal{O}(\boldsymbol{p}^4)$ modification of the 'external' geodesic Hamiltonian (Damour and Nagar, 2009, p. 10).

13.3 Radiation reaction effects

To include the radiation reaction effects, we switch to polar phase space variables r, p_r, ϕ, p_ϕ, in the equatorial plane $\theta = \frac{\pi}{2}$. Furthermore, we replace the radial momentum p_r by the momentum conjugate to the radial coordinate $R_* = \int dR(B/A)^{1/2}$, which yields $P_{R_*} = (A/B)^{1/2}P_R$ (Damour and Nagar, 2009, p. 14). The radiation reaction force now appears in the p_ϕ equation of motion only for the systems that we consider, as is explained in (Buonanno and Damour, 2000, pp. 9–12).

The conservative part of the dynamics has been constructed in the previous section. The result was a map between the real and the effective conservative energies, as given in equation 13.24. This energy map can be solved to obtain $E_{real}^{total} = \sqrt{s}$ in terms of $\mathcal{E}_{eff}$, and then by solving the effective Hamiltonian Jacobi equation to get $\boldsymbol{\mathcal{E}}_{eff}$ in terms of the effective phase space coordinates $\boldsymbol{q}_{eff}$ and $\boldsymbol{p}_{eff}$, the full effective one-body Hamiltonian is obtained. The result is given by

two nested square roots ($c = 1$):

$$\hat{H}_{EOB}(r, p_{r_*}, \phi) = \frac{H^{real}_{EOB}}{\mu} = \frac{1}{\nu}\sqrt{1 + 2\nu(\hat{H}_{eff} - 1)}, \tag{13.28}$$

where

$$\hat{H}_{eff} = \sqrt{p^2_{r_*} + A(r)\left(1 + \frac{p^2_\phi}{r^2} + z_3\frac{p^4_{r_*}}{r^2}\right)}, \tag{13.29}$$

with $z_3 = 2\nu(4 - 3\nu)$. $A(r)$ is the effective one-body metric function defined by Padé resumming the Taylor-expanded equation 13.15 obtained from matching the real and effective energy levels. The following rescaled dimensionless (effective) variables have been used: $r = \frac{R}{GM}$, $p_{r_*} = \frac{P_{R*}}{\mu}$, $p_\phi = \frac{P_\phi}{\mu GM}$, $t = \frac{T}{GM}$. This yields the following equations of motion, in which we define $A' = \frac{dA}{dr}$ (Damour and Nagar, 2009, pp. 14–15):

$$\frac{d\phi}{dt} = \frac{\partial \hat{H}_{EOB}}{\partial p_\phi} = \frac{A p_\phi}{\nu r^2 \hat{H}\hat{H}_{eff}} \equiv \Omega, \tag{13.30}$$

$$\frac{dr}{dt} = \left(\frac{A}{B}\right)^{1/2}\frac{\partial \hat{H}_{EOB}}{\partial p_{r_*}} = \left(\frac{A}{B}\right)^{1/2}\frac{1}{\nu\hat{H}\hat{H}_{eff}}\left(p_{r_*} + z_3\frac{2A}{r^2}p^3_{r_*}\right), \tag{13.31}$$

$$\frac{dp_\phi}{dt} = \hat{\mathcal{F}}_\phi, \tag{13.32}$$

$$\frac{dp_{r_*}}{dt} = -\left(\frac{A}{B}\right)^{1/2}\frac{\partial \hat{H}_{EOB}}{\partial r} \tag{13.33}$$

$$= -\left(\frac{A}{B}\right)^{1/2}\frac{1}{2\nu\hat{H}\hat{H}_{eff}}\left\{A' + \frac{p^2_\phi}{r^2}\left(A' - \frac{2A}{r}\right) + z_3\left(\frac{A'}{r^2} - \frac{2A}{r^3}\right)p^4_{r_*}\right\}. \tag{13.34}$$

The next step is to construct the ϕ-component of the gravitational radiation flux, $\hat{\mathcal{F}}_\phi$, from resumming the ϕ component of the radiation reaction. During the initial stage of the inspiral, in which the orbit is quasi-circular, $\hat{\mathcal{F}}_\phi$ is known in its post-Newtonian expanded form:

$$\hat{\mathcal{F}}^{Taylor}_\phi = -\frac{32}{5}\nu\Omega^5 r^4_\omega \hat{F}^{Taylor}(v_\phi), \tag{13.35}$$

where $v_\phi \equiv \Omega r_\omega$, and $r_\omega \equiv r[\psi(r, p_\phi)]^{1/3}$ is a modified effective one-body radius, with ψ defined as

$$\psi(r, p_\phi) = \frac{2}{r^2}\left(\frac{dA(r)}{dr}\right)^{-1}\left[1 + 2\nu\left(\sqrt{A(r)\left(1 + \frac{p^2_\phi}{r^2}\right)} - 1\right)\right]. \tag{13.36}$$

$\hat{F}^{Taylor}$ in equation 13.35 is then given by

$$\hat{F}^{Taylor}(v) = 1 + A_2(\nu)v^2 + A_3(\nu)v^3 + A_4(\nu)v^4 + A_5(\nu)v^5 + A_6(\nu, \log v)v^6 + A_7(\nu)v^7 + A_8(\nu = 0, \log v)v^8, \quad (13.37)$$

which includes the known 3.5PN-accurate comparable-mass result, and the small-mass-ratio 4PN contributions (Tagoshi and Sasaki, 1994) (Damour and Nagar, 2009, pp. 15–16).

However, these and higher-order results are rather slowly converging towards the exact value computed by perturbation theory in the small-mass limit $\nu = 0$, as can be seen in figure 13.2. Especially up to the last stable orbit the convergent properties are poor. The two resummation methods discussed in section 13.1 can be used to improve the convergence of the ϕ component of the radiation reaction $\mathcal{F}_\phi$ (Damour and Nagar, 2009, pp. 16–19).

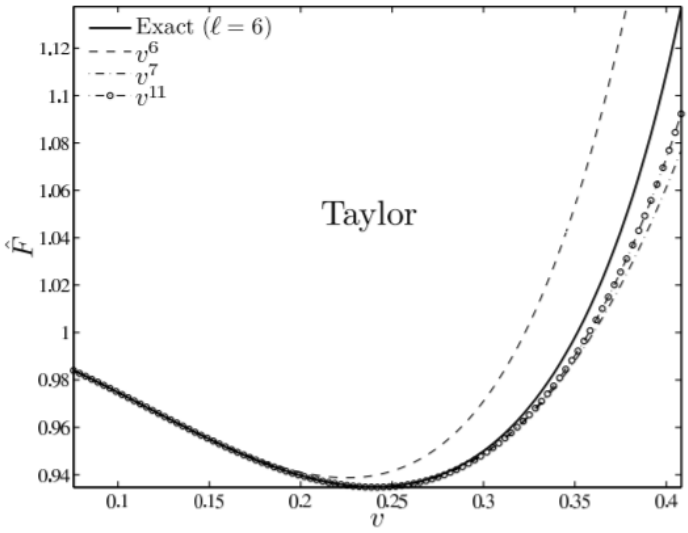

FIGURE 13.2: Illustration of the Taylor expansion of the flux emitted by a particle on circular orbits in the extreme mass ratio limit $\nu = 0$. The Taylor expansion has been performed around the numerical result (computed up to $l = 6$) obtained via perturbation theory (Damour and Nagar, 2009, p. 16).

The first step in applying the Padé resummation is to choose a number for v_{pole} which represents the value of the orbital velocity v_ϕ at which the exact angular momentum flux would become infinite if $\hat{\mathcal{F}}_\phi$ would be analytically continued beyond the last stable orbit. Given v_{pole}, the resummed radiation raction expression is given by

$$\hat{F}^{resummed}(v_\phi) = \left(1 - \frac{v_\phi}{v_{pole}}\right)^{-1} P_4^4 \left[\left(1 - \frac{v_\phi}{v_{pole}}\right) \hat{F}^{Taylor}(v_\phi, \nu = 0)\right], \quad (13.38)$$

where P_4^4 is a $(4, 4)$ Padé approximant as explained in section 13.1.1 (Damour and Nagar, 2009, pp. 17–18).

Figure 13.3 shows the results for the Padé resummation applied to the results from figure 13.2. The v_{pole} was set to be equal to $1/\sqrt{3}$, corresponding to standard Schwarzschild value for $\nu = 0$ (Damour and Nagar, 2009, p. 17) (Damour, Iyer, and Sathyaprakash, 1998). The resummed energy flux not only converges better, but the convergence is also monotonic, which was not the case for the Taylor expanded energy flux.

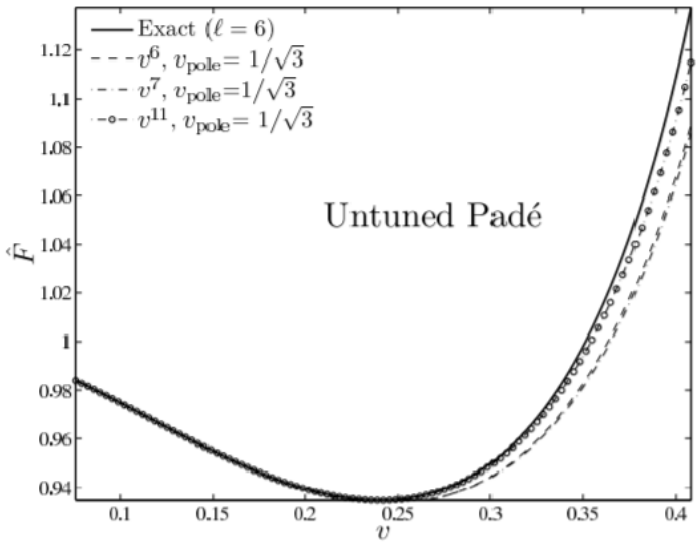

FIGURE 13.3: Illustration of the untuned Padé resummed expansion of the flux emitted by a particle on circular orbits in the extreme mass ratio limit $\nu = 0$. The standard Schwarzschild value $v_{pole} = 1/\sqrt{3}$ has been chosen here (Damour and Nagar, 2009, p. 18).

The resummed result can even be improved further by 'flexing' the value of v_{pole}. This means that v_{pole} is tuned until the difference between the resummed and the exact flux at the last stable orbit is minimal (Damour and Nagar, 2009, p. 18). The full explanation of this approach is given in (Damour and Nagar, 2008), and the results are given in figure 13.4.

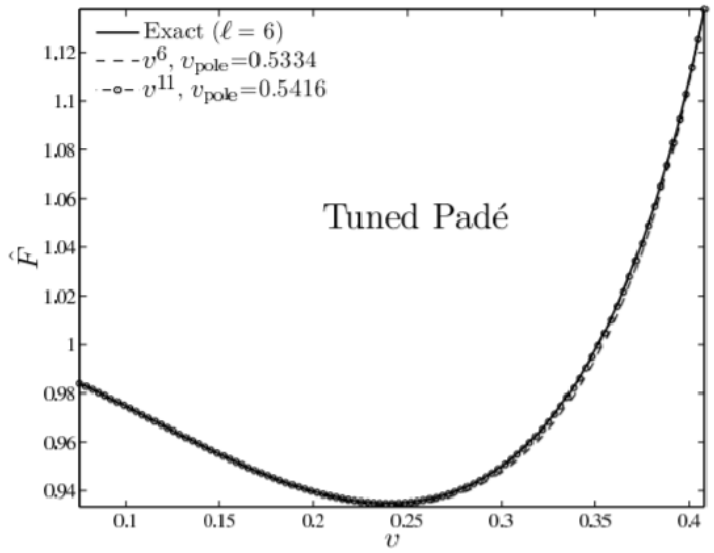

FIGURE 13.4: Illustration of the tuned Padé resummed expansion of the flux emitted by a particle on circular orbits in the extreme mass ratio limit $\nu = 0$. The value v_{pole} has been flexed as described in (Damour, Iyer, and Nagar, 2009) to improve agreement between the resummed and exact energy flux (Damour and Nagar, 2009, p. 18).

Chapter 14

Discussion of Part III

Conceptually, this part started from the results of the previous part, or from the post-Newtonian expanded action obtained through another method. The effective one-body description can be seen as an extension of the effective field theory from which both the finite-size effects and the potential modes are integrated out since in such a theory the two objects of the binary cannot be distinguished anymore. Another way of seeing the approach is as a generalisation of the test particle limit. Independent from the physical interpretation or conceptual understanding, the description of the system as an effective body moving through a fixed external spacetime geometry yields impressive results.

Two important tools for the effective one-body description are the applied resummation methods: Padé resummation, and multiplicative decomposition of the multipole waveform. The former is a general procedure to rewrite Taylor expansions up to a certain order. The latter is a new way to decompose the multipole waveform, the resummation uses a multiplicative, instead of the more standard additive, decomposition. Both resummation methods show to be effective on their own, and their strengths can be combined in the effective one-body description.

The overall procedure to match the effective one-body description to the two-body description is performed in a mapping of the energies of both descriptions. From this mapping in situations in which both the two-body and the one-body descriptions are well-known, such as the test particle limit, the coefficients can be fixed and the one-body description can be extended to apply in regions in which there is no accurate two-body description.

The electromagnetic case presented an interesting study because the availability of exact solutions to the Maxwell equations allows verifying the accuracy of the effective one-body description for a larger range of parameters. The mapping was performed in three different ways: by an expansion in the scalar field, one in the vector field, and one in the metric field. It showed that for both the effective scalar and effective vector descriptions a dependence on external parameters obscured the mapping, and hence reduces the ability to analytically describe situations outside of the range of validity of the post-Coulombian two-body description.

With this information, we immediately jumped to the effective metric description to construct the mapping in the gravitational theory. Although the full mapping and procedure to construct the effective one-body description that generates observable results for the waveform and phase of a gravitational wave is more extensive than the discussion in this part of the project, we were able to get an impression of the different tools and methods used in the approach. The full approach can generate waveforms in the inspiral, late-inspiral, plunge, and ringdown stages of a binary coalescence. An example of such a combined result of these descriptions of the stages of a waveform is given in figure 14.1.

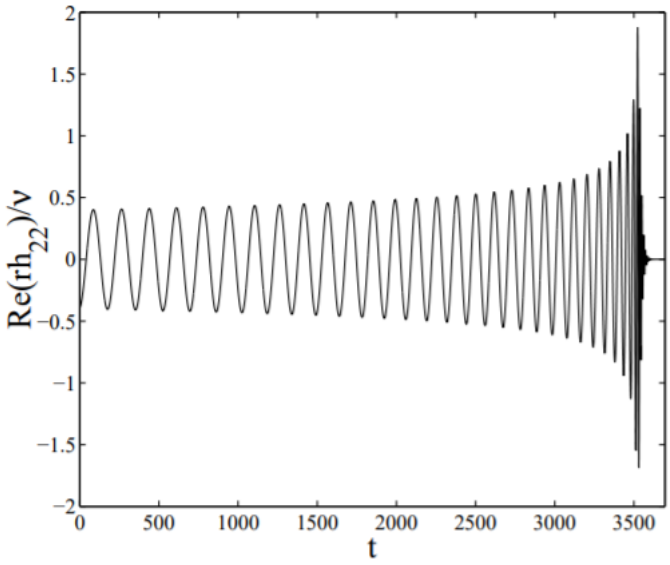

FIGURE 14.1: Complete resummed effective one-body quadrupolar $(l = 2, m = 1)$ waveform with ~ 29 cycles of inspiral, ~ 1 cycle during plunge, and ~ 4 cycles of ring-down (Damour, 2008, p. 15).

The post-Newtonian expansion gives an accurate description for the early inspiral of the merger up to the last stable circular orbit, corresponding to values of the expansion parameter up to $\frac{GM}{c^2 r} \sim \frac{1}{6}$. The Effective One Body approach generates a description of the dynamics and radiation for late inspiral, for $\frac{GM}{c^2 r} \gtrsim \frac{1}{12}$, and the subsequent plunge and merger stages. The ring-down parts of the description are often obtained by including numerical results (Damour and Nagar, 2009, p. 5).

Chapter 15

Conclusions

We have looked at a variety of breakthroughs in the development of gravitational wave theory. Now, to conclude this project, there are five observations, reflections and insights that I would like to share.

The first is the link between theoretical and experiment progress. Gravitational waves have shown to be a great example of the complementary nature of both areas. It is impossible to say that only theory has supported experimental research or vice versa. Instead, both have stimulated one another. Starting with the theoretical possibility for the existence of gravitational waves while there was still a seemingly insurmountable gap between the domain in which gravitational waves were expected and the domain of the experimental capabilities at the time. However, it was the experimental ambition of Joseph Weber that sparked experimental advances decreasing the gap, and later also renewed theoretical interest in the theory. Since the detection of gravitational waves was no longer deemed impossible, the two have worked closely together. Theoretical efforts are providing continuously improving effective descriptions which have been indispensable in constructing gravitational wave templates to extract the signal from the detector output. And the detections themselves offer important verification of these theoretical models and add to the ability to test predictions.

The second point to make here is that even though the concept of 'effective theories' that we have discussed here still is very abstract and broad, the mindset has become imperative in describing gravitational systems subject to General Relativity. In effective theories, there is always a compromise to be made between giving up on the fundamental description in a theory, and the feasibility of obtaining solutions. You could argue that explicit understanding of the effective theory mindset is not essential for using effective theories. The development of the effective theory mindset came at around the same time as the development of several effective theories such as effective field theory in particle physics, therefore it is hard to say which came first. However, it is also quite unnatural to view them as separate advancements. It pays off in both ways: understanding the conceptual foundation of effective theories in general can help to grasp the big outlines of a specific effective theory, while specific effective theories help to

understand the true trade-offs that are made for effective theories. The first holds for philosophy of science in its own discipline because even though scientists are best at doing science and do not require the ideas of philosophers, they are also often too close to their work to describe the nature of what they are doing. The second has been shown in practice in this project by first introducing the basic description of effective theories, and then giving two examples of how it is applied in practice, thus proving that the trade-offs being made do pay off in results and showing the variety of manifestations.

The next two observations are related to the two examples of effective theories that we have discussed: the effective field theory approach, and the effective one body approach. To put these two approaches into a broader context of the parameter space in which they can be applied, we consider figure 15.1. This diagram shows four different approaches to find solutions to the gravitational binary system central to this project. Note that the post-Newtonian description is a description that we have considered with the effective field theory approach and covers the upper half, non-relativistic and weak gravitational, domain. The effective one body description covers the whole diagram indicated by the dashed grey line.

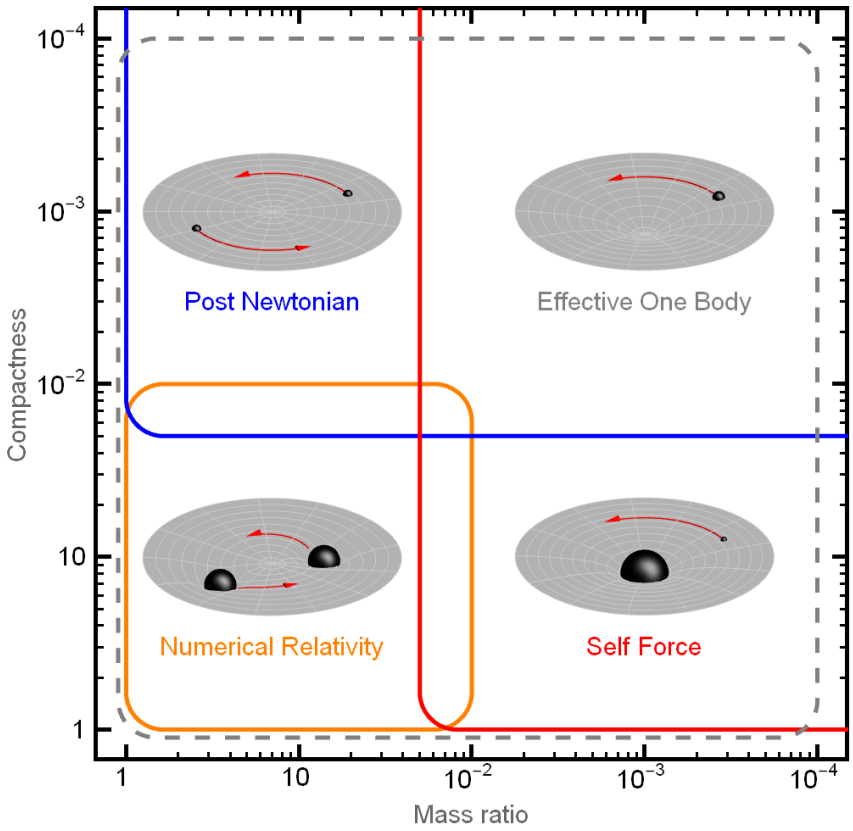

FIGURE 15.1: Diagram of the parameter space of compact binaries with the various approximation schemes and their regions of validity (van de Meent, 2015).

The third reflection concerns the effective field theory approach. While still not a trivial procedure, it is a very robust framework to systematically build an effective theory to find solutions. Familiarity with (effective) quantum field theories helps to see the rationale in the approach and even provides an amount of physical intuition to combine the various contributing effect. The use of the effective field theory can be classified as a combination between top-down and bottom-up. The former because it is a more comprehensive description of situations governed by General Relativity, and the latter because the ignorance about the exact dynamics on the smallest scales is integrated out and parameterized. This approach can be applied to other situations with a separation of scales. For example, Rafael Porto also discusses the effective theory of cosmological large scale structures (Porto, 2016, pp. 90–117). Hence we can conclude that the effective field theory approach is rich in its ability to solve complicated theories involving a large range of scales and versatile in its applications.

Fourthly, we address the effective one body approach. The biggest success of the approach lies in its region of validity in the parameter space. This enables the description to bridge gaps between other descriptions and combine the strengths from different approaches. However, the effective one body description compromises on the physical intuition supporting its validity in certain situations, and in those regions seems to be a clever trick to fine-tune the results. Its success also heavily relies on the descriptions it takes as input, such as the post-Newtonian expansion. Concerning the types of use of effective theories, the effective one body approach lacks a more fundamental describing theory, and therefore it is a bottom-up approach.

The last observation to make in this concluding chapter is the impressive results that both effective approaches yield individually, but more importantly, their combined strength. The appreciation for the accuracy of results that have been generated, and the boost in experimental abilities that this provides, grows even bigger when the complexity of the binary systems and all their interactions has been considered. To come back to the discussion of scientific progress from chapter 3.5, these theories or approaches are not incommensurable and therefore we do not have to choose which one is better or 'right'. Instead, the approaches have shown to be highly complementary, and in the case of the effective one body approach even dependent on the approaches generating the post-Newtonian description and other theories to generate the necessary input. The most impressive results are a virtue of the collective efforts of effective approaches to General Relativity.

These collective results have already been utilised in the confirmed detections of gravitational waves by several laser interferometers. For example, the detection of event GW150914 with which we have started the introduction of this thesis was facilitated by an enormous bank of templates constructed from models of the waveform that combine post-Newtonian theory, the effective one body formalism, and numerical relativity simulations (Abbott et al., 2016b, p. 6). Furthermore, where we ended the discussion in chapter 10 of part II by referring to the successful results of post-Newtonian descriptions up to 4PN order, the combined efforts

of post-Newtonian, post-Minkowskian, multipolar-post-Minkowskian, gravitational self-force, and Effective One Body approaches have been able to obtain the first partial results up to the 5th post-Newtonian order (Bini, Damour, and Geralico, 2019).

Let, therefore, after these remarks, the final conclusion be that instead of viewing 'effective' solely as 'practical' and 'not fundamental' when we talk about effective theories, we add another meaning of the word: 'successful'.

Bibliography

Abbott, B. P. et al. (Feb. 2016a). "Observation of Gravitational Waves from a Binary Black Hole Merger". In: *Phys. Rev. Lett.* 116 (6), p. 061102. DOI: 10.1103/PhysRevLett.116.061102. URL: https://link.aps.org/doi/10.1103/PhysRevLett.116.061102.

Abbott, B.P. et al. (Oct. 2016b). "Binary Black Hole Mergers in the First Advanced LIGO Observing Run". In: *Physical Review X* 6.4. ISSN: 2160-3308. DOI: 10.1103/physrevx.6.041015. URL: http://dx.doi.org/10.1103/PhysRevX.6.041015.

Arnowitt, R., S. Deser, and C. W. Misner (Dec. 1959). "Dynamical Structure and Definition of Energy in General Relativity". In: *Phys. Rev.* 116 (5), pp. 1322–1330. DOI: 10.1103/PhysRev.116.1322. URL: https://link.aps.org/doi/10.1103/PhysRev.116.1322.

Barausse, Enrico et al. (Aug. 2020). "Prospects for fundamental physics with LISA". In: *General Relativity and Gravitation* 52.8. ISSN: 1572-9532. DOI: 10.1007/s10714-020-02691-1. URL: http://dx.doi.org/10.1007/s10714-020-02691-1.

Bini, Donato, Thibault Damour, and Andrea Geralico (Dec. 2019). "Novel Approach to Binary Dynamics: Application to the Fifth Post-Newtonian Level". In: *Physical Review Letters* 123.23. ISSN: 1079-7114. DOI: 10.1103/physrevlett.123.231104. URL: http://dx.doi.org/10.1103/PhysRevLett.123.231104.

Blanchet, Luc (Feb. 2016). "Gravitational Radiation from Post-Newtonian Sources and Inspiralling Compact Binaries". In: *Living Reviews in Relativity* 17.1. ISSN: 1433-8351. DOI: 10.12942/lrr-2014-2. URL: http://dx.doi.org/10.12942/lrr-2014-2.

Blümlein, J. et al. (2020). "Fourth post-Newtonian Hamiltonian dynamics of two-body systems from an effective field theory approach". In: *Nuclear Physics B* 955, p. 115041. ISSN: 0550-3213. DOI: https://doi.org/10.1016/j.nuclphysb.2020.115041. URL: https://www.sciencedirect.com/science/article/pii/S0550321320301279.

Brezin, E., C. Itzykson, and J. Zinn-Justin (Apr. 1970). "Relativistic Balmer Formula Including Recoil Effects". In: *Phys. Rev. D* 1 (8), pp. 2349–2355. DOI: 10.1103/PhysRevD.1.2349. URL: https://link.aps.org/doi/10.1103/PhysRevD.1.2349.

Buonanno, A. and T. Damour (Mar. 1999). "Effective one-body approach to general relativistic two-body dynamics". In: *Physical Review D* 59.8. ISSN: 1089-4918. DOI: 10.1103/physrevd.59.084006. URL: http://dx.doi.org/10.1103/PhysRevD.59.084006.

Buonanno, Alessandra (Oct. 2000). "Reduction of the two-body dynamics to a one-body description in classical electrodynamics". In: *Physical Review D* 62.10. ISSN: 1089-4918. DOI:

10.1103/physrevd.62.104022. URL: http://dx.doi.org/10.1103/PhysRevD.62.104022.

Buonanno, Alessandra and Thibault Damour (Aug. 2000). "Transition from inspiral to plunge in binary black hole coalescences". In: *Physical Review D* 62.6. ISSN: 1089-4918. DOI: 10.1103/physrevd.62.064015. URL: http://dx.doi.org/10.1103/PhysRevD.62.064015.

Cannella, Umberto (2011). *Effective Field Theory Methods in Gravitational Physics and Tests of Gravity*. arXiv: 1103.0983 [gr-qc].

Chalmers, Alan (1999). *Wat heet wetenschap*. Amsterdam: Boom.

Chen, Chiang-Mei, James M. Nester, and Wei-Tou Ni (Feb. 2017). "A brief history of gravitational wave research". In: *Chinese Journal of Physics* 55.1, 142–169. ISSN: 0577-9073. DOI: 10.1016/j.cjph.2016.10.014. URL: http://dx.doi.org/10.1016/j.cjph.2016.10.014.

Clifford, William K. (1876). "On the Space Theory of Matter". In: *Proceedings in Cambridge Philosophical Society* 2, pp. 157–158.

Crowther, Karen (Nov. 2018). "What is the Point of Reduction in Science?" In: *Erkenntnis* 85, pp. 1437–1460. URL: https://doi.org/10.1007/s10670-018-0085-6.

Damour, T and G. Schäfer (Feb. 1988). "Higher-order relativistic periastron advances and binary pulsars". In: *Il Nuovo Cimento B* 101 (2), pp. 127–176. DOI: 10.1007/BF02828697. URL: https://doi.org/10.1007/BF02828697.

Damour, Thibault (Mar. 2008). "Introductory lectures on the effective one body formalism". In: *International Journal of Modern Physics A* 23.08, 1130–1148. ISSN: 1793-656X. DOI: 10.1142/s0217751x08039992. URL: http://dx.doi.org/10.1142/S0217751X08039992.

Damour, Thibault, Bala R. Iyer, and Alessandro Nagar (Mar. 2009). "Improved resummation of post-Newtonian multipolar waveforms from circularized compact binaries". In: *Physical Review D* 79.6. ISSN: 1550-2368. DOI: 10.1103/physrevd.79.064004. URL: http://dx.doi.org/10.1103/PhysRevD.79.064004.

Damour, Thibault, Bala R. Iyer, and B. S. Sathyaprakash (Jan. 1998). "Improved filters for gravitational waves from inspiraling compact binaries". In: *Physical Review D* 57.2, 885–907. ISSN: 1089-4918. DOI: 10.1103/physrevd.57.885. URL: http://dx.doi.org/10.1103/PhysRevD.57.885.

Damour, Thibault and Alessandro Nagar (Jan. 2008). "Comparing effective-one-body gravitational waveforms to accurate numerical data". In: *Physical Review D* 77.2. ISSN: 1550-2368. DOI: 10.1103/physrevd.77.024043. URL: http://dx.doi.org/10.1103/PhysRevD.77.024043.

– (2009). *The Effective One Body description of the Two-Body problem*. arXiv: 0906.1769 [gr-qc].

Damour, Thibaut (Sept. 1983). "Gravitational Radiation Reaction in the Binary Pulsar and the Quadrupole-Formula Controversy". In: *Phys. Rev. Lett.* 51 (12), pp. 1019–1021. DOI: 10.1103/PhysRevLett.51.1019. URL: https://link.aps.org/doi/10.1103/PhysRevLett.51.1019.

Dimastrogiovanni, Ema (Mar. 2021). *Lecture Notes March 3rd*.

Duff, M. J. (Apr. 1973). "Quantum Tree Graphs and the Schwarzschild Solution". In: *Phys. Rev. D* 7 (8), pp. 2317–2326. DOI: 10.1103/PhysRevD.7.2317. URL: https://link.aps.org/doi/10.1103/PhysRevD.7.2317.

Einstein, A. and A. D. Fokker (1914). "Die Nordströmsche Gravitationstheorie vom Standpunkt des absoluten Differentialkalküls". In: *Annalen der Physik* 349.10, pp. 321–328. DOI: https://doi.org/10.1002/andp.19143491009. eprint: https://onlinelibrary.wiley.com/doi/pdf/10.1002/andp.19143491009. URL: https://onlinelibrary.wiley.com/doi/abs/10.1002/andp.19143491009.

Einstein, Albert (1916). "Die Grundlage der allgemeinen Relativitätstheorie". In: *Annalen der Physik* 354.7, pp. 769–822. DOI: https://doi.org/10.1002/andp.19163540702. eprint: https://onlinelibrary.wiley.com/doi/pdf/10.1002/andp.19163540702. URL: https://onlinelibrary.wiley.com/doi/abs/10.1002/andp.19163540702.

– (1998). "To Karl Schwarzschild". In: *The Collected Papers of Albert Einstein*. Ed. by Ann M. Hentschel. Vol. 8. Princeton University Press. Chap. 194, p. 196.

Emparan, Roberto (Dec. 2020). *Effective Theories of Black Hole Dynamics*. International online lecture series.

Falcke, Heino (2020). *Licht in de duisternis. Zwarte gaten, het universium en wij*. Trans. by Jörg Römer. Amsterdam: Prometheus.

Feyerabend, Paul K. (1962). "Explanation, Reduction and Empiricism". In: *Scientific Explanation, Space, and Time*. Vol. 3. Minnesota studies in the philosophy of science. University of Minnesota Press, pp. 28–97.

Feynman, R. P. (1996). *Feynman lectures on gravitation*. Ed. by F. B. Morinigo, W. G. Wagner, and B. Hatfield.

Foffa, Stefano and Riccardo Sturani (Jan. 2014). "Effective field theory methods to model compact binaries". In: *Classical and Quantum Gravity* 31.4, p. 043001. ISSN: 1361-6382. DOI: 10.1088/0264-9381/31/4/043001. URL: http://dx.doi.org/10.1088/0264-9381/31/4/043001.

Galley, Chad R. and Adam K. Leibovich (Aug. 2012). "Radiation reaction at 3.5 post-Newtonian order in effective field theory". In: *Physical Review D* 86.4. ISSN: 1550-2368. DOI: 10.1103/physrevd.86.044029. URL: http://dx.doi.org/10.1103/PhysRevD.86.044029.

Goldberger, Walter D. (Jan. 2007). "Les Houches Lectures on Effective Field Theories and Gravitational Radiation". In: URL: https://arxiv.org/abs/hep-ph/0701129v1.

Goldberger, Walter D. and Ira Z. Rothstein (May 2006a). "Effective field theory of gravity for extended objects". In: *Physical Review D* 73.10. ISSN: 1550-2368. DOI: 10.1103/physrevd.73.104029. URL: http://dx.doi.org/10.1103/PhysRevD.73.104029.

– (Nov. 2006b). "Towers of gravitational theories". In: *General Relativity and Gravitation* 38 (11), pp. 1537–1546. ISSN: 1572-9532. DOI: 10.1007/s10714-006-0345-7. URL: https://doi.org/10.1007/s10714-006-0345-7.

Goldstein, H., C.P. Poole, and J.L. Safko (2002). *Classical Mechanics*. Addison Wesley. ISBN: 9780201657029.

Gupta, Suraj N. (Dec. 1954). "Gravitation and Electromagnetism". In: *Phys. Rev.* 96 (6), pp. 1683–1685. DOI: 10.1103/PhysRev.96.1683. URL: https://link.aps.org/doi/10.1103/PhysRev.96.1683.

Hartmann, Stephan (2001). *Effective Field Theories, Reductionism and Scientific Explanation*. URL: http://philsci-archive.pitt.edu/93/.

Hilborn, Robert C. (Mar. 2018). "Gravitational waves from orbiting binaries without general relativity". In: *American Journal of Physics* 86.3, 186–197. ISSN: 1943-2909. DOI: 10.1119/1.5020984. URL: http://dx.doi.org/10.1119/1.5020984.

Johansen, Nils Voje and Finn Ravndal (Mar. 2006). "On the discovery of Birkhoff's theorem". In: *General Relativity and Gravitation* 38.3, pp. 537–540. DOI: 10.1007/s10714-006-0242-0. URL: https://doi.org/10.1007/s10714-006-0242-0.

Kennefick, Daniel (2017). "The binary pulsar and the quadrupole formula controversy". In: *Eur. Phys. J. H* 42.2, pp. 293–310. DOI: 10.1140/epjh/e2016-70059-2.

Kol, Barak and Michael Smolkin (Feb. 2012). "Black hole stereotyping: induced gravito-static polarization". In: *Journal of High Energy Physics* 2012.2. ISSN: 1029-8479. DOI: 10.1007/jhep02(2012)010. URL: http://dx.doi.org/10.1007/JHEP02(2012)010.

Kraichnan, Robert H. (May 1955). "Special-Relativistic Derivation of Generally Covariant Gravitation Theory". In: *Phys. Rev.* 98 (4), pp. 1118–1122. DOI: 10.1103/PhysRev.98.1118. URL: https://link.aps.org/doi/10.1103/PhysRev.98.1118.

Kuhn, Thomas S. (1962). *The Structure of Scientific Revolutions*. Chicago: University of Chicago Press.

Kunze, M. and H. Spohn (2001). "Post-Coulombian Dynamics at Order c-3". In: *Journal of Nonlinear Science* 11, pp. 321–396.

Landau, L.D. et al. (1971). *The Classical Theory of Fields*. Course of theoretical physics v. 2. Pergamon Press. ISBN: 9780080160191.

LIGO Scientific Collaboration. *Burst Gravitational Waves*. URL: https://www.ligo.org/science/GW-Burst.php (visited on 05/24/2021).

– *Continuous Gravitational Waves*. URL: https://www.ligo.org/science/GW-Continous.php (visited on 05/24/2021).

– *Inspiral Gravitational Waves*. URL: https://www.ligo.org/science/GW-Inspiral.php (visited on 05/24/2021).

– *Sources of Gravitational Waves*. URL: https://www.ligo.org/science/GW-Sources.php (visited on 05/24/2021).

– *Stochastic Gravitational Waves*. URL: https://www.ligo.org/science/GW-Stochastic.php (visited on 05/24/2021).

Maggiore, Michele (2008). *Gravitational Waves. Volume 1: Theory and Experiments*. Oxford: Oxford University Press.

Magnan, Christian (2007). *Complete calculations of the perihelion precession of Mercury and the deflection of light by the Sun in General Relativity*. arXiv: 0712.3709 [gr-qc].

Nordström, Gunnar (Mar. 1913). "Zur Theorie der Gravitation vom Standpunkt des Relativitätsprinzips". In: *Annalen der Physik* 347, pp. 533 –554. DOI: 10.1002/andp.19133471303.

Oberheim, Eric and Paul Hoyningen-Huene (2018). "The Incommensurability of Scientific Theories". In: *The Stanford Encyclopedia of Philosophy*. Ed. by Edward N. Zalta. Fall 2018. Metaphysics Research Lab, Stanford University.

Peters, P. C. and J. Mathews (July 1963). "Gravitational Radiation from Point Masses in a Keplerian Orbit". In: *Phys. Rev.* 131 (1), pp. 435–440. DOI: 10.1103/PhysRev.131.435. URL: https://link.aps.org/doi/10.1103/PhysRev.131.435.

Poincaré, M. H. (Dec. 1906). "Sur la dynamique de l'électron". In: *Rendiconti del Circolo Matematico di Palermo (1884-1940)* 21 (1), pp. 129–175.

Porto, Rafael A. (May 2016). "The effective field theorist's approach to gravitational dynamics". In: *Physics Reports* 633, 1–104. ISSN: 0370-1573. DOI: 10.1016/j.physrep.2016.04.003. URL: http://dx.doi.org/10.1016/j.physrep.2016.04.003.

Ross, Andreas (June 2012). "Multipole expansion at the level of the action". In: *Physical Review D* 85.12. ISSN: 1550-2368. DOI: 10.1103/physrevd.85.125033. URL: http://dx.doi.org/10.1103/PhysRevD.85.125033.

Rothstein, Ira (Feb. 2016). *Classical Effective Field Theories*. School on Effective Field Theory across Length Scales. URL: https://www.ictp-saifr.org/wp-content/uploads/2015/05/ChapterCLEFT_Ira1.pdf.

Rothstein, Ira Z. (May 2014). "Progress in effective field theory approach to the binary inspiral problem". In: *General Relativity and Gravitation* 46 (6). DOI: 10.1007/s10714-014-1726-y. URL: https://doi.org/10.1007/s10714-014-1726-y.

Schutz, Bernard (2000). "Gravitational Radiation". In: *The Encyclopedia of Astronomy and Astrophysics*. DOI: 10.1888/0333750888/2110. URL: http://dx.doi.org/10.1888/0333750888/2110.

Schäfer, Gerhard and Piotr Jaranowski (Aug. 2018). "Hamiltonian formulation of general relativity and post-Newtonian dynamics of compact binaries". In: *Living Reviews in Relativity* 21.1. ISSN: 1433-8351. DOI: 10.1007/s41114-018-0016-5. URL: http://dx.doi.org/10.1007/s41114-018-0016-5.

Stewart, Iain (2013). *Effective Field Theory*. Lectures Spring Term.

Sturani, Riccardo (Dec. 2014). *Gravitational waves and effective field theory methods to model binaries*. ICTP SAIFR course: 'Effective field theory methods applied to the 2-body problem in General Relativity. URL: https://www.ictp-saifr.org/wp-content/uploads/2013/07/cursoGW-ICTP-Sturani1.pdf.

Tagoshi, H. and M. Sasaki (Oct. 1994). "Post-Newtonian Expansion of Gravitational Waves from a Particle in Circular Orbit around a Schwarzschild Black Hole". In: *Progress of Theoretical*

Physics 92.4, 745–771. ISSN: 1347-4081. DOI: 10.1143/ptp/92.4.745. URL: http://dx.doi.org/10.1143/ptp/92.4.745.

Taylor, J. H., L. A. Fowler, and P. M. McCulloch (Feb. 1979). "Measurements of general relativistic effects in the binary pulsar PSR1913+16". In: *Nature* 277 (5696), pp. 437–440. DOI: 10.1038/277437a0. URL: https://doi.org/10.1038/277437a0.

van de Meent, Maarten (Aug. 2015). *Diagram of the parameter space of compact binaries with the various approximation schemes and their regions of validity*. URL: https://upload.wikimedia.org/wikipedia/commons/a/a1/GR2bodyparameterspace.png.

Weisberg, J. M., D. J. Nice, and J. H. Taylor (Sept. 2010). "Timing Measurements of the Relativstic Binary Pulsar PSR B1913+16". In: *The Astrophysical Journal* 722.2, 1030–1034. ISSN: 1538-4357. DOI: 10.1088/0004-637x/722/2/1030. URL: http://dx.doi.org/10.1088/0004-637X/722/2/1030.

Wells, James D. (2011). *When effective theories predict: the inevitability of Mercury's anomalous perihelion precession*. arXiv: 1106.1568 [physics.hist-ph].

– (Jan. 2012). *Effective theories in physics. From planetary orbits to elementary particle masses*. DOI: 10.1007/978-3-642-34892-1.

Wimsatt, William C. (1976). "Reductive Explanation: A Functional Account". In: *PSA 1974: Proceedings of the 1974 Biennial Meeting Philosophy of Science Association*. Ed. by R. S. Cohen et al. Dordrecht: Springer Netherlands, pp. 671–710. ISBN: 978-94-010-1449-6. DOI: 10.1007/978-94-010-1449-6_38. URL: https://doi.org/10.1007/978-94-010-1449-6_38.

– (Aug. 2006). "Reductionism and its heuristics: Making methodological reductionism honest". In: *Synthese* 151, pp. 445–475. URL: https://doi.org/10.1007/s11229-006-9017-0.

Zee, A. (2010). *Quantum field theory in a nutshell*. second edition. Princeton University Press.